STUDIES ON LASER INDUCED OPTOGALVANIC EFFECT IN CERTAIN GAS DISCHARGES

P R SASI KUMAR

THESIS SUBMITTED
IN PARTIAL FULFILMENT OF THE REQUIREMENTS
FOR THE DEGREE OF
DOCTOR OF PHILOSOPHY

LASER DIVISION
DEPARTMENT OF PHYSICS
COCHIN UNIVERSITY OF SCIENCE AND TECHNOLOGY
COCHIN - 682 022, KERALA, INDIA

1994

DEDICATED TO MY PARENTS

ACKNOWLEDGEMENTS

DECLARATION

Certified that the work presented in this thesis entitled "STUDIES ON LASER INDUCED OPTOGALVANIC EFFECT IN CERTAIN GAS DISCHARGES" is based on the original work done by me under the guidance of Prof VPN Nampoori at the Department of Physics, Cochin University of Science and Technology, Cochin-22, and has not been submitted previously for the award of any diploma or degree.

Cochin-22

20-8-1994

P. R Sasi Kumar

CERTIFICATE

Certified that the work presented in this thesis entitled "*STUDIES ON LASER INDUCED OPTOGALVANIC EFFECT IN CERTAIN GAS DISCHARGES*" is based on the original work carried out by Mr. P R Sasi Kumar, under my guidance at the department of Physics, Cochin University of Science and Technology and has not been included in any other thesis submitted previously for the award of any degree.

Prof. V P N NAMPOORI

(Supervising Teacher)

Department of Physics,

Cochin-22

20-8-1994

Cochin University of Science & Technology,

Cochin-682 022.
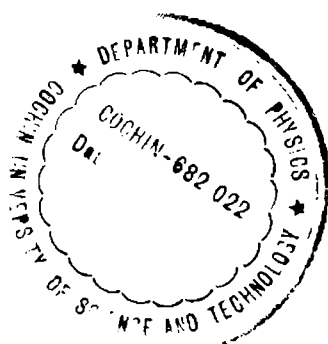
PREFACE

Electrical gas discharges have been the subject of numerous investigations from the last century due to their growing interest in technological and fundamental applications. Absorption of electromagnetic radiation by a gas discharge result into a change in electrical impedance due to a significant perturbations in the steady state population of excited levels and the degree of ionization. This change in impedance produced by resonant absorption of radiation is known as optogalvanic (OG) effect, where as that is produced by injecting electrons in to the discharge by photoelectric emission is usually known as photoemission optogalvanic (POG) effect. With the development of lasers and sophisticated electronic equipment, these effects have established their importance in analytical and spectroscopic measurements. The present thesis deals with the work carried out by the author in the field optogalvanic effect during the past few years at the Department of Physics in Cochin University of Science and Technology. The results and the observation are summarized in nine chapters and the references to the literature is made at the end of each chapter.

In the first chapter a general introduction to the subject with a comprehensive review of the OG effect is presented. Details of rf and dc discharge configurations of experimental schemes and some important applications to spectroscopy are

included in this chapter   Various features and advantageous over other spectroscopic methods are also given.   A brief description of the physical mechanism involved and different models of the OG effect, using rate equation approach for important excitation and de-excitation processes are discussed in the second chapter.   The third chapter consists of a detailed description of the experimental technique employed in the present study.   The details of the different discharges used, with continuous gas flow and sealed discharge cell configuration are presented here. Description of the laser system used for optical excitation, details of the instruments utilized for the experiment and the experimental layout are also presented in this chapter

The details of the OG spectrum of molecular nitrogen corresponding to the first positive system $(B^3\Pi_g - A^3\Sigma_u^+$ transition) using ring dye laser has been described in chapter four.   Details of the OG resonances for a large number of rotational lines in the $17179 - 17376$ cm^{-1} spectral region of the $(10,6)$, $(11,7)$ and $(12,8)$ bands recorded under high resolution optogalvanic spectroscopy are also included in this chapter.

The selective excitation of energy level population in a discharge using lasers of high spectral intensity will produce noticeable modifications in the plasma characteristics.   Chapter five presents the simultaneous investigation of OG effect and the laser modified emission characteristics under resonant laser excitation corresponding to $1s_5 \rightarrow 2p_2$ and $1s_5 \rightarrow 2p_4$ transitions

of neon in a hollow cathode discharge at 5882 Å and 5945 Å.

Results obtained from spectral profile studies by using high resolution optogalvanic spectroscopy of certain selected transitions of neon and nitrogen molecule are included in the sixth chapter. Spatial dependence study of the OG effect in neon glow discharge is also presented.

Chapter seven describes the POG effect under pulsed and cw laser excitation. Two photon absorption, laser power and voltage dependence of the POG effect in a Ne/Mo hollow cathode, and the monitoring of discharge instability by POG signal are described in this chapter.

The eighth chapter includes the investigations on non-linear dynamics of the plasma in hollow cathode discharges. With the discharge current as the control parameter the bifurcations structure and the period doubling route to chaos in the plasma dynamics are described in this chapter

The concluding chapter gives the summary of the investigations presented in the preceding chapters.

Part of the investigations presented in this thesis has been presented/published/communicated in the form of following papers in Symposia/Journals.

1 Observation of two-photon induced photoemission optogalvanic effect, P R Sasi Kumar, G Padmaja, A V Ravikumar, VPN Nampoori and CPG Vallabhan, Pramana, J.Phys. 36 (1991) 423.

2 Photoemission optogalvanic effect studies in N_2, NO_2 and Ar discharges under pulsed laser excitation, P R Sasi Kumar, VPN Nampoori and CPG Vallabhan, J. Phys. D: Appl. Phys. 26 (1993) 1.

3 High resolution optogalvanic study in nitrogen discharge, P R Sasi Kumar, B Ambadi, VPN Nampoori and CPG Vallabhan, Pramana, J. Phys. 40 (1993) 113.

4 High resolution optogalvanic spectrum of N_2-rotational structure of (11,7) band in the first positive system, P R Sasi Kumar, S S Harilal, VPN Nampoori and CPG Vallabhan, Pramana, J. Phys. 42 (1994) 231.

5 Modification of spectral characteristics and optogalvanic response in neon hollow cathode discharge under laser excitation, P R Sasi Kumar, VPN Nampoori and CPG Vallabhan, Pramana, J. Phys. 42 (1994) 427.

6 Photoemission optogalvanic effect in a Ne-Nd hollow cathode, P R Sasi Kumar, VPN Nampoori and CPG Vallabhan, (accepted in J Phys. D, Appl. Phys. 1994).

7 Subcritical Hopf bifurcation in Ne-Nd Hollow cathode discharge P R Sasi Kumar, VPN Nampoori and CPG Vallabhan (Recommended in Phys. Lett. A 1994).

8 Measurement of collision cross section and line broadening coefficient for $1p_8 \rightarrow 4d_4$ transition in neon, P R Sasi Kumar, S S Harilal, VPN Nampoori and CPG Vallabhan, High resolution spectroscopy technical digest (Optical Society of America) 1 (1993) 92.

9 Quantum efficiency of two photon absorption in N_2 using photo emission Optogalvanic effect, P R Sasi Kumar, B Ambadi, VPN Nampoori and CPG Vallabhan, (12th Symposium of the Optical Society of India, April 1992, Sameer, Bombay).

10 High resolution optogalvanic spectrum of N_2 at 17382.8 cm^{-1}, P R Sasi Kumar, B Ambadi, V P N Nampoori and C P G Vallabhan (APSYM-CUSAT-92 Symposium).

11 High resolution laser optogalvanic study of (11,7) band of the $B^3\Pi_g$— $A^3\Sigma_u^+$ transition of N_2. P R Sasi Kumar, VPN Nampoori and CPG Vallabhan, *(Trombay Symposium on radiation and Photo chemistry, BARC, Bombay, 1994)*.

12 Non-linear plasma dynamics in a hollow cathode discharge – observation of bifurcation windows, P R Sasi Kumar, VPN Nampoori and CPG Vallabhan, *(National workshop on recent advances in quantum optics, March 1994, CAT, Indore)*.

CONTENTS

OPTOGALVANIC EFFECT AND ITS APPLICATIONS-AN OVERVIEW

1.1 INTRODUCTION

The passage of electricity through gases usually produces a great variety of luminous phenomena which are typical for different kinds of the electrical discharges. Conversely, electrical phenomena can be generated in gases by absorption of light. Optogalvanic (OG) effect is such a phenomenon in which impedance of a gas discharge changes due to the absorption of radiation by atoms, molecules, ions etc. of the gaseous sample or the electrode material present in the discharge. Early experiments on this effect usually involved two discharge tubes; one tube was used as a source of excitation which perturbs the population of species present in the second tube by exciting atoms from a lower to a higher energy state. Penning in 1928 [1] observed a change in the breakdown voltage when a discharge tube was irradiated with light emitted from an identical discharge. Joshi and co-workers [2] have also observed change in the threshold potential of an electrical discharge in presence of light; which they termed as *light effect*. Variation of voltage across He-Ne laser tube has been observed when it begins to lase [3] and in gas lasers this is much pronounced under certain operating conditions of the discharge.

Although the OG effect has been observed and used for a

number of applications over the years, the usefulness of this effect for spectroscopic and analytical studies was realized only after the development of tunable dye lasers. With the use of tunable laser systems it is possible to study this effect under much better and refined conditions and this has stimulated an increased interest in the studies of fundamental as well as of applied nature. Green and co-workers in 1976 [4], using a dye laser source, have demonstrated the sensitivity of the method in determining sodium contamination by detecting sodium atoms in a lithium hollow cathode lamp.

Absorption of photons by atomic or molecular species will significantly affect the relative population of various levels in the discharge. This results a change in ion generation rate, which in turn, causes a change in impedance of the discharge requiring a different voltage to sustain it. The OG signal can correspond to an increase or decrease in the discharge current depending on the kinetics of the levels whose populations are perturbed by the laser. If the laser excite atoms from a level with a small probability of ionization to a level with a large probability of ionization, the discharge current will increase and the discharge voltage will decrease. Alternatively if the laser excites atoms from a level with a large probability of ionization to a level with a small probability of ionization the discharge current will decrease and the discharge voltage will increase. The latter situation often arises when the lower level

has a high probability of collisional ionization, and upper level is a short lived resonance level [5].

The importance of OG effect in spectroscopy and spectrochemical analysis was first demonstrated by Green [4] The use of OG effect for plasma diagnostics or for laser plasma interaction is possible only if we have a detailed information on various processes in the discharge under investigation. However, for many spectroscopic applications, any ionized gas can be considered to be a *black box* whose impedance and electrical output is specifically controlled by the input of a monochromatic light. In general, the small change in the discharge voltage ΔV can be considered as proportional to the change in local population of the excited states, ΔN_i as generated by the absorption of radiation through [6]

$$\Delta V = \sum_i \alpha_i \Delta N_i \qquad (1.1)$$

where

$$\alpha_i = \partial V / \partial N_i, \quad i = 1, 2, \qquad (1.2)$$

This concept is based on the variation in density for each excited state within the discharge volume. Zelewski et al [7] have also shown that the relative variation of the plasma impedance for weak OG signal depends on the relative optical absorption and the temperature.

Laser optogalvanic spectrum is recorded by monitoring the

3

change in voltage across the discharge tube as a function of wavelength of the probe laser beam. An experiment involving OG effect compliment the usual experiment in atomic or molecular spectroscopy, where the spectra are recorded using a spectrograph on a photographic film or with monochromator and photo detectors. Line width observed in OG spectrum is that of the dye laser which is considerably smaller than those obtained with usual methods. With a single mode ring dye laser and by making use of Doppler free techniques, resolution up to of a few MHz can be easily obtained. OG detection is distinguished from other spectroscopic methods by the presence of a sustained discharge with an electron gas at a relatively high temperature. Because of this high temperature in the discharge, there are significant atomic and molecular populations in excited states and hence transitions between the excited levels in atoms or molecules can be detected. Refractory elements, which have very high melting point, can be conveniently studied with this technique.

Several types of electrical gas discharges are currently used for OG spectroscopy (OGS). Some of them are low pressure positive columns, hollow cathodes, and plane diode type discharges [8]. The properties and mechanism of these discharges are thoroughly discussed in many standard books on ionized gases [9-12]. An electrical discharge can be produced by applying a high voltage between two electrodes within the cell which is filled with a gas at pressures of a few torr   Under the

4

influence of the electric field, this gas will get ionized and most of the discharge properties are characterized by various excitation and de-excitation processes of the species present in the discharge. The simple experimental setup for observing OG effect consists of an electrical discharge produced in a gas cell, provided with two electrodes between which a stable dc voltage is applied[4]. A ballast resistance is used to limit the current in the circuit. The modulated laser beam is passed through the cell, which results in a change in impedance of the discharge by resonant absorption of radiation. A coupling capacitor blocks the dc voltage and the change in impedance can be measured directly on an oscilloscope. Pulsed or cw lasers can be used for exciting the discharge medium.

The advantages of OG effect over other spectroscopic methods are that the voltage signal can be directly used for spectroscopic or analytic measurements eliminating the need to monitor irradiating source optically as in absorption or emission spectroscopy. Since no optical measurement is required in monitoring the signal, the problems associated with the collection efficiency, scattered light etc., do not limit the sensitivity. From an experimental point of view, the method is simple and convenient; the discharge medium acts as the sample and a pair of electrodes with a coupling capacitor are sufficient for detection.

Main source for noise in the experiments are statistical

fluctuations of electrons arising from plasma instabilities, if the cell is not operated in a range of current corresponding to a stable discharge region[13]. If the discharge remains stable, the noise can be minimized to the level of shot noise determined by the current flow through the resistance which is in series with the cell. For OGS studies the selection of gases, electrode material, cell configuration, applied voltage, pressure etc. must be such that the random fluctuations of the electrical output leading to noise is minimum.

Significant progress has already been made in understanding the OG effect both qualitatively and quantitatively. The aim of many investigations made with different experimental and discharge conditions has been to understand the mechanisms which regulate the OG signal production. Laser optogalvanic spectroscopy is particularly a powerful technique for providing spectroscopic information unobtainable from conventional spectroscopic methods. The optogalvanic studies, to date, have been carriedout using visible laser radiation. The OG detection provides valuable tool for studies in the ultra violet and infrared region of the spectrum as well. UV photons have energies of the same order of magnitude as the ionization potential of many atoms/molecules and the OG effect refers to a perturbation in the ionization states and hence OGS in the UV region is quite practicable[14]. Laser optogalvanic signals in molecular discharges produced by IR laser excitation have been reported for

several molecules [15-16].   Current interests of OG effect are
mostly for a wide variety of spectroscopic and analytical
applications with particular interest in high resolution studies
due to its high sensitivity and selectivity[17].

1.2 GAS DISCHARGES - EXCITATION METHODS

Two type of schemes commonly used for producing discharges
are by direct current (dc) and radio frequency (rf)
excitation[8]. In dc OG technique, an electrical discharge
produced by a stable dc voltage is irradiated with a laser beam.
A resistance, which limits the current in the circuit, is
connected in series with the cell (fig 1.1). The gas pressure
and the discharge current are adjusted to get a minimum noise
level and the output is taken via a coupling capacitor which
blocks the dc component.   Plane diode type or positive column
discharges are commonly used for gaseous samples and hollow
cathodes are used for solids, including refractory metals.   More
details of the discharge cells and about the experimental aspects
are discussed in chapter 3.

Detection of optical resonant absorption in gases with radio
frequency excitation, in an electrodeless cylindrical discharge
tube was first demonstrated by Staciulescu et al [18].   Another
simple scheme for observing optogalvanic effects in the rf
discharge has also been reported by Suzuki[19] is as shown in fig
1.2.   In this method, the discharge is produced by applying an rf

7
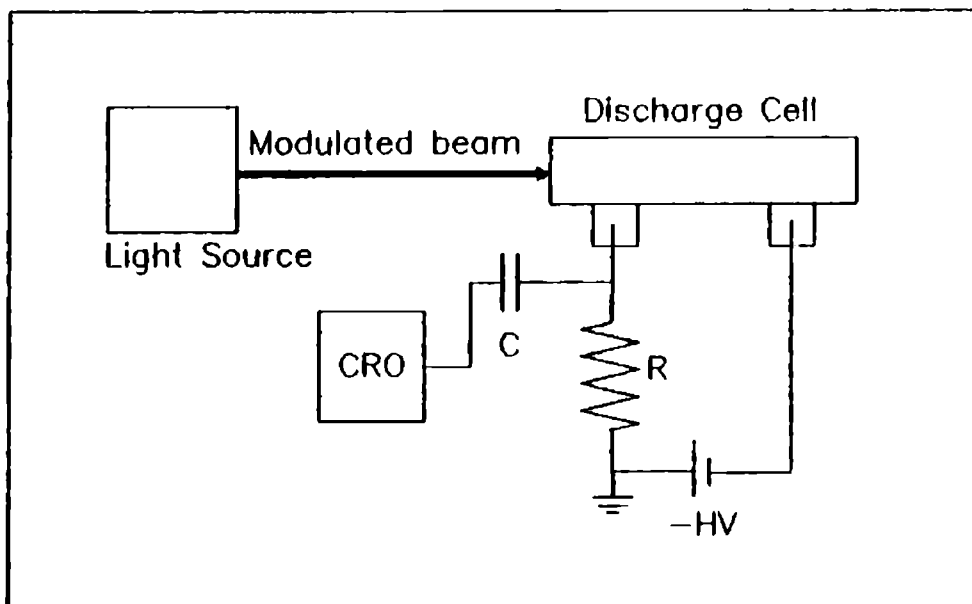
Fig 1.1 Simple experimemtal arrangement for OG effect.
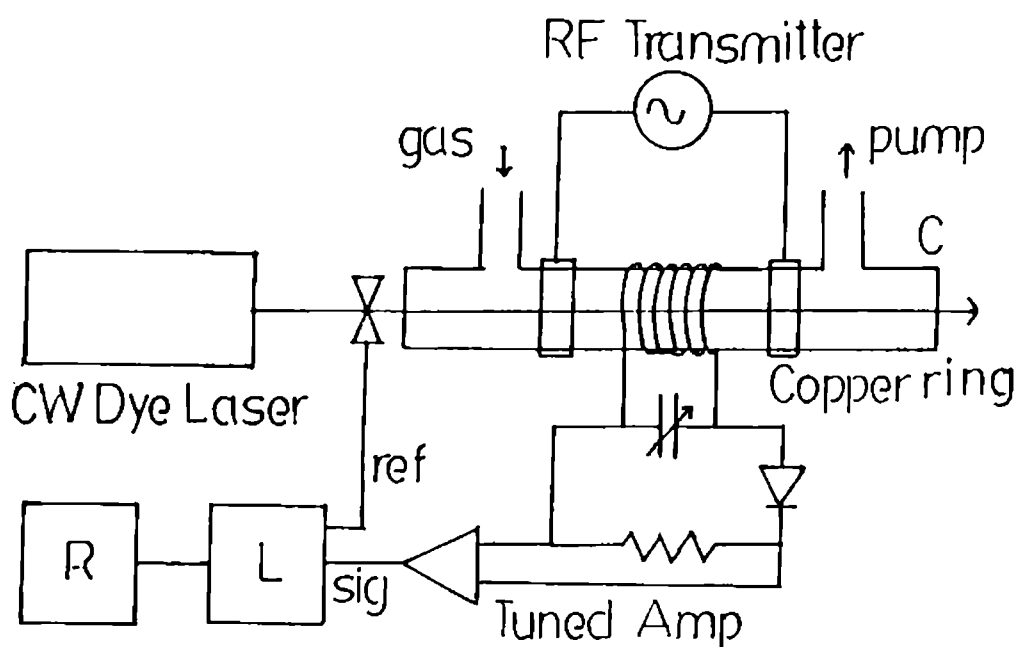
Fig 1.2 OG effect with rf excitation (C-discharge cell,
L-lock-in amplifier and R-chart recorder)

field having an output power of $\simeq$ 50 watts, to two electrodes separated by 5 to 10 cm of a glass tube of length $\simeq$ 40 cm and diameter 10-30 mm. The electrodes are copper plates with a width of 1 cm which are wound around the tube. A pickup coil around the tube and the capacitor forms a tank circuit which is adjusted to be resonant with the applied rf field. Signal picked up by the coil are rectified and passed through an amplifier tuned to the modulation frequency. The output is monitored by an oscilloscope and measured with a lock in amplifier. The discharge condition and the magnitude of the signal depends on the gas pressure, tube diameter, electrode spacing, rf power, laser power and molecular species. The best combination of these parameters which gives maximum signal is different for each molecules.

In rf electrodeless discharges, the entire plasma is approximately neutral and diffusion controlled which often resembles the positive column of an equivalent dc discharge without the complications of the cathode and anode regions observed as in dc glow discharge. In contrast to dc discharges, the use of high frequency electrodeless discharges for OGS has certain advantages viz., (a) much lower discharge power level minimizes broadening due to the collision of electrons and the line shift of spectral lines, (b) spatially homogeneous plasma (c) high electron temperature allows the excitation of a number of levels and (d) a complete elimination of the noise caused by the cathode sputtering. High frequency detection technique is

9

readily adaptable for the studies of unstable molecules which are reactive to metal electrodes in the discharge tube. A simple theory of the OG effect in low pressure rf discharges of Ar and Cesium has given by Bulyshev [20].

The rf detection appears to be suitable for Rydberg state spectroscopy [21], high resolution spectroscopy[22,23] etc. and using these methods optogalvanic detection of negative ions of molecules [24] Ar metastables [25], frequency stabilization [26], measurements of predissociation rates of $\bar{A}$ state of HCO [27] etc. have been reported. Investigations on OG effect in microwave discharges have also been reported in the literature[28,29]

1.3 OG EFFECT IN FLAME

In contrast to electrically sustained discharges, flame is a chemically sustained plasma and the laser induced galvanic studies can also be adopted to flame. OGS in flames, also known as laser enhanced ionization (LEI) spectroscopy, has become a most promising tool for the quantitative method for the trace analysis of elements[5,30-33]. The common atom reservoirs for analytical atomic spectrometry are atmospheric pressure flames, furnaces and electrical plasmas. Such environments promote some level of ionization of atomic and molecular species, depending on the ionization potential of the species. Enhanced ionization rate due to the thermal collisions of laser excited and other species constitute the basis of the OG effect in flames or in

laser enhanced ionization.

In LEI method, samples to be analyzed are aspirated into the flame, where they are vaporized and decomposed to atomic form (fig 1.3) The flame commonly used in atomic absorption spectrometry utilizes a pneumatic nebulizer for introducing the solution into the flame-gas mixture. The acetylene flame with either air or nitrous oxide as oxidant seems to be the most practical in terms of good atomization. In most cases, the air acetylene flame which burns at a temperature of about 2500 K is used. Many refractory elements in the form of oxides require
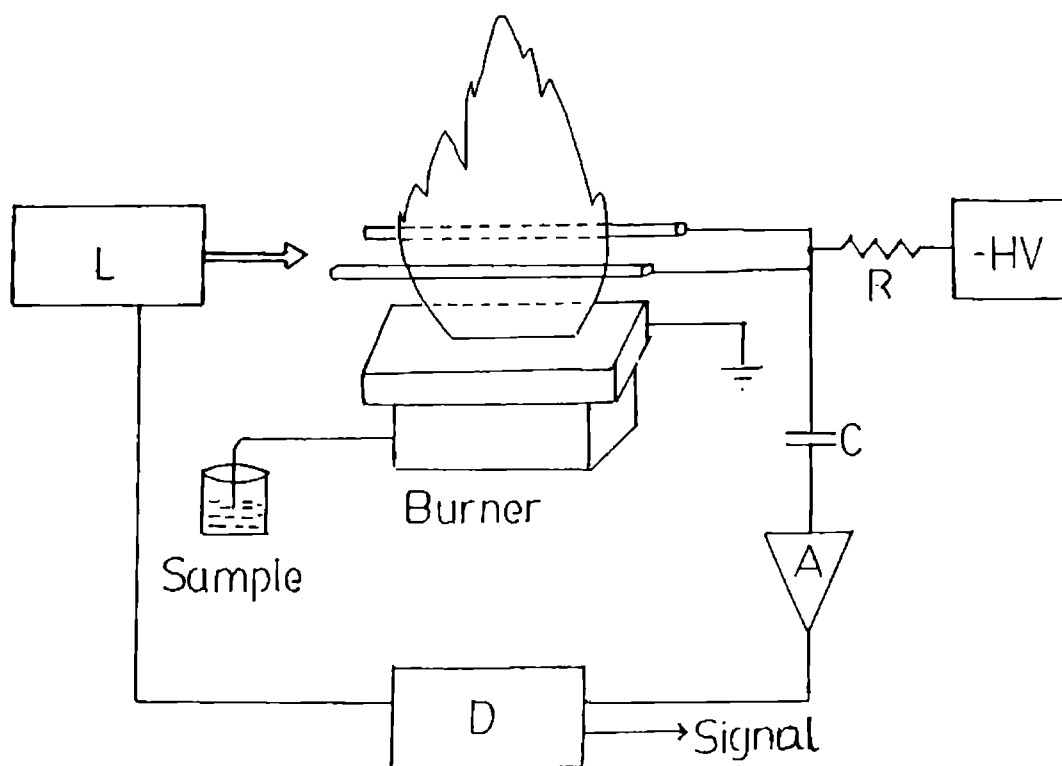
Fig 1.3 Optogalvanic effect in flame (L-pulsed dye laser, D-gated detection system and A-current amplifier).

hotter nitrous oxide flame (3000 K) to achieve efficient atomization. Use of a tunable dye laser for the resonant excitation of the element of interest results in a significant perturbation of the population of energy levels. The enhanced rate of collisional ionization of the resulting excited atoms relative to those in the ground state is the basis of the laser enhanced ionization technique. To detect the occurrence of the LEI, a voltage is applied across the flame and the resulting current is monitored. LEI signal appears as change in this current, and is thus most easily detected by using pulsed or amplitude modulated cw lasers with synchronous detection. Even with no bias voltage, enhanced ionization always occurs in flames when the species are optically excited. It is only to collect the free charge carriers created by LEI that an external electric field is necessary. In general, the signal is caused by the motion of electrons and ions from the laser irradiation zone towards the biased electrodes. Due to the difference between ion and electron mobilities there is a build up of net positive space charge sheath in an electrical field distribution which resembles that of negative Langmuir probe. The alignment of the laser beam close to the cathode within the cathode sheath greatly increases the collection efficiency of charged species. Theoretical and experimental developments of LEI in flame are studied in some details by many workers [30-34]. Numerous elements have been investigated by LEI spectroscopy using single and multistep laser

excitation. The limit of detection is in the range of $1-10^{-3}$ ng/ml [30]. Besides the trace element analysis, the OG effect in flame is also suitable for diagnostics of combustion phenomena and spectroscopy of molecules and radicals.

The applicability of multi photon optogalvanic techniques to probe the hydrogen plasma is reported by Ausschnitt [35]. Report on the use of OG effect for dark space diagnostics of a hollow cathode discharge [36], investigations of cathodic region of neon discharge [37] and space charge effects [38], analysis of Townsend discharge [39], measurement of electric field, absolute metastable density and temperature in the cathodic region of a glow discharge [40,41] etc. are also available in literature.

1.4 APPLICATION TO ATOMIC AND MOLECULAR SPECTROSCOPY

Experimental simplicity is one of the most attractive aspects of optogalvanic spectroscopy. Optogalvanic detection provides a convenient means of observing an optical transition without requiring any conventional optical detectors [42-45].

Laser induced galvanic study of electrical discharges, flames and plasmas have provided a wealth of information on spectral properties of atomic and molecular species. Unlike emission or absorption spectroscopy, which require the use of optical detectors, optogalvanic spectroscopy is based on the detection of variations in electrical impedance caused by resonant absorption of laser by atoms or molecules. In the latter

13

case the discharge itself acts as both spectroscopic sample and detector of the perturbed atoms/molecules in the medium. Generally, the impedance variations are controlled by various ionization processes in the discharge. For most of the spectroscopic applications, however, a detailed knowledge of the laser plasma interaction mechanism is not necessary. Laser induced OGS is particularly a powerful technique for providing spectroscopic informations which are unobtainable using other spectroscopic techniques such as laser induced fluorescence, absorption etc. and is widely used for Doppler free spectroscopy [46], level crossing OGS [47-49], two photon spectroscopy [50-56], Rydberg spectroscopy [57-59], penning ionization spectroscopy [60,61] etc.

Many refractory elements are best studied in hollow cathode discharge (hcd), where ions or electrons colliding with the cathode remove atoms from the cathode by sputtering, making the sputtered atoms accessible to gas phase optical spectroscopy. Since these materials are part of the discharge, OGS provides the most straight forward technique for studying them. Due to a relatively high temperature in the plasma, there are significant atomic and molecular populations in levels far from the ground state. Hence OG effect can be used to detect transitions between excited levels in atoms/molecules and the spectra of ions, free radicals etc. of refractory elements. OGS investigations using multistep laser excitation with dye laser has been demonstrated

as another technique for studying highly excited atomic levels.

OGS provides an important alternative to absorption or fluorescence studies for the determination of spectroscopic data such as relative oscillator strength, electron temperature, isotope and hyperfine structure measurements, determination of transition energies [62], measurements of line broadening and line shifts, determination of Lande g factor [63] etc. Use of OG effect in various other fields like for the study of Zeeman effect [64], autoinization spectrum of Kr [65], frequency stabilization [66-70], intracavity atomic absorption measurements [71], the detection of photons [72], etc. have also been reported.

It is only recently that laser optogalvanic spectroscopy has been applied to study molecular species. Feldmann [73] extended this technique to molecular species; although the signals were weaker by several orders of magnitude as compared with those of atoms. At present OGS has been successfully used to record the spectra of molecules in the visible and IR [74-78] region. Webster et al [15] have studied the LOG signal of molecules in the IR wavelength region by using tunable diode laser Results of investigations of simple diatomic molecules like I_2 [79-85], N_2 [19,73] and of many complex molecules are also available in the literature. OGS technique has been applied to the detect positive molecular ions [86], negative ions [24,87], and for the measurement of photo detachment [15] phenomena. Several lines

belonging to the ν_2 band of NH_3 at 9.5μm and the ν_3 band of NO_2 at 6.2μm have been studied by Webster [15] and found that absorption spectrum is directly comparable with LOG spectrum. Singh et al [88] have studied low pressure dc discharges of ammonia from excitation of ground as well as excited vibrational states with a line tunable CO_2 laser and have estimated the vibrational and rotational temperature of the discharge.

Even though OGS overcomes most of the limitations in the conventional studies of gaseous media, it does have limitations of its own. The technique has, inherently, very high sensitivity, although attaining this sensitivity may require some effort to produce an electrically quiet discharge. The pressure and current necessary to operate the discharge in a stable regime may perturb the atomic or molecular energy levels of interest, although this generally does not appear to be a significant effect in moderate resolution spectroscopy.

1.5 OSCILLATOR STRENGTH MEASUREMENTS

Zelewski et al [7] have observed that for certain transitions in a neon hollow cathode discharge, magnitude of the impedance change is proportional to the product of the wavelength, degeneracy of the initial level and the oscillator strength. Keller et al [89] have also demonstrated that, laser induced impedance changes could be used for the determination of oscillator strength and electron temperature of an electrical

discharge. These authors measured the laser induced impedance change for some transitions of neon and uranium for which the magnitude of the impedance change depends only upon the properties of the initial level i, such that

$$\frac{\Delta Z_{ij}}{I_{ij}} \propto \lambda_{ij} f_{ij} [A]$$

(1.3)

where ΔZ_{ij} is the laser induced impedance change at λ_{ij}, I_{ij} is the laser intensity which is a normalizing factor in these measurement, f_{ij} is the oscillator strength of the transition and $[A]$ is the concentration of the level i, given by,

$$[A] \propto g_i \exp\left(-\frac{E_i}{k_b T}\right)$$

(1.4)

where g_i is the degeneracy of the state i. Then,

$$\frac{\Delta Z_{ij}}{I_{ij}} \propto \lambda_{ij} g_i f_{ij} \exp\left(-\frac{E_i}{k_b T}\right)$$

(1.5)

Thus, $\log\left(\Delta Z_{ij}/I\lambda gf\right)$ verses E_i plot will be a straight line from which oscillator strength and the temperature of the discharge can be evaluated. However in the case of calcium, Bechor et al [90] have observed a large inaccuracy in measuring the oscillator strength by this method. Major uncertainties in the measurement of oscillator strength are due to the following reasons.

1) The OG effect has a strong spatial dependence.

17

2) The interaction of laser beam with plasma is a complex process and is usually non-linear with respect to parameters such as number density, electron density, the temperature etc.

1.6 WAVELENGTH CALIBRATION

In laser spectroscopy, as in classical spectroscopic methods, it is often necessary to have a source of accurately reproducible reference wave numbers. The desirable characteristics of a reference spectrum are; it should be easily and conveniently observable, lines of the spectrum should be highly reproducible and the source should have a good spectral distribution of useful reference lines. A number of sources have been proposed and used for laser wavelength calibration. The most widely used source for this purpose is the absorption spectrum of molecular iodine. It has good spectral coverage and easy to use, but its accuracy is limited by the unresolved hyperfine structure and asymmetric Doppler brodended lines.

King et al [91] have shown that OG effect provides a simple and accurate technique to measure laser profile and for direct wavelength calibration of spectral lines. The technique is equally successful for cw and pulsed lasers. Calibration spectrum is recorded with a portion of the reflected laser beam, using a beam splitter, which provides simultaneous measurement of the laser wavelength and the spectra derived from the experiment. Thus the laser wavelength in any spectral region can be

calibrated by utilizing an appropriate discharge lamp. OG effect in hollow cathode discharge (hcd) lamps has been extensively used in spectroscopy for calibrating dye laser wavelength [14,91-100]. Most of the commercially available hcd lamps, which contain selected cathode material and filled with a buffer gas like neon or argon, are suitable for this.

Transitions associated with rare gases are often used for wavelength calibration because of their high intensity. Investigations of OG spectrum of neon and argon in a wide spectral region, which is useful to calibrate both cw and pulsed lasers, have been reported. The use of transitions in uranium and thorium discharges have been proposed as being well suited for this purpose because of their narrow line width and the availability of a large number of lines in the IR, visible and UV spectral range. Many lines covering a broad spectral region are easily observable in most of the commercially available hcd lamps. The accuracy in the wavelength measurement of lines using these lamps is limited only by Doppler broadening and the line shifts due to collision process.

As an aid to wavelength calibration, Keller et al [99] have studied the relative intensity of the laser induced voltage change with the intensity of the corresponding emission line of neon over a wide wavelength region. In a Uranium hcd at constant current the ratio of the voltage change to the laser intensity for cw laser excitation is given by

$$\frac{\Delta V_{ij}}{I} \propto \lambda_{ij} f_{ij} g_i \exp\left\{-\frac{E_i}{k_b T}\right\}$$

(1.6)

ΔV_{ij} is the observed voltage change when the laser wavelength λ_{ij} corresponds to the $E_i \rightarrow E_j$ transition, f_{ij} is the oscillator strength of this transition, g_i degeneracy of the initial (i^{th}) state, E_i is the energy of this state and I is the laser intensity. The intensity of the emission line is given by

$$F_{ji} \propto \frac{g_i}{g_j} \frac{f_{ij}}{\lambda_{ij}^3} g_j \exp\left\{-\frac{E_j}{k_b T}\right\}$$

(1.7)

In this case the initial state is the jth level. For a small wavelength region λ_{ij} does not change appreciably and $E_j = E_i + h\nu_{ij}$. Thus these equations can be rewritten for comparison over a small wavelength region as

$$\frac{\Delta V_{ij}}{I} \propto f_{ij} g_i \exp\left\{-\frac{E_i}{k_b T}\right\}$$

(1.8)

and

$$F_{ji} \propto f_{ij} g_i \exp\left\{-\frac{E_j}{k_b T}\right\}$$

(1.9)

where the factor λ^{-3} and exp $(-h\nu/k_b T)$ have been incorporated in the proportionality constant. Inspection of eqns (1.8) and (1.9) indicates that there should be a correspondence between the laser

induced voltage and the intensity of the emission line. This correspondence indicates that OG effect is useful for wavelength calibration.

Effect of photoelectric emission on OG effect is another emerging area of light-matter interaction. Photoelectric emission is troublesome especially in the ultraviolet region where the photon energy exceeds the work function of the cathode material. As the photon energy approaches the work function, the entire surface can contribute to photoelectric emission and there is a large increase in the OG signal Hence, when this method is used for wavelength calibration in the UV spectral region, photoelectric emission from the cathode will mask the OG signal. This is especially true for pulsed excitation where it can be a serious problem even in the visible region. Construction of the discharge tube with a clear optical path through the cathode would be very useful at shorter wavelength. Dovichi et al [100] have constructed a tubular hollow cathode discharge tube such that the laser light can pass through the centre of the discharge without striking the cathode surface. The use of this tubular hcd eliminates interferences from photo emission and permits wavelength calibration of pulsed lasers at shorter wavelengths. Babin et al [101] have also developed a convenient iron hcd for measuring the reference wavelength in the 210-300 nm region which is suitable to use for high resolution measurements.

Recently, a fully automatic wavelength calibrator has been

developed to calibrate the dye laser system [102]. In this system when a target wavelength is put into the keyboard, the computer scans the laser wavelength and takes OG signal of the hcd lamp which is installed in the dye laser system. Then the wavelength of the laser is tuned to the target comparing with the reference OG line. In this system the reproducibility in the absolute wavelength calibration over a spectral range from 220-740 nm is better than $\pm$ 1 cm^{-1}

1.7 SPECTRAL PROFILE OF THE OG SIGNAL

Spectral profile of a transition in a gas discharge has a finite width and the characteristic shape is determined by the conditions existing in the source. Different processes that affect spectral profile are due to natural broadening, Doppler broadening and the broadening as a result of interaction of absorbing or emitting atoms with the neighboring particles.

Doppler broadening is caused as a result of random distribution of transition frequencies due to the random thermal motion of atoms in the discharge medium [103]. The shape and width of the spectral lines radiated from a discharge lamp is Doppler broadened. The Doppler width can be reduced by cooling and operating the discharge at low currents. In laser spectroscopy, there are several techniques to eliminate this. Intermodulated optogalvanic spectroscopy, polarization intermodulated excitation, optogalvanic double resonance

spectroscopy etc. are the commonly used methods for this purpose.

Interaction between atoms, molecules, ions or electrons will perturb the state of radiative atom and will cause line broadening, line shift or distortions in the spectral profile which can also be investigated by OGS [104]. Due to a small line width and the tunability of the lasers along with a high selectivity of OGS, measurement up to a few MHz could be easily attained [105].

The use of OG effect for spectral profile investigation has been discussed by many authors. For instance, Bechor et al [90] have compared OG and absorption line profiles and have observed that, for low discharge currents, the line profile obtained by both methods are similar. The measurements of temperature from the Doppler width of the OG line profile have also been reported [8,106]. The Doppler width $\Delta\nu_D$ depends only on the temperature T and the atomic weight M according to the formula,

$$\Delta\nu_D = \frac{2}{c}(2R \log 2)^{1/2}\nu_0(T/M)^{1/2} \qquad (1.10)$$

where R is the gas constant and c is the velocity of light. The fraction of the incident light of frequency ν that passes through an absorbing region of the discharge of length l is given by [107]

$$I(\nu) = I_0 \exp(-k(\nu)l) \qquad (1.11)$$

where $I(\nu)$ and I_0 are the transmitted light intensities with and without absorption respectively and $k(\nu)$ is the absorption

23

coefficient as a function of frequency. The integral of the absorption coefficient is expressed as [108]

$$\int k(\nu)d\nu = \frac{\lambda_0^2}{8\pi} \frac{g_2}{g_1} NA \qquad (1.12)$$

where λ_0 is the wavelength of the transition, g_1 and g_2 are the statistical weights of the lower and the upper states respectively, N is the atom density at the lower level and A is the Einstein coefficient. When the Doppler broadening is dominant, the absorption coefficient at the line centre is given by

$$k(\nu) = k_0 \exp\left\{-\left[2(\nu-\nu_0)(\log 2)^{1/2}/\Delta\nu_D\right]^2\right\} \qquad (1.13)$$

where ν_0 and k_0 are the frequency and the maximum absorption coefficient at the line centre. Integrating eqn (1.12) one obtains

$$k_0 = \frac{\lambda_0^2}{4\pi\Delta\nu_D} \left(\frac{\log 2}{\pi}\right)^{1/2} \left(\frac{g_2}{g_1}\right) NA \qquad (1.14)$$

Thus, from the OG spectral profile, the temperature T is obtained directly from the Doppler width and the atomic density of the lower level N is obtained from the maximum absorption coefficient.

1.8 HIGH RESOLUTION OG SPECTROSCOPY

Random thermal motion of atoms or molecules in a discharge causes their resonance frequencies, as seen by a stationary observer, to be shifted by the Doppler effect. Since the sample as a whole consists of atoms and molecules moving in all different directions with a large range of velocities, the additive effect of this individual shift is to broaden the spectral lines. This Doppler broadening is often the factor that limits the resolution obtainable in a standard spectroscopic experiment. Several techniques have been developed to overcome this limitation and to obtain a much better resolution. The Doppler free saturation spectroscopy and two photon spectroscopy have recently been combined with optogalvanic detection to increase the range of applications of these methods to high resolution spectroscopy.

Doppler free intermodulated optogalvanic spectroscopy (IMOGS), similar to saturation spectroscopy, is first described by Lawler [109]. In this method, radiation from a single mode laser is split in to two beams of roughly equal intensity, and both beams mechanically chopped at two different frequencies f_1 and f_2 are passed through the discharge from opposite directions (fig 1.4). If the laser is tuned to the centre of a transition, both beams will interact with the same group of atoms, having zero velocity component along the beams, and thus avoids the Doppler shift. In this case, non-linearity caused by these two
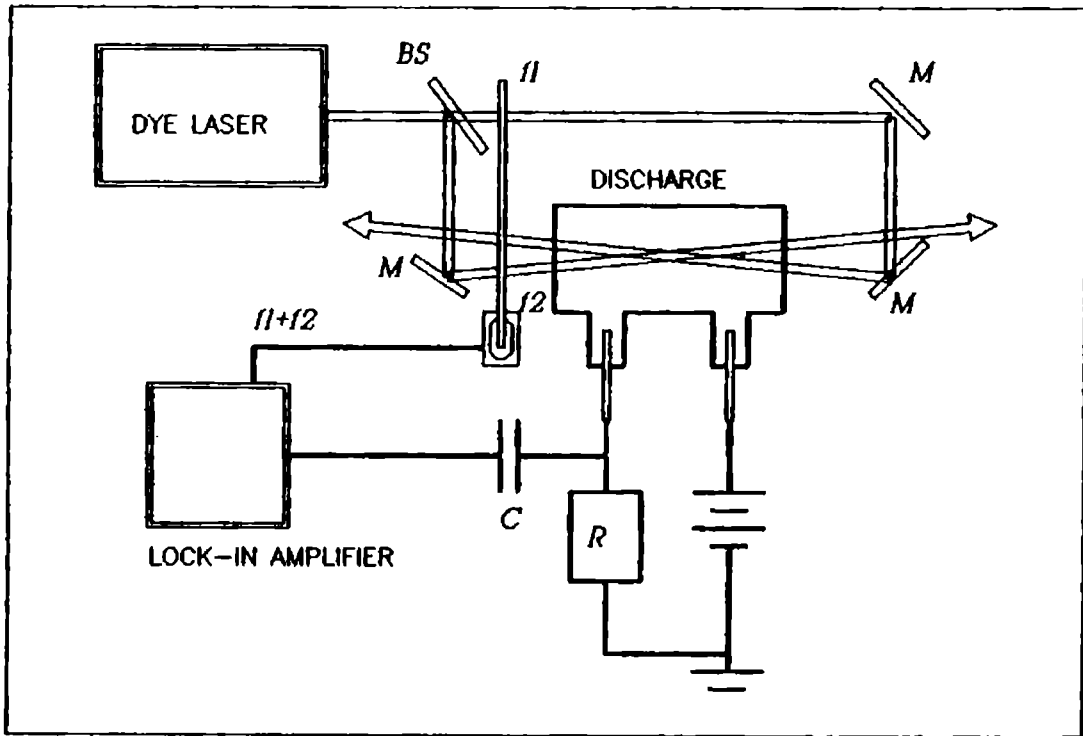
Fig 1.4 Experimental scheme for intermodulated
optogalvanic spectroscopy.
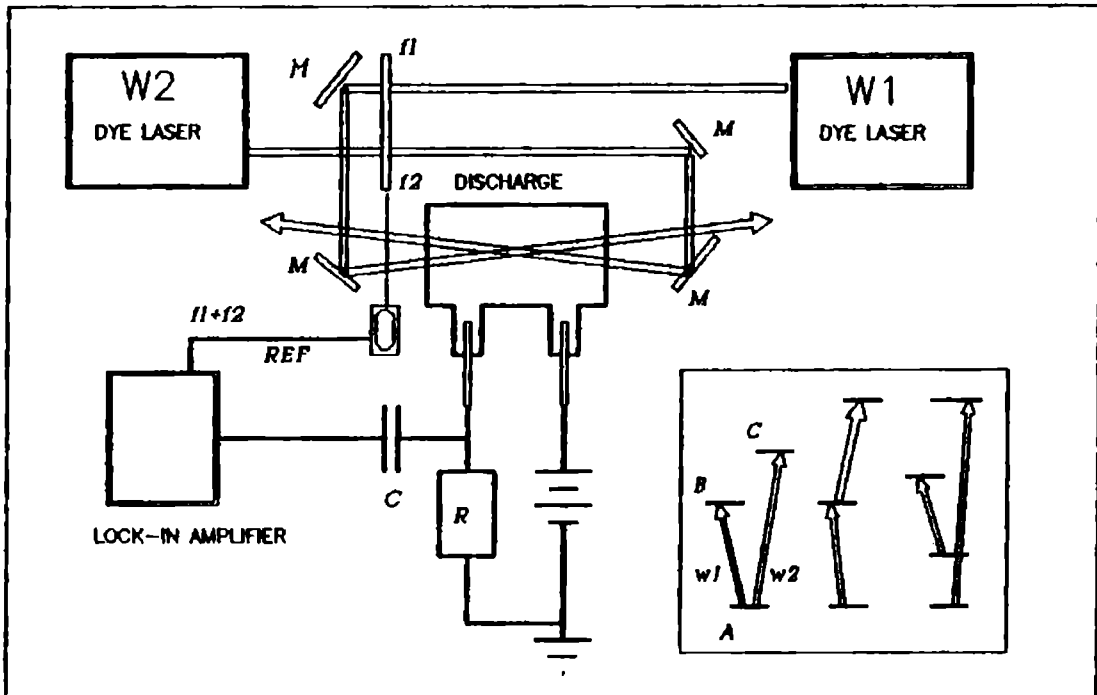
Fig 1.5 Principle of optogalvanic double resonance
spectroscopic experiment.

beams saturate the same group of atoms to produce Doppler free signals modulated at frequencies $(f_1 + f_2)$ and $(f_1 - f_2)$ in addition to the Doppler broadened signals at f_1 and f_2.

Comparison of intermodulated optogalvanic spectroscopy and Doppler free saturated absorption spectroscopy indicates that IMOGS is more sensitive than the saturation absorption spectroscopy. This method is an extremely simple technique and is most useful when low noise detectors or high quality optical components are unavailable. Doppler free IMOGS is widely used for isotope shift measurements, hyperfine structure studies and a large number of atomic and molecular spectroscopic investigations. Bevereni et al [110] have demonstrated that Doppler free intermodulated optogalvanic detection could be applied to Zeeman spectroscopy of volatile and non-volatile elements in hcd without loss of accuracy or resolution for magnetic fields larger than 120 Gauss.

When the gas pressure in the discharge cell is of the order of 0.1 torr or greater, the recorded Doppler free spectra show sharp peaks on the top of broad pedestal. These pedestals are attributed to velocity changing collisions which tend to redistribute the population of the ground or metastable level atoms over the original Maxwellian distribution and thus reducing the velocity selection of the saturating beams consequently resulting into the Doppler broadened spectrum. This problem can be eliminated by the method of polarization intermodulated

27

excitation (POLINEX) developed by Hansch [111]. In POLINEX, the polarization of one or both of the beam is modulated rather than the intensity of the beam as in IMOGS. In this way, by modulating the polarization rather than the intensity, the detected Doppler free signal arises from light induced atomic orientation, and the atoms which suffered a velocity changing collision will no longer contribute to signal if their orientation are destroyed. POLINEX can take advantage of the rules for the absorption of the polarized light to yield information on the angular momenta of the participating energy levels.

Another interesting technique for state selective atomic and molecular spectroscopy proposed by Vidal [112,113] is by making use of optogalvanic double resonance (OGDR). In this method, discharge is irradiated by two tunable lasers operating at frequencies ω_1 and ω_2. The two laser beams, modulated at frequencies f_1 and f_2 respectively, are passed into the discharge tube from opposite directions. The laser-induced change in the discharge current is detected by a lock-in amplifier at a frequency $(f_1 - f_2)$ or $(f_1 + f_2)$. The principle of the method is explained in fig 1.5. Laser 1 is tuned to a transition ω_{ab} and induces an intensity dependent change in the population densities of levels a and b. Depending on the ionization rates of levels a and b, this gives rise to a modulation of the plasma discharge current detectable at modulation frequency f_1. Similarly, laser

2 is able to generate a detectable signal at modulation frequency f_2, if it is tuned to some other transitions of the system under investigation. If, however, both lasers simultaneously pump transitions that have one state in common, one can generate laser-induced changes of the plasma discharge current that are proportional to the product of the two laser intensities involved and that can be detected at a frequency $(f_1 - f_2)$ or $(f_1 + f_2)$.

In the OGDR experiment, frequency ω_1 of laser 1 is tuned to a particular transition frequency ω_{ab}. An OG signal at frequency $(f_1 - f_2)$ or $(f_1 + f_2)$ can be detected by scanning the laser 2 if laser 2 coincides with a transition that has state a or b in common. One, therefore, has a state-selective version of OGS.

1.9 ISOTOPE ANALYSIS

Since for low laser intensities, OG effect is proportional to the density of the absorbing species, it was suggested by Keller at al [89] that, isotopic analysis of elements could be performed by laser induced optogalvanic spectroscopy in hollow cathode plasma. Due to the presence of Doppler broadening and hyperfine structure, the accurate measurement of isotope shift by classical method is very difficult. However, using Doppler free methods such as IMOGS [109], POLINEX OGS [111] etc., the optical isotope shift with an accuracy of a few MHz could be measured. Hollow cathodes are extensively used for isotope analysis, since they are characterized by narrow spectral line with electron

temperature $\simeq$ 3500 K and hence any element including refractory material can be investigated. Details of the dependence of the OG signal strength on isotope concentration in uranium hcd was first reported by Planorasa et al [114].

The transition energy for atoms of different isotopes from a level of energy E' to a lower level of energy E'' will be

$$E'_\alpha - E''_\alpha = h\nu_\alpha \quad \text{and} \quad E'_\beta - E''_\beta = h\nu_\beta \qquad (1.15)$$

where α and β denotes heavier and lighter isotopes respectively. Then $h(\nu_\beta - \nu_\alpha)$ corresponds to optical isotope shift which can be measured by scanning the laser wavelength over the transition.

The determination of the ratio $^\alpha N \diagup ^\beta N$ of any two isotopic pairs α and β of an element by OGS consists of measuring the densities $^\alpha N$, $^\beta N$ of these two isotopes, that being in two given isotope shifted energy levels, which absorb the incident laser photons. This absorption can, in principle, produce positive and negative OG signals, where, the sign depends on the particular level being excited and hence on the configuration to which it belongs. For a given isotope pair, whose energy difference is due to the isotope-shift term belong to the same configuration. It follows that in most cases for a given isotope pair, the OG signals will have the same sign.

The OG signal $S(\nu)$ for a transition at a frequency ν is related to the absorbed laser intensity $\Delta I(\nu)$ by

$$S(\nu) = CD \Delta I(\nu) \qquad\qquad (1.16)$$

where D is the geometrical cross section of the laser beam and C is a proportionality factor which is constant for a given transition, for all isotopes. In the case of a homogeneous absorbing layer of length l illuminated by a laser-beam of intensity I which is sufficiently low so as to avoid saturation, equation 1.16 becomes

$$S(\nu) = CDI\{1 - \exp[-k(\nu)l]\} \qquad\qquad (1.17)$$

where $k(\nu)$ is the frequency dependent absorption profile of the transition. For small absorptions $k(\nu)l \ll 1$, eqn.(1.17) can be written as

$$S(\nu) = CDIk(\nu)l \qquad\qquad (1.18)$$

The explicit $k(\nu)l$ dependence of $S(\nu)$ can be used to relate $S(\nu)$ to the atom density in the lower level of the transition by using the relation,

$$\int k(\nu)d\nu = \frac{\lambda_o^2[J']AN}{8\pi[J]} \qquad\qquad (1.19)$$

where $[J] = 2J+1$; J and J' are the statistical weights of the lower and upper levels, respectively, A is the Einstein

transition probability and N is the isotope population in the lower level. In a hcd, the significant line broadening effect is the Doppler broadening due to thermal motion of the atoms. Atomic absorption line shapes are then well approximated by a Gaussian profile and eqn(1.19) can be rewritten as

$$\int k(\nu)\,d\nu = \frac{1}{2}\left(\frac{\pi}{\log 2}\right)^{1/2} k_0 \Delta\nu_D \qquad (1.20)$$

where k_0, the absorption coefficient at the line center is given by

$$k_0 = \frac{\lambda_0^2 [J'] A}{4\pi [J] \Delta\nu_D}\left(\frac{\log 2}{\pi}\right)^{1/2} N \qquad (1.21)$$

and $\Delta\nu_D$, the Doppler width of the transition (FWHM), is given by

$$\Delta\nu_D = \frac{2.147 \times 10^{12}}{\lambda_0}\left(\frac{T}{M}\right)^{1/2} \qquad (1.22)$$

with λ_0 in Angstroms, T in kelvins and M in amu. Thus from equations (1.17), (1.18) and (1.21), one obtains the relationship between the OG signal at the line center S_0 and the density of the absorbing atoms N as

$$N = \frac{4\pi [J] \Delta\nu_D}{\lambda_0^2 [J'] A}\left(\frac{\pi}{\log 2}\right)^{1/2}\left[-\frac{1}{l}\log\left(1 - \frac{S_0}{CD/l}\right)\right] \qquad (1.23)$$

for strong absorption and

$$N = \frac{4\pi[J]\Delta\nu_D}{\lambda_0^2[J^{\prime}]A}\left[\frac{\pi}{\log 2}\right]^{1/2}\frac{S_o}{CD[l}$$ (1.24)

for weak absorption.

Eqns. (1.23) and (1.24) are valid for isotopes having zero nuclear angular momentum. In the case of odd isotopes for which the nonzero nuclear angular momentum produces hyperfine splitting of the atomic transitions, then the relation between the integrated OG signal and the density of the atoms can be written as [114],

$$N = \frac{8\pi[J]}{\lambda_0^2[J^{\prime}]AC[D[l}\int S(\nu)d\nu$$ (1 25)

Studies on uranium isotopes [114] indicates that the concentration and the measured OG signal at the line centre for different isotopes, for weak absorption, satisfies the relation

$$\frac{^{234}U}{^{238}U} = \frac{^{234}S_o}{^{238}S_o}$$ (1 26)

The Theoretical detection limit attainable for even isotopes is of the order of 10^6 atoms/cm^3 [114]. Isotope splitting of transitions in U, Mo, Ne etc have been reported by many researchers by employing OGS techniques [25,89,114-117]

1.10 HYPERFINE STRUCTURE ANALYSIS

Hyperfine structure of atom arises mainly as a result of the interaction of magnetic moment of a nucleus with the electric field produced by the valence electrons. Wave number T_F of the F component of an atomic level is given by the expression [118]

$$T_F = T_0 + A\frac{C}{2} + B \frac{[3C(C+1) -4I(I+1)J(J+1)]}{8I(2I+1)J(2J+1)} \qquad (1.27)$$

where

$$C = F(F+1) -I(I+1) -J(J+1) \qquad (1.28)$$

and

$$F = I+J, \ I+J-1, \ . \qquad |I-J| \qquad (1.29)$$

T_0 is the wave number of the level if there were no hyperfine interactions and I is nuclear spin. The splitting constants A and B due to magnetic and electric interactions are respectively given by

$$A = \frac{\mu_I H_J(0)}{IJ} \qquad (1.30)$$

and

$$B = eQV(0) \qquad (1.31)$$

where μ_I is the magnetic dipole moment of the nucleus, $H_J(0)$ is the magnetic field produced by the electrons at the nucleus, Q is the nuclear quadrapole moment and $V(0)$ is the average of the field gradient at the nucleus. According to the equation (1.27),

the magnetic and the electric interaction between the nucleus and the orbital electron splits a fine structure multiplet level of quantum number J into a multiplet of hyperfine structure levels. The number of levels is equal to the number of possible orientations of I and J ie. $2I+1$ if $J \geq I$ and $2J+1$ if $I \geq J$.

The small magnitude of the hyperfine splitting and the large Doppler width of the spectral lines makes accurate measurements very difficult. Development of high resolution laser spectroscopy have resulted into a variety of interesting and powerful technique to measure hyperfine splitting. For accurate measurement of hfs, the Doppler free methods have to be used. However, for heavier elements the Doppler broadening at room temperature is in the range of 600-900 MHz while the hyperfine splittings are in the range of a few GHz, so that Doppler limited techniques are sufficient [119].

The sensitivity of OGS technique is quite high as compared with other methods and it can be used for the study of most of the elements in the periodic table. In this method, atoms are sputtered from the cathode of a hollow cathode lamp, filled with an appropriate buffer gas at a suitable pressure. The sputtering technique eliminates the need to have a high temperature cell or a heat pipe oven and is readily applicable even for refractory metals. Another advantage is that highly excited state or singly ionized atoms can be produced in sufficient density so that spectroscopy in these species can be easily carried out without

the need of multistep excitation. Results of the hfs interactions using OGS applied to sputtered atoms in hollow cathode lamps for a large number of elements are available in the literature [116,119-123].

1.11 PHOTOEMISSION OPTOGALVANIC EFFECT

The change in impedance of a gas discharge can also be generated by injecting electrons into the discharge via photoelectric effect which is known as photoemission optogalvanic (POG) effect. In this non-resonant process the photon energy required is greater than the work function of the cathode material. The photoelectrons will further interact with the discharge species and the current in the circuit will be the resultant of the original plasma current and that produced by the interaction of photoelectrons with the plasma. The essential difference between the OG and POG effect is that the former is due to the resonant absorption of radiation where as the latter is by the non-resonant absorption processes. The POG effect has numerous practical applications in real time monitoring of metal or semiconductor surfaces [124], surface characterization [125], diagnostics of electrode surfaces in a discharge lamp [126], etc. More about the effect is described in chapter 7

Studies of the OG effect in ionized gases are at present largely developed in connection with various applications in physics and chemistry. Possibilities of this powerful

spectroscopic tool have opened wide range of research areas in for atomic and molecular spectroscopy; high resolution, Rydberg, multi photon spectroscopy, isotope and hyperfine structure analysis; diagnostics of electrical discharges, flames and plasmas; analytical chemistry; wavelength calibration; laser frequency stabilization etc.

REFERENCES

1 F H Penning, Physica 8 (1928) 137

2 S S Joshi, Current Sci. 8 (1939) 548, Proc. Ind. Acad. Sci. 21 (1945) 389

3 A Garscadden and P Bletzinger, J. Appl. Phys. 35 (1964) 3432

4 R B Green, R A Keller, G G Luther, P K Schenck and J C Travis Appl. Phys. Lett. 29 (1976) 727

5 J E M Goldsmith and J E Lawler, Contemp. Phys. 22 (1981) 235

6 E M van Veldhuizen, F J de Hoog and D C Schram, J. Appl. Phys. 56 (1984) 2047

7 E F Zalewski, R A Keller and E Engleman Jr. , J. Chem. Phys. 70 (1979) 1015

8 I I Popescu, Trends in quantum electronics (Ed. A M Bokhorove and I Ursu Springer Verlag, Berlin 1986) p391

9 A Von Engle, Ionized gases (Oxford University Press, London) 1965

10 A Von Engle, Electric Plasmas; their nature and uses (Tayler and Francis Ltd, London 1983)

11 C Brown, Basic data on plasma physics (Wiley, New York, 1959)

12 Yuri P Raizer, Gas discharge physics (Springer Verlag, Berlin 1991)

13 R A Keller and E F Zalewski, Appl. Opt. 19 (1980) 3301

14 M Hippler and J Pfab, Opt. Comm. 97 (1993) 347

15 C R Webster and R T Menzies, J.Chem.Phys. 78 (1983) 2121

16 D J Jackson, E Arimondo, J E Lawler and T W Hansch,
       Opt.Comm. 33 (1980) 51

17 P Camus, J.de Physique 44 (1983) C7

18 C Stanciulescu, R C Bobulescu, A Surmeian, D Popescu and
       I Popescu, Appl.Phys.Lett. 37 (1980) 888

19 T Suzuki, Opt.Comm. 38 (1981) 364

20 A E Bulyshev, N V Denisova and N G Preobrazhenskii,
       Opt.Spectrosc. 64 (1988) 590

21 P Labastie, F Biraben and E Giacobino, J.Phys.B At.Mol.Phys.
       15 (1982) 2595

22 D R Lyons, A L Schawlow and G Y Yan, Opt.Comm. 38 (1981) 35

23 T Suzuki and M Kakimoto, J.Mol.Spectrosc. 93 (1982) 423

24 T Susuki and T Kasuya, Appl.Phys.B 51 (1990) 374

25 D E Murnic, R B Robinson, D Stoneback, M J Colgan and F A
       Moscatelli, Appl.Phys.Lett. 54 (1989) 792

26 C C Tsai, T Lin, C Y Shieh, T C Yen and T T Shy, Appl.Opt. 30
       (1991) 3842

27 R Vasudev and R N Zare J.Chem.Phys. 76 (1982) 5267

28 H Sekiguchi and A Masuyama, J.Appl.Phys. 58 (1985) 154

29 C Hameau, J Wascat, D Dangoisse and P Glorieux, Opt.Comm. 49
       (1984) 423

30 J C Travis, P K Schenck, G C Turk and W G Mallard, Anal.Chem.
       51 (1979) 1516

31 J C Travis, Anallytical Laser Spectroscopy (Ed. S Martellucci
       and A N Chester, Plenum Press, New York 1985) p213

32 J C Travis, G C Turck and R B Green, Anal.Chem. 54 (1982)
       1006A

33 P K Schenck, W G Mallard, J C Travis and K C Smith
       J.Chem.Phys. 69 (1978) 5147

34 O Axner and S Sjostrom, Spectrochem. Acta 47B (1992) 245

35 C P Ausschnitt, G C Bjorklund and R R Freeman, Appl.Phys.Lett.
       33 (1978) 851

36 F Babin and J M Gagne, Appl. Phys. B 54 (1992) 35

37 E De Marinus and A Sasso, J. Appl. Phys. 63 (1988)649

38 N S Kopeika, T Karcher and C S Ih, Appl. Opt. 18 (1979) 3513

39 M P Scheer, F Vermeersch and F J de Hoog, J. Phys. D: Appl. Phys.
      26 (1993) 1700

40 E A Den Hartog, D A Doughty and J E Lawler, Phys. Rev. A 38
      (1988) 2471

41 D K Dougty and J E Lawler, Appl. Phys. Lett. 45 (1984) 611

42 D S King and P K Schenck, Laser Fucus (March 1978) 50

43 A I Fergueson, Phil. Trans. R. Soc. Lond. A 307 (1982) 645

44 W B Bridges, J. Opt. Soc. Am 68 (1978) 352

45 K Arnett, R Anderson and R Alexander, Am. J. Phys 49 (1981) 767

46 C J Lorenzen and K Niemax, Opt. Comm. 43 (1982) 26

47 P Hannaford and H W Series, J. Phys. B: At. Mol. Phys. 14 (1981)
      L661

48 P Hannaford and H W Series, Phys. Rev. Lett. 48 (1982) 1326

49 J N Dodd, J. Phys. B: At. Mol. Phys. 16 (1983) 2721

50 J E M Goldsmith, A J Ferguson, J E Lawler and A L Schawlow,
      Opt. Lett. 4 (1979) 230

51 J E M Goldsmith and A V Smith, Opt. Comm. 32 (1980) 403

52 R Shuker, A Ben-Amer and G Erez, Opt. Comm. 39 (1981) 51

53 R Shuker, A Ben-Amer and G Erez, Opt. Comm. 49 (1984) 263

54 H Wakata, S Saikan and M Kimura, Opt. Comm. 38 (1981) 271

55 A Wada, Y Adachi and C Hirose, Opt. Comm. 66 (1988) 203

56 M Duncan and R Devonshire, Chem. Phys. Lett 187 (1991) 545

57 B N Ganguly and A Garscadden, J. Appl. Phys. 57 (1985) 4856

58 D H Katayama, J M Cook, V E Bondybey and T A Miller,
      Chem. PHys. Lett. 62 (1979) 542

59 C Delsart, J C Keller and C Thomas, J. Phys. B: At. Mol. Phys. 14
      (1981)3355

60 K C Smith, B C Bentz, C G Bruhn and W W Harrison,
      J. Am. Chem. Soc. 101 (1979) 749

61 A Ben-Amer, R Shuker and G Erez, Appl. Phys. Lett. 38 (1981) 783

62 M A Khan, M A Gondal and M H Rais, J. Phys. B 57 (1993) 123

63 P Hannaford and H W Series, Opt. Comm. 41 (1982) 427

64 Lanlois E and J M Gagne, J. Opt. Soc. Am. B 4 (1987) 1222

65 A Wada, Y Adachi and C Hirose, J. Phys. Chem. 90 (1986) 6645

66 E David and J M Gagne, Appl. Opt. 29 (1990) 4489

67 M J Kavaya, R T Menzies and U P Oppenheim, IEEE J. Quantum
        Electron. 18 (1982) 19

68 J T Shy and T C Yen, Opt. Comm. 60 (1986) 306

69 L Ph. Roesch, Opt. Comm. 44 (1983) 259

70 A L S smith and S Moffatt, Opt. Comm. 30 (1979) 213

71 E F Zalewski, R A Keller and C T Apel, Appl. Opt. 20 (1981) 1584

72 G A Petrucci and J D Winefordner, Spectrochemica Acta 47B
        (1992) 437

73 D Feldman, Opt. Comm. 29 (1979) 67

74 R E Muenchausen, R D May and G W Hills, Opt. Comm. 48 (1984)
        317

75 M Van Roozendael, G W Hills and M Herman, Opt. Comm. 58 (1986)
        319

76 M H Begemann and R J Saykally, Opt. Comm. 40 (1982) 277

77 R C Carlson, L A Cross and T M Dunn, Chem. Phys. Lett. 113 (1985)
        515

78 C Hameau, E Arimondo, J Wascat and P Glorieux, Opt. Comm. 53
        (1985) 375

79 C T Rettner, C R Webster and R N Zare, J. Phys. Chem. 85 (1981)
        1105

80 I M Beterov and N V Fateyev, Opt. Comm. 40 (1982) 425

81 V Kumar, A K Rai and D K Rai, Pramana-J. Phys. 31 (1988) L421

82 A K Rai, S B Rai, S N Thakur and D K Rai, Chem. Phys. Lett. 138
        (1987) 215

83 C R Webster and I S McDermid, J. Chem. Phys. 78 (1983) 646

84 C Demuynck and J L Destombes, IEEE J Quatum Electron. 17 (1981)
        575

85 D A Haner, C R Webster, P H Flamant and I S Mcdermid, Chem.
        Phys. Lett. 96 (1983) 302

86 R Walkup, R W Dreyfus and Ph Avouris, Phys. Rev. Lett. 50 (1983)
1846

87 H Amemiya and T Suzuki, Jap. J. Appl. Phys. 29 (1990) L1712

88 K Singh, R D Cunha and V B Kartha, Opt. Comm. 79 (1990) 33

89 R A Keller, R Engleman Jr. and E F Zalewski, J. Opt. Soc Am. 69
(1979) 738

90 H A Bachor, P J Manson and R J Sandeman, Opt. Comm. 43 (1982)
337

91 D S King, P K Schenck, K C Smyth and J C Travis, Appl. Opt. 16
(1977) 2617

92 J R Nestor, Appl. Opt. 21 (1982) 4154

93 A Duckworth, R S Adrain and B A Tozer, Opt. Laser Tech. 24
(1992) 39

94 B R Reddy and P Venkateswarlu, Opt. Comm. 85 (1991) 491

95 C J Sansonetti and K H Weber, J. Opt. Soc. Am. B 1 (1984) 361

96 K Narayanan, G Ullas and S B Rai, Chem. Phys. Lett. 156 (1989) 55

97 B R Reddy, P Venkateswarlu and M C George, Opt. Comm. 75
(1987) 257

98 M C Su, S R Ortiz and D L Monts, Opt. Comm. 61 (1987) 257

99 R A Keller, R Engleman Jr. and B A Palmer, Appl. Opt. 19 (1980)
836

100 N J Dovichi, D S Moore and R A Keller, Appl. Opt. 21 (1982)
1468

101 F Babin, P Camus, J M Gagne, P Pillet and J Boulmer,
Opt. Lett. 12 (1987) 468

102 Y Oki, T Izuha, M Meada, C Honda, Y Hasegawa, H Futami,
J Izumi and K Matsuda, Jap. J. Appl. Phys. 30 (1991) L1744

103 Alan Corney, Atomic and laser spectroscopy (Oxford university
Press, Oxford, 1977)

104 K Naveedullah and A S Naqvi, Opt. Comm. 56 (1985) 117

105 T Masaki, Y Adachi and C Hirose, Appl. Spectrosco. 42 (1988)54

106 D K Doughty, E A Den Hartog and J E Lawler, Appl. Phys. Lett.
46 (1985) 352

107 M Hiramatsu, M Sakakibara, M Mushiga and T Goto,
    Meas. Sci. Technol. 2 (1991) 1017

108 A C G Mitchell and M W Zemansky, (University Press,
    Cambridge, 1961)

109 J E Lawler, A I Ferguson, J E M Goldsmith, D J Jackson and
    A L Schawlow, Phys. Rev. Lett. 42 (1979) 1046

110 N Beverini, M Galli, M Inguscio, F Strumia and G Bionducci,
    Opt. Comm. 43 (1982) 261

111 T W Hansch, D R Lyons, A L Schawlow, A Siegel, Z Y Wang and
    G Yan, Opt. Comm. 38 (1981) 47

112 C R Vidal, Opt. Lett. 5 (1980) 158

113 R Engleman Jr. and R A Keller, Opt. Lett. 5 (1980) 465

114 P Pianarosa, Y Demers and J M Gagne, J. Opt. Soc. Am. B 1 (1984)
    704

115 B M Suri, R Kapoor, G D Saksena and P R K Rao, Opt. Comm. 49
    (1984) 29

116 G N Rao, M N Reddy and R Singh, Phys. News (DEC 1988) 132

117 A Siegel, J E Lawler, B Couillaud and T W Hansch, Phys. Rev. A
    23 (1981) 2457

118 H Kopfermann and E E Schneider, Nuclear Moments (Academic
    Press, New York, 1958)

119 M N Reddy and G N Rao, Physica C 150 (1988) 457

120 R Singh, G N Rao and R K Thareja, Pramana-J. Phys. 38 (1992)
    363

121 R Singh, G N Rao and R K Thareja, J. Opt. Soc. Am. B 8 (1991) 12

122 G H Guthohrlein and H P Keller, J. Phys. B: At. Mol. Phys. 21
    (1988) 2353

123 M N Reddy, S A Ahmad and G N Rao, J. Opt. Soc. Am. B 9 (1992) 22

124 S W Downey, A Mitchell and R A Gottscho, J. Appl. Phys. 63
    (1988) 5280

125 G S Selwyn, B D Ai and J Singh, Appl. Phys. Lett. 52 (1988)
    1953

126 M B Schulman and D R Woodward, Appl. Phys. Lett. 55 (1989) 1618

THEORY OF OPTOGALVANIC EFFECT

2.1 GENERAL FEATURES OF A GAS DISCHARGE

Electrical discharge is an electrically energized matter in gaseous state. In general, it consists of three components; neutral atoms or molecules, charged particles (in the form of positive ions, negative ions and electrons) and photons permeating the plasma-filled space. The atoms or molecules can be either in their ground state or in excited states.

A distinct feature of the discharge is the presence of a bright luminous region extending all along the tube. General features of a glow discharge in which the distribution of glow intensity, potential, longitudinal field, electronic and ionic current densities, charge densities and space charge [1] with respect to distance from the cathode are shown in fig 2.1. If the inter electrode separation is sufficiently large, an electrically neutral plasma region with fairly weak field is formed between the cathode and the anode. This homogeneous electro neutral region is generally known as positive column. Sometimes positive column has a periodic layer structure called striations. The formation of striations is not inevitable or they may not be resolvable. In such cases positive column emits light uniformly up to the anode region. In contrast to the cathode layer, whose existence is vital for the glow discharge
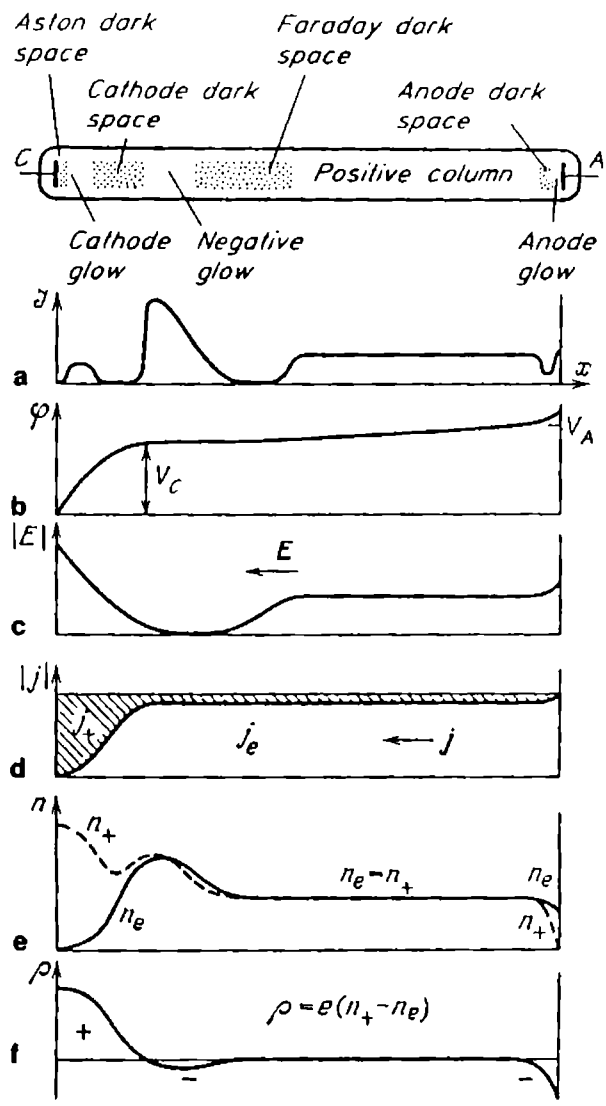
Fig 2.1   Glow discharge in a tube and the
distribution of a) glow intensity, b) potential φ,
c) longitudinal field E, d) electric and ionic
current densities j_e and j_+, e) charge densities
n_e and n_+ and f) space charge ρ

44

the positive column is not an essential part for a discharge. The discharge in each gas has a characteristic set of colours exhibiting its spectrum, and most of the properties being sensitive to specific conditions.

2.2 EXCITATION AND DECAY PROCESSES IN DISCHARGES

Ionization of atoms and molecules by electron-impact is the most prominent mechanism of charge generation in the bulk of a gas discharge. The rate of this process, with electron density n

$$\left(\frac{dn}{dt}\right)_i = \gamma_i n$$

(2.1)

is characterized by the ionization rate γ_i, which is the number of ionization events performed by an electron per second. If the temperature (T) of a gas discharge is substantially lower than that required for ionization indicated by the ionization potential(ε), then

$$\gamma_i = N \bar{v} C_i (\varepsilon + 2k_b T) exp\left[- \frac{\varepsilon}{k_b T}\right]$$

(2.2)

where $\bar{v} = (8k_b T/\pi m)^{1/2}$ is the average velocity, N is the number of atoms per unit volume and C_i is the ionization cross section. The atoms of a weakly ionized gas are mostly ionized from the ground state. If the gas is highly ionized, many excited atoms, molecules and ions may be involved and step wise ionization will be dominant. Atoms are first excited by electron impact and then

45

ionized by subsequent collisions. Long lived metastables and excited particles play an important role in this processes for which ionization cross sections are rather high.

Some of the important excitation and ionization processes are given below.

electron-impact excitation $A + e^- \longrightarrow A^* + e^-$

electron-impact ionization $A + e^- \longrightarrow A^+ + 2e^-$

electron-impact ionization of excited states $A^* + e^- \longrightarrow A^+ + 2e^-$

excited state-excited state collisions $A^* + A^* \longrightarrow A^+ + A + e^-$

penning ionization $A^* + B \longrightarrow A + B^+ + e^-$

charge transfer $A^+ + B \longrightarrow A + B^+$

photo ionization $A + h\nu \longrightarrow A^+ + e^-$

associative ionization $A^{**} + A \longrightarrow A_2^+ + e^-$
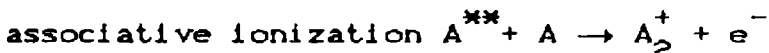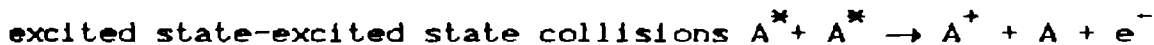
Here A,B are ground state atoms A^* is the excited or metastable state and A^+, B^+ are the positive ions.

Some of the important decay processes in the discharges are

1) Radiative and non-radiative decay

2) Recombination and dissociation by various collision effects (electron ion, ion-ion dissociation etc.)

3) Formation and the decay of negative ions (called attachment and detachment processes) and

4) diffusion losses (low pressure gas discharges are usually affected by electron losses due to the diffusion towards walls) These losses are irreversible and the electrons go into the metal or attach to the dielectric where they recombine with ions. The

mean electron life time with respect to the diffusional loss is $\tau_d = \Lambda^2/D$, where D is the diffusion loss coefficient and Λ is the characteristic diffusion length. For a cylinder of radius r and length ℓ, $(1/\Lambda)^2 = (2.4/r)^2 + (\pi/\ell)^2$ [1]

The steady state of an electrical discharge results from the stabilization of numerous excitation and de-excitation processes, involving various species of atoms molecules or ions present in the discharge. Then, the plasma is composed of free electrons and neutrals or ionized elements with energies spread over all the possible states. The density of the neutral particles is much higher than that of the charged particles and the plasma produced is known as weakly ionized or low temperature plasma. When a steady state condition is achieved, the population density is stationary and the plasma represents an internal constant impedance fixed by the experimental conditions. OG effect essentially represents the perturbation in the population distribution, and hence the impedance of the discharge, as a result of interaction between electromagnetic radiation and the species present in the discharge.

2.3 OG EFFECT

Illumination of a glow discharge with electromagnetic radiation perturbs the steady state of population distribution. In general the collisinal ionization rates from different levels are unequal, so that the ionization conditions in the discharge

are altered and another equilibrium corresponding to a different current-voltage point is created in presence of the electromagnetic radiation. An important feature of the OG effect is that the change in impedance, and hence the voltage across the discharge can be an increase or decrease so that both positive and negative OG signals are generally observed.

There are two significant mechanisms proposed for the origin of the laser induced optogalvanic (OG) effect in electrical gas discharges; viz.

1) laser excitation of atoms to higher electronic states leading to a modification in the ionization rate and hence the electrical impedance of the discharge and 2) Laser excitation that perturbs the equilibrium between the electron temperature and the atomic excitation temperature.

The basis of the increased electron temperature mechanism is that an equilibrium is established between thermal electrons and the atomic excitation, such that, the electron temperature and the electronic excitation temperature are equal - at least to the first approximation. This equilibrium come out as a result of many elastic and superelastic collisions between atoms and the electrons. The laser irradiation creates a small perturbation to this processes. The importance of electron temperature to generate laser induced impedance changes has been reported by many workers[2-5]. It is generally assumed that both mechanisms do occur simultaneously and the contribution of each mechanisms

depends on the levels involved in the transitions and the experimental conditions.

Spatial and temporal measurements using cw and pulsed lasers have played an important role in elucidating discharge mechanisms, energy storage or transfer pathways. In the case of cw irradiation, excited species can be continuously produced so that there is a steady state concentration of potential reactants. The dynamical features of the OG effect can be studied by using pulsed dye lasers. The decay time of the signal is typically of the order of a few micro seconds. When the pulsed lasers are employed, either the pulse widths or the excited state life time become key parameter, and if the laser pulse is shorter than the life time of the state that determines the time dependence of the potential reactants. In most cases, the upper level of the transition does not participate in the OG effect as the radiative life time of the upper level is too short to alter the ionization rate in the discharge. In principle, time resolved profile of OG signal under resonant pulsed laser excitation contains informations on high lying levels, long lived states, population inversion and on the dynamics of various reaction channels for ionization processes. Experimental and theoretical investigations on OG effect under pulsed laser excitation in a variety of discharges have been discussed by many workers[6-9].

The improved understanding of this effect in a variety of

discharges has made it an important tool for quantitative diagnostics of electrical discharges, flames and plasmas. Most of the theoretical models of this effect were developed only by considering a certain transitions in a particular type of discharge where the effect is produced and is based on the specific experimental conditions assumed to be existing. The difficulty in developing a more general model is due to a large number of parameters that characterize the discharge system. A simplified theory of optogalvanic effect based on the multiplication of electrons within the plasma has been reported by Erez et al [6]. The modeling reported by Lawler [10] in terms of the perturbed steady state rate equations, including the dynamic impedance to describe the OG effect in a He positive column discharge is in good agreement with the experimental results. This approach is especially useful in cases where many of the collision cross section are not known. Daughty et al [11] and Stewart et al [12] extended this approach to explain transitions in neon over a wide range of discharge conditions. The theory of Pepper[13], Meada et al [4] and Veleantinili et al [14] in terms of the electron temperature and the density variations have explained the observed sign changes and the magnitude of the signal in metal vapour-rare gas discharges. Considering a three level atom model interacting with two intense amplitude-modulated laser beams, Tewari et al [15] have reported the theory of the resonant optogalvanic effects in optical double

resonance spectroscopy. Experimental and theoretical investigation of OG effect in HgAr discharge [16] and the population monitoring in the B-X system of HgBr are also available in the literature [17].

2.4 GENERAL MODEL OF THE OG EFFECT

A general model, proposed by Erez et al[6] has been successfully applied by many researchers [8,9]. Using this model the relative magnitude, sign and temporal behavior of the OG signal and its dependence on current or pressure can be predicted qualitatively for both cw and pulsed laser excitation. Consider a dc discharge cell, in which an electron excites or ionizes some of the atoms on its way to the anode and there by generating more electrons. The positive ions travel towards the cathode and may undergo several processes including production of secondary electrons so that a large number of electrons are generated by the avalanche caused by the multiplication. If the multiplication factor, α is less than unity, current decays and if, it is greater than unity, current will increase. In an OG experiment, the laser beam interacts with the discharge species and in the steady state conditions,

$$d\alpha = \left[\frac{\partial \alpha}{\partial V}\right]_{N_i} \Delta V + \sum_i \left[\frac{\partial \alpha}{\partial N_i}\right]_{V, N_j, j \neq i} \Delta N_i = 0 \qquad (2.3)$$

where V is the voltage across the tube ΔV is magnitude of the

OG signal, N_i are the various atomic or ionic populations and ΔN_i are their deviations from the steady state. Thus from equation (2.3)

$$\Delta V = -\beta \sum_i a_i \ \Delta N_i \qquad\qquad (2.4)$$

$$\text{where } \beta = \left[\frac{\partial \alpha}{\partial V}\right]_{N_i}^{-1} \qquad\qquad (2.5)$$

$$\text{and } a_i = \left[\frac{\partial \alpha}{\partial N_i}\right]_{N_i, V} \qquad\qquad (2.6)$$

β is always positive since a voltage increase enhances the ionization probability. Similarly $a_i > 0$, for all i. In general, a_i increases with the energy of the state i ΔN_i obeys the dynamical equations,

$$\frac{d(\Delta N_i)}{dt} = \sum_j \gamma_{ji} \Delta N_j - \sum_j (N_i - N_j) \sigma_{ij} \ I_{ij} \qquad\qquad (2.7)$$

$\sigma_{ij}(=\sigma_{ji})$ are the optical cross section for the respective transitions and I_{ij} is the appropriate light intensity. Consider a two level system in which the absorption of a monochromatic laser beam at the resonance frequency corresponding to the transition 1 $\rightarrow$ 2, and since there are many levels j, they can be treated collectively, with a characteristic energy relaxation times T_1, which characterize the steady state after illumination.

We can write time dependence of ΔN_1 as

$$\frac{d(\Delta N_1)}{dt} = \frac{\Delta N_1}{T_1} - (N_1 - N_2)\sigma_{12} I_{12} \qquad (2.8)$$

$$\frac{d(\Delta N_2)}{dt} = \frac{\Delta N_2}{T_2} - (N_2 - N_1)\sigma_{21} I_{21} \qquad (2.9)$$

These equations can be used to explain the behavior of the OG signal ΔV for various modes of the laser illuminations.

FUNCTIONAL FORM OF THE OG SIGNAL

CASE I *CW LASER EXCITATION:*

In this case $\frac{d(\Delta N)}{dt} = 0$ so that

$$\Delta N_1 = -(N_1 - N_2) \sigma_{12} I_{12} T_1$$

and $\Delta N_2 = (N_1 - N_2) \sigma_{12} I_{12} T_2$

Thus $\Delta V = -\beta \sigma_{12} I_{12} (a_2 T_2 - a_1 T_1)(N_1 - N_2)$ \qquad (2.10)

Here 1 is the lower level $(N_1 > N_2$ and $a_2 > a_1)$. Hence ΔV is negative unless $a_1 T_1 > a_2 T_2$. OG signal is thus negative except for excitation from metastable levels, where the positive signal may be expected. Since the relaxation times of metastable levels are quite sensitive to changes in the plasma, a positive signal may change sign with increasing current [17] due to a decrease in relaxation time (T_1) caused by enhanced collision with electrons.

Moreover, in the small signal limit the amplitude of the OG signal will be proportional to (N_1-N_2) and the time profile of the ΔV is nearly same as that of the laser intensity.

CASE II *PULSED LASER EXCITATION:*

Consider the laser pulse width to be short as compared to the time scale in the processes with in the plasma. During the pulse, the only relevant dynamics are those connected with the illumination,

$$\frac{d(\Delta N_1)}{dt} = (N_2-N_1)\sigma_{12}I_{12} = -\frac{d(\Delta N_2)}{dt}$$

After the termination of the laser pulse

$$\frac{d(\Delta N_1)}{dt} = -\frac{\Delta N_1}{T_1} \qquad \frac{d(\Delta N_2)}{dt} = -\frac{\Delta N_2}{T_2}$$

Also, $-\Delta N_1(t=0) = \Delta N_2(t=0) = \sigma_{12}(N_1-N_2)\int I_{12}(t)\,dt = Q(N_1-N_2)$

Thus

$$\Delta V = -\beta\, Q(N_1-N_2)(a_2 exp[-t/T_2] - a_1 exp[-t/T_1]) \qquad\qquad (2.11)$$

The temporal behavior of the signal can be deduced from the equation (2.11) for ΔV The factor $\beta\, Q(N_1-N_2)$ is positive and does not affect the shape.

Erez et al [6] studied the OG signal in Argon and Neon at various pressure and current conditions and have found to be in agreement with this theory. Extension of this theory to model

the pulsed OG effect in neon by considering four relevant energy levels to investigate the transient effects such as fast relaxation of levels, population density and the population inversion has also been reported [7]. However application of this simplified theory will not explain the observed OG phenomena completely.

2.5 RATE EQUATION FORMALISM OF OG EFFECT IN NEON POSITIVE COLUMN DISCHARGE

A generalized model of the OG effect includes the interaction of photons with atomic system in a discharge perturbed by an external optical source such as laser. The interaction of photons with the atomic species in the plasma affects the population and increase or decrease in impedance of the discharge depends on the resultant redistribution of population.

The principal features of the OG effect can be described by using rate equations of the atomic system. Most of the works on the theory of OG effect is to formulate the rate equations that describes the dominant processes in a discharge medium and to calculate the laser induced perturbation by solving these equations. Description of the main features involved in resonant laser irradiation in a neon positive column discharge have been reported by Kane[19,20] and Daughty[11]. Due to the complex processes present in OG phenomenon involving a large number of

atoms in different states, these authors have assumed a simplified energy level diagram. However Sasso et al [21] have developed a more general model in which all the states are considered separately in spite of the previous works.

The lowest excited levels in neon are $1s_i$ ($i=2,3,4$ and 5) of the $2p^5 3s$ configuration (in Paschen's notations). The $1s_5$ and $1s_3$ are true metastable levels where as $1s_2$ and $1s_4$ are radiatively coupled to the ground state. The next excited state configurations are ten $2p_j$ levels which are all radiatively coupled to the $1s_i$ levels. In this model, the separate contribution of four $1s_i$ levels and the collisional mixing between the upper $2p_j$ levels with the neighboring levels were also included. The relevant energy level diagram of neon including the ground state, four $1s_i$, ten $2p_j$ ($i=2,3,4,5$, $j = 1$ to 10 in Paschen notation) levels and the continuum with their principal excitation and de-excitation mechanisms that contribute to OG signal production are shown in fig 2.2.

In a neon discharge, ion-electron pairs are produced by single step and the multistep processes. The most important multistep process involves the long lived, low lying metastable levels of Ne. The electron-impact excitation of the radiative $1s_4$ and $1s_2$ levels of neon are followed by the emission of VUV photons at 743.7 and 735.9 Å respectively. Along with single-step electron collision, two step and multistep collisions are the dominant ionization processes of neon atoms in the
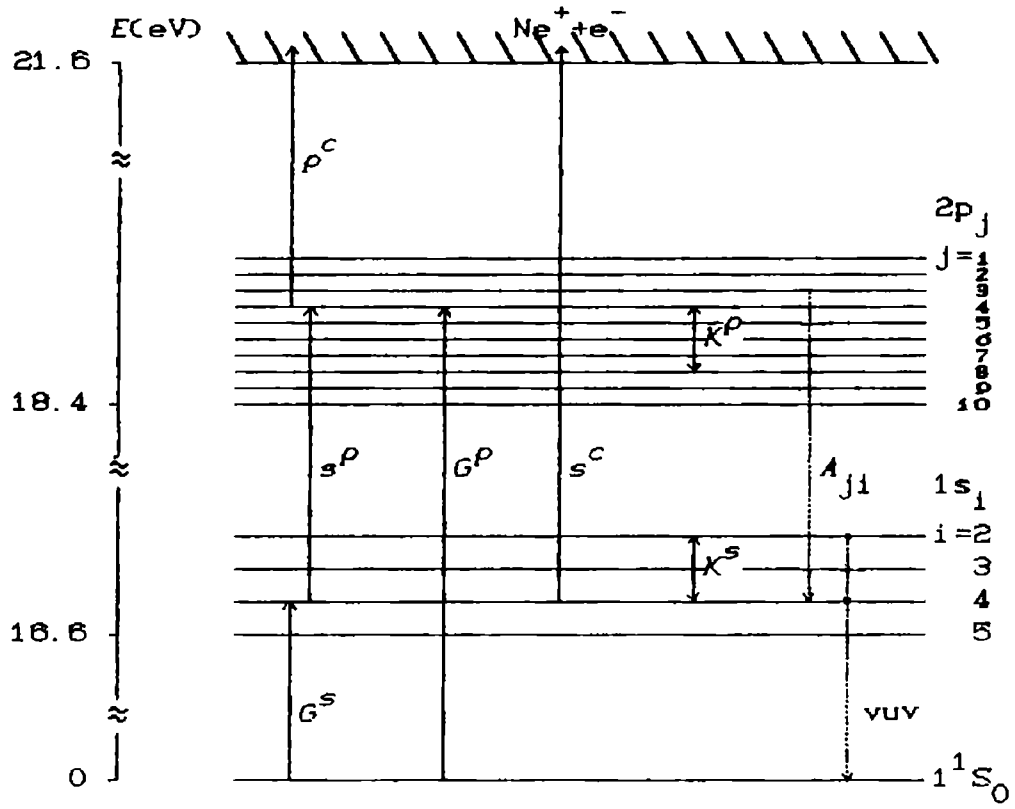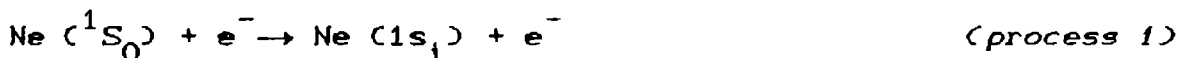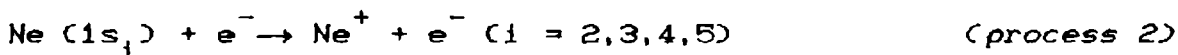
56

Fig 2.2 Simplified energy level diagram of neon including the $^1S_0$ ground state, the four $1s_i$, the ten $2p_j$ levels and the continuum [21].
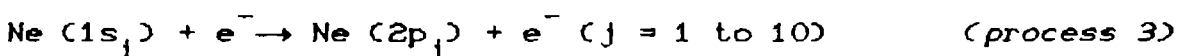
positive column. In two step ionization process the $1s_i$ levels are populated by the processes

$$Ne\ (^1S_0) + e^- \rightarrow Ne\ (1s_i) + e^- \qquad\qquad \textit{(process 1)}$$

and they are ionized through the collisions

$$Ne\ (1s_i) + e^- \rightarrow Ne^+ + e^- \quad (i = 2,3,4,5) \qquad \textit{(process 2)}$$

In the multistep processes the ionization occurs through the highly excited $2p_j$ levels.

$$Ne\ (1s_i) + e^- \rightarrow Ne\ (2p_j) + e^- \quad (j = 1\ to\ 10) \qquad \textit{(process 3)}$$

$$Ne\ (2p_j) + e^- \rightarrow Ne^+ + 2e^- \qquad\qquad \textit{(process 4)}$$

For both two step and multi-step ionization processes the role played by the metastable $1s_i$ of neon atoms is essential.

Irradiation of a positive column discharge by laser light that is resonant with the $1s_{3,5} \rightarrow 2p_j$ transitions results into depletion of the population of metastable $1s_{3,5}$ and reduces the rate of reaction (2) and (3). Correspondingly the electron density gets depleted so that the current in the circuit decreases. However when the laser excites a transition from radiative $1s_{2,4}$ levels, the metastable density is increased by the spontaneous decay from the upper $2p_j$ laser excited level down to the $1s_{5,3}$ levels. In this case, both the ionization probability and the magnitude of the discharge current are increased. This description does not take into other competitive effects that contribute to the OG phenomenon. At high current and at high laser intensity, where a large $2p_j$ population is produced, the ionization reaction (4) from the laser-excited

level can be more efficient than the reaction (2) from the laser depleted level. This mechanism produces an increase of current in the circuit.

Considering various prominent processes in the discharge, the rate equation for 1s levels are

$$\frac{dS_i}{dt} = G_i^s N_g n + \sum_{j=1}^{10} A_{ji} P_j + N_g \sum_{\substack{j=2 \\ j \neq i}}^{5} K_{ji}^s S_j - N_g S_i \sum_{\substack{j=2 \\ j \neq i}}^{5} K_{ij}^s - \left[s^P + s_i^c \right] S_i n$$

$$- TS_i \sum_{j=2}^{5} S_j - \omega_i S_i - \sigma F_L \left[S_m - \frac{g_m}{g_n} P_n \right] \delta(i=m)$$

$$i = 2,3,4,5 \qquad\qquad (2.12)$$

Here, S_m and P_n are the populations of the $1s_m$ and $2p_n$ levels perturbed by the laser.

The rate equations that describes the evolution of $2p_j$ populations are

$$\frac{dP_j}{dt} = n \sum_{i=2}^{5} s^P S_i + \frac{\alpha_r}{10} n^2 + G^P N_g n + N_g \sum_{\substack{l=1 \\ l \neq j}}^{10} K_{lj}^s P_l$$

$$+ \sigma F_L \left[S_m - \frac{g_m}{g_n} P_n \right] \delta(j=m) - N_g P_j \sum_{\substack{l=1 \\ l \neq j}}^{10} K_{j,l}^P - P_j \sum_{i=2}^{5} A_{ji} - P^c P_j n$$

$$j = 1, 2. \quad .10 \qquad\qquad (2.13)$$

and the rate equation for the electron density will be

59

$$\frac{dn}{dt} = n\left[\sum_{i=2}^{5} s_i^P S_i + \sum_{j=1}^{10} P^c P_j\right] + \alpha_T \upsilon_d n + \frac{T}{2}\sum_{j=2}^{5}\sum_{\substack{j'=2 \\ j \neq j'}}^{5} S_j\, S_{j'} + T\sum_{i \neq 2}^{5} s_i^2$$

$$- D_a\left(\frac{2.4}{r}\right)^2 n - \alpha_r n^2 \qquad\qquad (2.14)$$

Various rate constants used in the above equations are listed below.

S_i — $1s_i$ level population

P_j — $2p_j$ level population

G_j^* — rate coefficient for the metastble or radiative $1s_i$ level's population produced by the excitation of process (1)

N_g — ground state atom density

n — electron density

A_{ji} — radiative transition rate for $j \rightarrow i$ transition

K_{ij}^0 — rate constant for population transfer between $1s_i$ level produced by collision of ground state neon atoms for the transfer from i to the j level.

s_i^c — rate constant for collisions with electrons for the production of direct ionization (process 2)

s_i^P — rate constant for collision with electrons producing Ne $(2p_j)$ excited state atoms.

T — rate constant for collision between two excited Ne($1s_i$) atoms

α — the absorption cross section for laser excited transition

F_L — Photon flux of the laser beam

g_m, g_n — statistical weight of the laser excited $1s_m$ and $2p_n$ levels respectively

w_i — loss rate of $1s_i$ levels

α_r — dependence of the dissociative recombination coefficient of the electrons

α_T — Townsend coefficient

v_d — electron drift velocity

$D_a \left(\frac{2.4}{r}\right)^2$ — The ambipolar diffusion loss rate for electrons.

For the unperturbed discharge the electron density are consistent with the direct relationship to the discharge current

$$i = 2\pi h_0 e r^2 v_d n \qquad (2.15)$$

where e is the electron charge, r is the radius of the discharge plasma and $2h_0$ is the Tonks- Langmuir constant that relates the average and axial electron concentration. When the laser radiation is resonant with a $1s_i \rightarrow 2p_j$ neon transitions the overall $1s_i$ and $2p_j$ level populations and consequently the electron density are modified. The OG signal can be considered as a perturbation in the discharge current given by the relation

$$\Delta i = 2h_0 \pi e r^2 \left[v_d(n)_{laser\ on} + \frac{\partial v_d}{\partial E} \Delta E(n)_{laser\ on} - v_d(n)_{laser\ off} \right]$$

$$(2.16)$$

The modification ΔE in the electric field within the discharge is

derived by considering that in the experimental arrangement a constant voltage power supply feeds the discharge tube with length l and a ballast resistor Z in series with the discharge. Thus

$$l\Delta E + Z\Delta i = 0 \qquad\qquad (2.17)$$

and

$$\Delta i = \frac{2h_0 \pi r^2 v_d [(n)_{laser\ on} - (n)_{laser\ off}]}{1 + 2h_0 r^2 e(\partial v_d / \partial E)\frac{Z}{l}(n)_{laser\ on}} \qquad (2.18)$$

This relation represents general description of the OG effect in positive column of neon discharge. This model of OG effect is based on the steady state rate equations describing the population of four $1s_i$ levels, ten $2p_j$ levels and the electron density which confirms the key role played by the metastables, electron impact ionization and the collisional mixing between the excited states in the discharge.

Spatial dependence of the OG signal in the cathode region of a neon glow discharge shows that secondary electron emission from the cathode surface is dominant as compared to the direct current variation induced by the neon multistep ionization [22]. The bombardment of the cathode surface by metastables VUV photons and ions also plays dominant roles in sustaining the discharge and producing the OG signal. Mechanism of OG effect in the obstructed glow discharge [23], neon Townsend discharge [24], hollow cathode discharge[3] etc. are available in the literature.

The primary importance of OG effect is for spectroscopic applications which relays on the measurement of impedance change of a discharge as a function of wavelength corresponding to an absorption. For most of the spectroscopical applications, a detailed knowledge of the mechanism of laser matter interaction is not required. However, to increase the sensitivity of detection and for the diagnostics of gas discharge, plasma and flame a theoretical understanding of the process is very essential. Since the process involving laser plasma interaction is very complex, a general model of this effect is not practicable. Even though, from the sensitive nature of the detection and by considering prominent excitation and de-excitation processes in the discharge, quantitative evaluation of various physical quantities can be accurately made.

REFERENCES

1 Yuri P Raizer Gas discharge physics, (Springer-Verlag, Berlin 1991)

2 R A Keller, B E Warner, E F Zalewski, P Dyer, R Engleman Jr. and B A Palmaer, J. de Physique 44 (1983) c7-23

3 C Dreze, Y Demers and J M Gagne, J. Opt. Soc. Am 72 (1982) 912

4 M Meada, Y Nomiyama and Y Miyazoe, Opt. Comm. 39 (1981) 64

5 E F Zalewski, R A Keller and R Engleman Jr, J. Chem. Phys. 70 (1979) 1015

6 G Erez, S Lavi and E Miron, IEEE J. Quantum Electron. QE-15 (1979) 1328

7 A Ben Amer, G Erez and R shuker, J. Appl. Phys. 54 (1983) 3688

8 R Shuker, A Ben Amer and G Erez, Opt Comm. ,42 (1982) 29

9 B R Reddy and Venkateswarlu Opt. Comm. , 85 (1991) 491

10 J E Lawler, Phys. Rev. A 22 (1980) 1025

11 D K Doughty and J E Lawler, Phys. Rev. A 28 (1983) 773

12 R S Stewart, K W McKnight and K I Hamad, J. Phys. D:
        Appl. Phys. 23 832 (1990)

13 D M Pepper, IEEE J. Quantum Electron. QE-14 971 (1978)

14 H B Velentini, Opt. Comm. 53 313 (1985)

15 S P Tewari and M K Krishna, J. Phys. B: At. Mol. Opt. Phys.
        22 (1989) 1115

16 W H Richardson, L Maleki and E Garmire, Phys. Rev. A 36 (1987)
        5713

17 V Kumar, A K Rai, S N Thakur and D K Rai, Chem. Phys. Lett.
        142 (1987) 217

17 H A Bachor, P J Manson and R J Sandeman, Opt. Comm. 43 (1982)
        337

19 D M Kane, Opt. Comm. 47 (1983) 317

20 D M Kane, J. Appl. Phys. 56 (1984) 1267

21 A Sasso, M Ciocca and E Arimondo, J. Opt. Soc. Am. B 5 (1988)
        1484

22 E de Marinus and A Sasso, J. Appl. Phys. 63 (1988) 649

23 D K Doughty and J E Lawler, Appl. Phys. Lett. 42 (1983) 234

24 M P Scheer, F Vermeersch and F J de Hoog, J. Phys. D:
        Appl. Phys. 26 (1993) 1700

EXPERIMENTAL DETAILS OF OPTOGALVANIC SPECTROSCOPY

3.1 INTRODUCTION

Optogalvanic spectroscopy (OGS) is one of the versatile techniques for elucidating the energy levels of atoms and molecules. Besides the experimental simplicity, the high signal to noise ratio has made it a very useful method for spectroscopic investigation[1]. As described in chapter 2, OG signal arises when impedance of a low pressure gas discharge changes in response to the absorption of radiation by atomic or molecular species present in the discharge. The resulting increase or decrease in ionization gives a measurable change in voltage across the discharge tube [2]. This voltage change is observed in all kind of discharges; like hollow cathodes, positive column, arc, microwave discharges, as well as in flames and plasmas. Generally, electrical impedance variation is controlled by collisional ionizations, involving optically modified states as well as the transport properties within the plasma. The plasma itself acts as a sensitive non-optical detector of the perturbation of states produced by the absorption of photons.

In general, the experimental aspects for observing OG effect consists of 1) highly stable electrical discharge medium with suitable electrodes, 2) optical excitation of various species in the discharge medium using tunable pulsed or cw laser and

3) detection of the resulting OG signal   The interaction of radiation with the discharge will produce change in voltage which can be measured using appropriate detection systems.   The experimental simplicity along with the remarkable sensitivity is the most important aspect of the OGS that makes it a versatile tool for many spectroscopic applications.

The choice of discharge cells for dc optogalvanic studies depend on the nature of experimental requirements and samples. In general, a discharge cell consists of two electrodes filled with gas at a few torrs of pressure.   A stable dc voltage is applied to the electrodes in order to sustain the discharge.   In principle, most of the metals in the periodic table can be used as the electrode material and any of the atomic or molecular gas can be used as the gaseous medium.   Properties of both electrodes and gases have considerable influence in generating the OG effect.   The discharge environment provides a relatively high effective electron temperature which is potentially important factor in generating the OG signal.   The existence of the significant amount of excited state populations in the discharge enables one to observe transitions between excited states in this method.

Spatial and temporal measurements using both cw and pulsed lasers have played an important role in elucidating discharge mechanisms, energy storage and transfer pathways.   The dynamical features of the OG effect can be studied using pulsed dye lasers

[3,4]. Important features of the OG effect is its positive or negative characteristics and the spatial dependence (ie. the dependence of the OG signal on the position where the laser beam interacts within the plasma) due to space wise distribution of the species in the discharge medium. Hence for most of the applications, the configuration of the cell must be such that the interaction of laser beam with the plasma should result in a maximum voltage change.

The cells commonly used for OGS are hollow cathodes, positive column and diode type glow discharges [5]. Both sealed types and continuous flow gas cells are employed. In general, most of the commercially available hollow cathodes are sealed type, provided with cylindrical hollow cathode and a ring anode filled with a rare gas at a suitable pressure. Even though, experiment is possible using this cells only for a fixed gas pressure at which the cell is sealed, the discharge noise due to pressure variations is negligible and are particularly useful for high resolution spectroscopic studies. Continuous-flow type cells are best suited for the study of gases and for the study of the dynamics of interaction of laser beam with the discharge. In this case, even though, there are some problems due to the presence of noise induced by random pressure fluctuations, a wide range of pressure can be employed. The cells with de-mountable electrodes are convenient to change or clean the electrodes, so that the problems associated with de-gasing effects on the

electrode surfaces can be minimized and hence even reactive gases can be investigated. The design criteria and performance of de-mountable hollow cathodes for high resolution spectroscopy of refractory elements [6,7], wavelength calibration [8,9] etc. have been reported by various workers   Discharge cell for laser induced OGS with a fully adjustable electrode position suitable for the study of molecular gases using both cw and pulsed laser excitation has been developed [10,11]. Discharges with plane electrodes and positive column or other types with suitable electrode configuration having minimum noise are also commonly utilized for various spectroscopic and analytic measurements [12-18]. The OG effect has also been observed in commercially available indicator lamp [19], which is in general consist of two electrodes separated by a few mm of distance and filled with neon gas at a low pressure.

The commercial hollow cathode discharge (hcd) lamps are inexpensive and are readily available. However, their use is limited since the hollow cathode cup design is not appropriate and the buffer gas cannot be changed. See-through cylindrical hollow cathodes have to be used in order to get a well defined location of the probing laser beam. The design of a hollow cathode for high resolution spectroscopy must be optimized for a given element and transition.

Since the spectroscopic measurements are performed in a discharge environment, much care is necessary to reduce the

perturbations. The line broadening due to Doppler effects and collision between charged and neutral particles caused by the electric field are the causes of such perturbations. The major difficulties that arise during OG studies are due to the presence of random discharge noise as a result of fluctuations in current caused by the variations in gas pressure or applied voltage and the sputtering from the electrodes. The noise can be minimized by maintaining the gas pressure at a steady level and by using a highly regulated power supply. The noise due to sputtering from the cathode surface or arcing between the electrodes can be minimized by using clean and polished surfaces. Configuration of the discharge cell and the operating conditions will also considerably affect the discharge noise. The spatial dependence of the signal on discharge parameters can also lead to difficulties in signal detections. However, this is advantageous in certain plasma diagnostic studies.

3.2 DISCHARGE CELLS

3.2.1 Continuous gas flow positive column discharge cell

In certain cases, sealed cells are not suitable for prolonged use where de-gasing effects will upset the same experimental conditions. So it is better to use continuous gas flow de-mountable cells. This type of cells are best suited for molecular gases that react with electrode material in which case, the cell can be cleaned if necessary. A cell with adjustable

electrode position with respect to the probe laser beam would not only be advantageous in optimizing the generated signal, but would also allow the study of fundamental discharge mechanisms which produce signal of a particular polarity or its time evolution.

Fig 3.1 shows details of the de-mountable continuous gas flow discharge cell fabricated in our laboratory. It has been used for high resolution spectroscopic study of nitrogen gas. The electrodes, made up of stainless steel, are cylindrical in shape, placed at both ends of a Borosil glass tube having an inner diameter 6mm and length 5cm. Glass windows are provided at both ends on the other side of the cylindrical hollow electrodes. Nozzles made of stainless steel for gas inlet/outlet and for connecting pressure gauge are also provided. The couplings which are not in direct contact with the discharge are made with brass and all the joints are vacuum tightened by "O" rings. The inner surface of the electrodes are well polished and there is no sharp edges so that the arcing is eliminated. The separation between the electrodes is altered by choosing glass tube of appropriate length. A constant gas pressure is maintained by using needle and diaphragm valves which are provided at the inlet and the outlet sections of the cell

The cleaned cell is first evacuated with a vacuum pump and then flushed by passing experimental gas. A digital pirani gauge is used for monitoring pressure (Vacuum Techniques Model VT
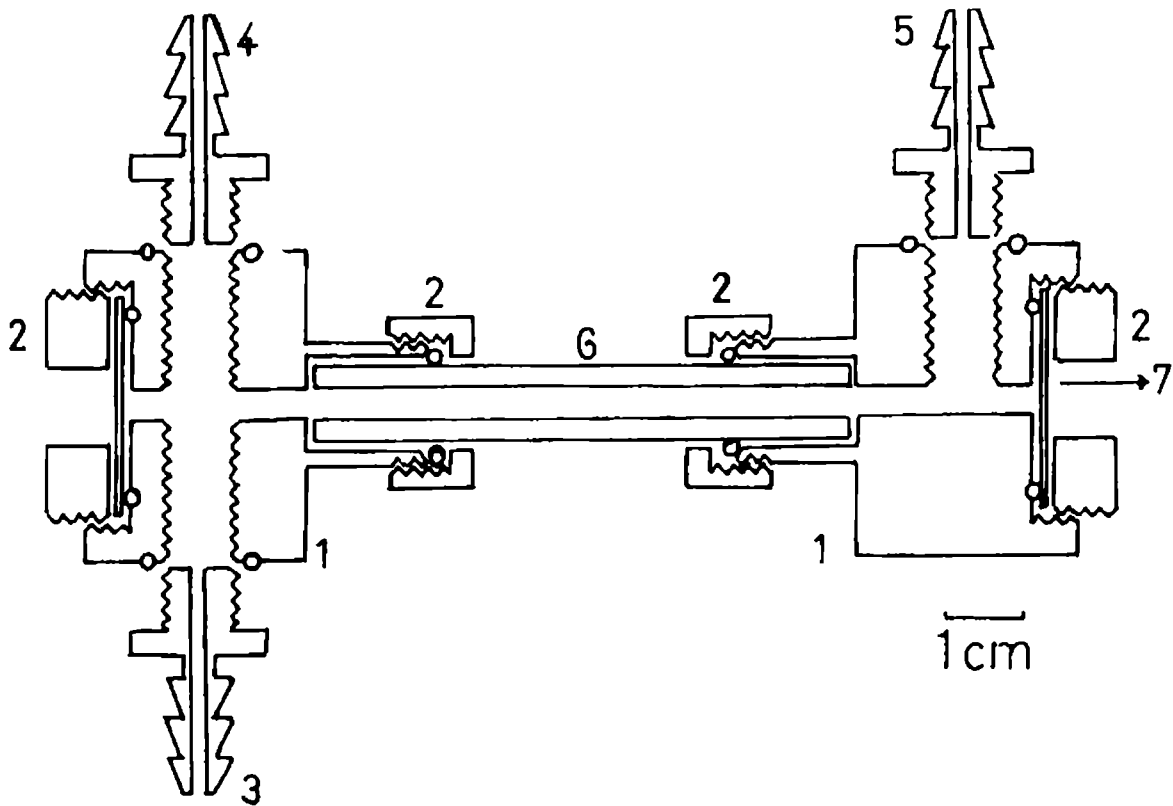
Fig 3.1 Continuous gas flow positive column discharge cell
1) stainless steel electrodes, 2) brass couplings, 3) gas
inlet, 4) pressure gauge, 5) gas outlet to pump, 6) glass
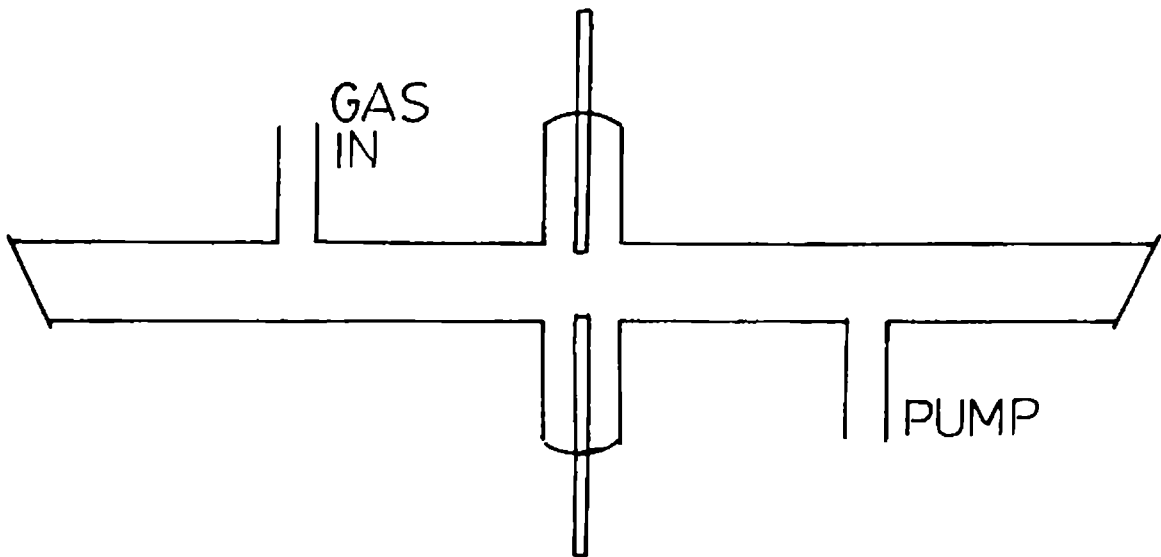tube and 7) glass window

Fig 3.2 Continuous gas flow glow discharge cell
with tungsten electrodes

DPC-11) The inlet and the outlet valves are adjusted to maintain a steady gas flow so that the gas pressure inside the cell remains constant. A well regulated dc high voltage is applied through a ballast resistance. The discharge is then run for a long time at a slightly higher current than the actual current at which the experiment is performed, so that the presence of impurities in the cell is minimized. The discharge noise is then monitored and the pressure of the gas is adjusted such that it is minimum. It is observed that for cell with electrode separation of 5 cm nitrogen gas at about 0.1 to 5 torr and the discharge current below 5mA, discharge noise is about 2mV.

3.2.2 Continuous gas flow discharge cell for photoemission study

For photoemission optogalvanic effect studies, we have used another continuous gas flow discharge cell with tungsten electrodes with an inter electrode separation of 1cm (fig 3.2). These electrodes are placed in a glass tube of inner diameter 1cm and length 15 cm with optical windows on both ends. Two side tubes of 0.6 cm inner diameter are also provided for the inlet of the experimental gas (N_2, NO_2 and Ar) and for outlet of the gas as shown in the fig 3.2.

3.2.3 Hollow cathode discharge lamp

Hollow cathode discharge (hcd) lamp consists of a ring shaped anode and a hollow cylindrical cathode filled with a buffer gas taken at about a few torrs [20] Most of the

72

commercially available light sources are of this type and they serve as a convenient source of radiation with narrow spectral lines for most of the solid elements in the periodic table. The wide range of applicability of such a source lies in the fact that the emitting metal atoms are produced not by thermal evaporation as in most other sources but by the process of ion bombardment. When a discharge is struck in a hcd lamp, positive ions of the carrier gas are accelerated towards the hollow cathode and bombard the inner surface with sufficient energy to eject atoms of the cathode material A certain number of metal atoms then diffuse away from the cathode surface into the central region of the bore where they may become excited by electron impact. The hcd is suitable not only as a source for emission lines of atoms but also as a reservoir of atoms for carrying out experiments on atomic resonance absorption and fluorescence.

In thermal methods, the temperature needed to produce plasma with a suitably high electron density varies greatly from element to element and in the case of refractory metals a temperature in the range of 2000K to 3000K are required. The absorption line, of any element in a vapor, produced by sputtering in a gas discharge are narrow and the broadening is predominantly by Doppler effect, with width closely corresponding to that at the ambient temperature of the gas (300K). Sputtering methods permit studies to be carried out in metastable atoms and ions, since they can be produced with sufficiently high density in the

discharge and the plasma sample to be investigated is more localized than that in other discharge configurations. The density remains very stable over a long period of time and can be adjusted in a well controlled manner by altering the discharge current.

In a low pressure gas discharge, the cathode is continuously bombarded by the energetic ions which have been accelerated in the high field of the cathode dark space and by fast neutral atoms produced by charge exchange. The bombarding ions and fast neutrals possess a wide range of kinetic energies. The species ejected during sputtering of a metastable target consists predominantly of ground state neutral atoms and a certain small fractions may also be in the form of excited atoms, ions and small clusters of atoms. The sputtered atoms rapidly lose their high kinetic energy of ejection by elastic collisions with rare gas atoms and become thermalized. Many of the atoms diffuse back to the cathode, while a small number of them escape towards the wall of the cells. As the sputtered atoms pass through the negative glow region some may get excited or ionized by electron impact or by collision with metastable atoms or ions present in the discharge. In this way, it is possible to accumulate neutral atoms, metastables and charged ions in a reasonably high density suitable for carrying out atomic absorption and fluorescence experiments.

Fig 3.3 shows the schematic diagram of the commercial hollow

74

cathode discharge lamp. The hcd we used are commercially available Ne/Nd and Ne/Mo lamps (Cathodean UK) which consist of a bulb having a glass window into which a hollow cylindrical cathode and a ring shaped anode have been inserted. The atmosphere within the bulb consists of neon gas at a pressure of 10 Torr. The construction has been designed to increase the negative glow there by achieving a high spectral intensity. With a suitable voltage applied between the electrodes of the hcd lamp, a glow discharge occurs. Electrons pass from the interior of the cathode to the surface of the hollow cathode region towards the anode. This causes ionization of the gas within the lamp through non-elastic collision with the gas atoms. Positive gas ions are accelerated by the electric field and collide with the cathode surface. The kinetic energy of the ion causes material to be sputtered from the cathode surface in the form of single atoms which are at the lowest energy or ground state. Simultaneously, electrons accelerated by the electric field towards the anode collide with ground state metallic atoms so that they are excited to higher energy states. The excited atoms de-excite to the lower state emitting spectral line characteristic to the element. In addition to this, radiation due to the transitions corresponding to the buffer gas atoms in the lamp are also obtained. Intensity, stability, noise and spectral profile etc. are strongly influenced by the nature of the gas, pressure, the element used for the cathode and its
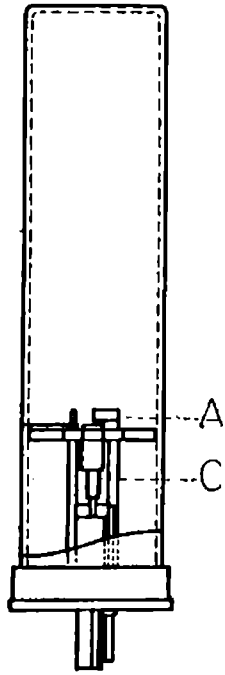
Fig 3.3
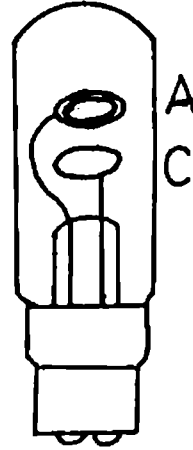Hollow cathode
discharge lamp
A-ring anode,
C-hollow cathode

Fig 3.4
Neon glow discharge
indicator lamp
A-ring anode,
C-disk cathode

surface state, the electrode construction, discharge current and the applied voltage.

3.2.4 Glow discharge indicator lamp

OG effect in commercially available indicator glow discharge lamp filled with neon and argon gases has been reported [19,21]. While the OG resonances of these discharges are of some spectroscopic interest, the primary motivation for the investigation lies in the use of these lamps as calibration devices for tunable dye lasers. These lamps, in general, consist of two electrodes very close to each other, filled with rare gases at a reduced pressure and usually operated at very low voltages showing the characteristic glow of the fill gas. We have used an indicator lamp having ring shaped anode and a disk cathode (of diameter 1cm) with an inter electrode separation of about 2.5 mm in which neon gas is filled as the discharge medium (fig 3.4).

3.2.5 High voltage power supply

One of the serious problem that limit the sensitivity in OG experiment is the presence of large discharge noise due to random fluctuations in the pressure or current. This can arise as a result of variations in gas pressure or the applied voltage, presence of impurities, sputtering from the cathode etc. Hence it is essential to maintain the discharge with a minimum noise using an extremely stable and ripple free voltage source. The voltage source used is a stable well regulated high voltage power

supply having very low ripple factor (2mV peak to peak), and the output controllable from 100V to 2800V up to a maximum current of 5mA (Thorn EMI PM28B) [22]   The unit is provided with a switch controlling the output in 200 V steps from 100 - 2300 V and a five turn potentiometer for fine voltage control giving range of 0 - 500V.

3.3 OPTICAL EXCITATION SYSTEMS

3.3.1 The cw laser source

I) Argon ion laser

The cw laser used is a 12 Watt argon ion laser (Spectra Physics 171) capable of providing discrete lines of wavelength 514.5, 496.5, 488, 476.5 nm etc or a multiline output containing all the lasing wavelengths [23].   The discrete lines can be obtained by tuning the prism which is placed in the cavity.   The output has a gaussian profile and has a frequency stability 60 MHz/$^{\circ}$C and a stability of $\pm$ 0.5% when used in the light control mode.   The laser is also provided with power meter to continuously monitor the output power

II) Single mode ring dye laser

For tunable laser output, which is very important for OGS, radiation from Spectra Physics 380D ring dye laser [24] pumped by above argon ion laser is used (fig 3.5).   The ring dye laser has a travelling wave, ring resonator with tunable high power, single frequency radiation.   The ring resonator consists of a pump

mirror, which focuses the pump laser beam into the dye jet and has four additional mirrors which constitute the cavity. In the cavity, the beam travels in a pattern of figure eight. A unidirectional device which introduces a directional anisotropy into cavity is used to select a particular propagation direction. The output power is concentrated in a nearly single frequency beam with a narrow line width. Because the emission gain curve of the lasing dye extends over several nanometers, simultaneous lasing can occur at a large number of cavity mode frequencies. Single frequency selection is achieved by using a birefringent filter with a fine etalon (FSR = 900 G HZ) and an electrically tunable single frequency etalon (FSR = 75 GHZ). The spectral range of these three selection elements are such that loss is introduced for all other cavity modes except the particular one where lasing is desired.

To scan the output frequency, the cavity modes with a spacing of about 200 MHz are tuned by changing the length of the laser resonator using two galvoplates. The index of refraction of the plate is higher than that of air, there by changing the effective cavity length. By scanning the inter etalon separation at the same rate as the dual galvoplates scan the cavity mode frequency, the output frequency of the single frequency dye laser can be scanned.

Stabilock system is used to achieve narrow line width and tc avoid mode hops during scanning. The dye laser frequency is
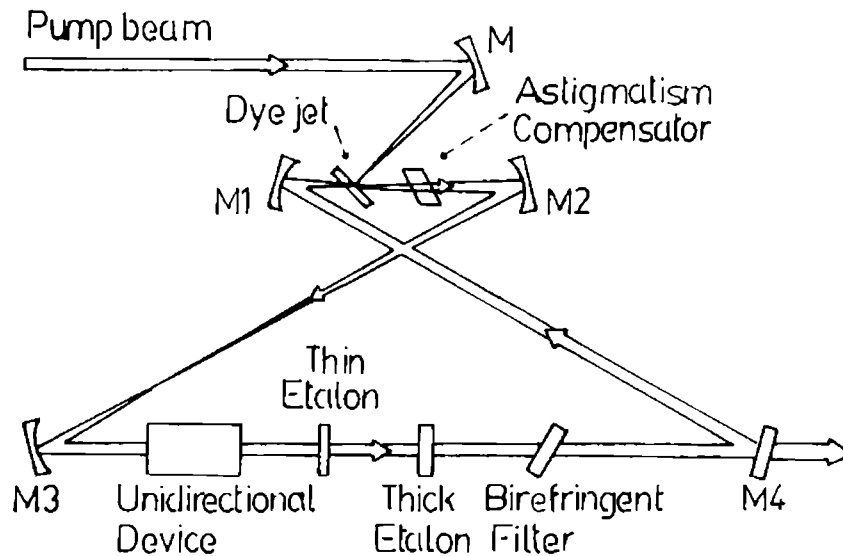
Fig 3.5 Block diagram of the ring dye laser

stabilized by locking it to a fringe of an external reference
interferrometer (FSR = 0.5 GHz). Frequency deviations are
detected by an error signal fed back to the PZT maintained mirror
M_2 and the galvoplates. When the laser try to hop the mode,
another 10 GHz interferometer circuitry takes up and returns the
laser frequency to the correct fringe and then the frequency
control hands over to the 0.5GHz interferometer.

The tunable range of this laser with Rh6G dye is from ~
570-600 nm having line width of a few MHz and the output

power/wavelength are extremely stable. The continuous tunability over a wide spectral region, narrow line width and the stability of this laser system has made it very suitable for high resolution spectroscopy.

3.3.2. The pulsed dye laser

Pulsed dye laser source used in the present studies is Quanta Ray PDL 2 dye laser system in which Rh 6G is taken as the lasing medium. It is pumped by the second harmonic output at 532nm of a Q-switched Nd:YAG laser (Quanta Ray DCR 11) [25,26]. This dye laser provide a continuous wavelength output from 540-580 nm peaking at ~564nm. Wavelength tuning is performed by a stepper motor attached to the grating element with a minimum speed of 0.04nm/step. The wavelength reading is obtained from the factory calibrated readout provided on the dye laser assembly.

3.4 DETECTION SYSTEMS

I) Wavemeter

The Burleigh WA-20 VI wave meter is used for the measurement of the wavelength or frequency of the cw laser   Using this instrument measurement with an accuracy of 0.01 cm^{-1} can be made. It consists of a scanning Michelson interferometer coupled to a fringe counting system. The wavelength or the frequency determination is made by counting number of fringes of the input laser beam simultaneously that of the reference He-Ne laser for

which the wavelength is accurately known [27]

In a typical experimental setup, a small portion of the laser to be measured is coupled into the wavemeter by a beam splitter. The alignment of the laser to the wavemeter is facilitated by the tracer He-Ne laser beam from inside of the wavemeter. Continuous automatic monitoring of the laser wavelength can be performed while the laser is tuned. If the indicating wavelength is incorrect, the display will not update and will show some error message on the wavemeter. Only a very low power (0.1mW) of the sample laser beam through the 2mm input aperture is required for accurate wavelength measurements and this can be tapped from the main beam with only negligible loss.

II) Spectrum analyzer

Spectrum analyzer (Spectra Physics 470) [28] is a mode degenerate spherical mirror Fabry-Perot interferometer used as a scanning spectrum analyzer for high resolution optical spectroscopy. Its operating range is 550-650nm and the separation between the adjacent transmission maxima (free spectral range) is 2 G Hz. A free spectral range will be scanned in the time required to change the mirror separation by 1/4 wavelength. Using Spectra Physics 476 scanning interferometer drive [29], the spectral dispersion, position of the displayed spectra, repetition rate and amplitude can be varied over a continuous range. Since the free spectral range of the spectrum analyzer is known to be 2 GHz, the repetitive feature of the

display can be used to calibrate the observed spectrum which is very important in high resolution spectroscopy.

III) **Laser energy meters**

The laser energy/power that is used in the experiments is measured by using laser power meters (Scientech model 362 and EG&G model 460-1A) [30,31]. Usually the measurements are taken in the main beam path before or after the experimental data has been recorded.

IV) **Monochromator**

A monochromator system essentially contains, an entrance slit, a collimator a dispersive element (in the present case a grating), a second mirror or lens to focus the dispersed light and an exit slit. The height and width of the slits are generally variable. Jarrell-Ash (Model No. 5) is a 0.5m grating monochromator having a maximum resolution of 0.02nm. This instrument provides smooth scanning motion in eight speeds ranging from 0.2nm/min to 50nm/min. The output from the Jarrell-Ash monochromator is detected by an EMI model 9683 KQB photo multiplier tube that can directly mounted at the exit face of the monchromator. Model 9683 is a head on type PMT having S-20 cathode and performs well in the 300-800nm region.

V) **Modulation**

Modulation of the incident laser beam is essential for the detection of the OG signal. For cw source, mechanical choppers EG&G 192 and Stanford SR 540 [32,33] are used to square wave

modulate the intensity of optical signals. The modulation frequency output is provided as reference to lock-in amplifier.

VI) Oscilloscope

To monitor the signal 20 MHz analog oscilloscopes (L&T, Aplab) and 200 MHz digital storage oscilloscope (Iwatsu DS-8621) are used. The digital storage oscilloscope has signal averaging and data storing facilities which can also be used to obtain hardcopy of signal shapes using plotter/printer [34]

VII) Lock-in amplifier

Lock-in amplifiers are used to detect and measure very small AC signals accurately. It uses a technique known as phase sensitive detection in which signal at frequencies other than the reference frequency are rejected and do not affect the measurement. Typically in an experiment, the sample is excited at a fixed frequency (this reference signal is a square wave from the mechanical chopper) and the lock-in detects the response from the experiment at the reference frequency. Only the signal at the reference frequency will be processed and a voltage proportional to the rms signal amplitude is obtained as the output. For the present measurements we have used two lock-in amplifiers, EG&G 5208 [35] which is computer interfaced with RS 232 and SR 850 [36] which has disk drive facility for data storage.

3.5 GENERAL EXPERIMENTAL SET UP

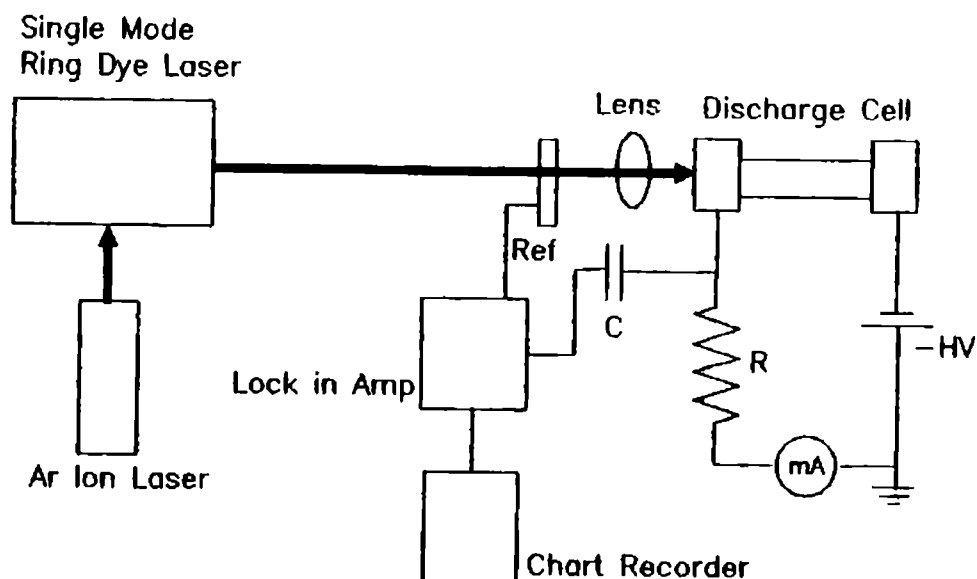General scheme of experimental setup (fig 3.6) consists of

Fig 3.6 Schematic experimental setup for
optogalvanic spectroscopy using cw laser

the measurement of galvanic effect produced in the electrical

discharge by the absorption of laser   Commercial hollow

cathodes, neon indicator lamp and home made continuous gas flow

cells with N_2 gas or tungsten electrodes/N_2, NO_2 and Ar gas

discharges are used as the discharge medium.   A current limiting

resistance and a milliammeter are connected in series with the

cell and the discharge is maintained by applying a stable dc

voltage.   The discharge condition is adjusted by varying gas

pressure, applied voltage etc. so as to get a minimum electrical

discharge noise.   Radiation from the pulsed dye laser or

intensity modulated cw laser is passed into the cell.   For OG

studies laser beam is passed without falling on the electrodes so

that the photoelectric emission is completely eliminated whili for photoemission optogalvanic measurements the beam is allowe to fall on the cathode surface. The AC signal is measured wit CRO, lock-in etc. by blocking the dc voltage with a capacitor Measurement were carried out by monitoring laser wavelength laser power, gas pressure, discharge current, spatial positioi where the laser beam is interacted within the discharge etc Specific details about the experimental aspects are discussed ii the subsequent chapters.

REFERENCES

1   R B Green, R A Keller, G G Luther, P K Schenck and J C Travis
        Appl. Phys. Lett. 29 (1976) 727

2   J E M Goldsmith and J E Lawler, Contemp. Phys. 22 (1981) 235

3   T Sakurai, N Goto and H Morisawa, Opt. Comm. 61 (1987) 266

4   Y Yasuda, N Sokabe and A Murai, Opt. Comm. 55 (1985) 319

5   I I Popescu, Trends in quantum electronics (Ed. A M Bokhorove
        and I Ursu, Springer Verlag, Berlin 1986) p391

6   B Barbieri, N Beverini, M Galli, M Inguscio and F Strumia, IL
        Nuovo Cimento D 4 (1984) 172

7   J E Lawler, A Siegel, B Couillaud and T W Hansch, J. Appl. Phys.
        52 (1981) 4375

8   N J Dovichi, D S Moore and R A Keller, Appl. Opt. 21 (1982) 14(

10 F Babin, P Camus, J M Gagne, P Pillet and J Boulmer,
        Opt. Lett. 12 (1987) 468

11 C R Wbster, Rev. Sci. Instrum. 54 (1983) 1454

12 C R Webster, R T Menzies, J. Chem. Phys. 78 (1983) 2121

13 S P Kravis and S C Haydon, J. Phys. D: Appl. Phys. 14 (1981) 151

14 N S Nogar and G L Keaton, Chem. Phys. Lett. 120 (1985) 327

15 H Maeda, Y Nomiyama and Y Miyazoe, Opt. Comm. 39 (1981) 64

16 E M van Veldhuizen, F J de Hoog and D C Schram, J. Appl. Phys.
    56 (194) 2047

17 De Marinus, A Sasso and E Arimondo, J. Appl. Phys. 63 (1988) 6

18 D M Kane, J. Appl. Phys. 56 (1984) 1267

19 G Y Yan, K I Fujii and A L Schalow, Opt. Lett. 15 (1990) 142

20 P Hannaford, Contemp. Phys. 24 (1983) 251

21 J R Nestor, Appl. Opt. 21 (1982) 4154

22 Thorn EMI model PM28B high voltage power supply instruction

23 Spectra Physics Model 171 Argon ion laser instruction manual

24 Spectra Physics Model 380D ring dye laser instruction manual

25 Quanta Ray model DCR 11 Nd:YAG Laser instruction manual

26 Quanta Ray Model PDL-2 pulsed dye laser instruction manual
    manual

27 Burleigh model WA-20 IV wavemeter instruction manual

28 Spectra Physics Model 470 spectrum analyzer instruction
    manual

29 Spectra Physics Model 476 scanning interferometer driver
    instruction manual

30 Scientech model 362 laser power meter instruction manual

31 EG&G model 460-1A laser power meter instruction manual

32 EG&G model 192 mechanical chopper instruction manual

33 Stanford Reseach systems model SR 540 mechanical chopper
    instruction manual

34 Iwatsu model DS-8621 digital storage oscilloscope
    instruction manual

35 EG&G model 5208 lock-in amplifier instruction manual

36 Stanford Reseach systems model SR 850 lock-in amplifier
    instruction manual

HIGH RESOLUTION OPTOGALVANIC SPECTRUM OF NITROGEN

4.1 INTRODUCTION

Spectroscopically one of the most studied diatomic system i molecular nitrogen. As the principal constituent of air nitrogen molecules play a significant role in the atmospheri phenomena. Nitrogen spectra are produced in a variety o laboratory discharges and afterglows. No satisfactory explanatio has yet been advanced to account for all the spectroscopi features of nitrogen molecule. It is only recently that man complexities regarding certain transitions of this molecule hav been deduced theoretically. The nature of energy level an electronic structure of N_2 molecule is now better known. Ther remains, however, numerous details to be worked out, especiall for the exited states. Experimental data on life time intensities and identification of various branches in th electronic spectra are yet to be obtained accurately. Variou: aspects of the spectrum of nitrogen molecule based on comprehensive review of the literature has been given by Lofthu: [1].

Deactivation of electronically excited molecules play a ver important role in the emission of light and the observation of band system in the emission spectrum depends on th characteristics of the discharge and the sources used foi

exciting the medium. Bands of the first and second positive system of N_2 molecule can be easily observed in the positive column of discharge tubes containing nitrogen gas at low pressure of a few torr.

There are large number of band systems attributed to the neutral nitrogen molecule. The energy level scheme (fig 4.1) and details of the main systems are summarized by Pearse [2] and Lofthus [1]. In each systems, there are several bands so that the rotational structure is too complex. The first positive system $(B^3\Pi_g - A^3\Sigma_u^+)$ is one of the most prominent band, that readily appears in most type of N_2 discharges, notably in the positive column and it consists of numerous multiple band heads extending from infrared to blue region. Because of its high intensity, this system was the first to be studied by early investigators and has been the subject of many detailed investigations. The rotational structure and the nature of the transitions involved in this band system was first reported by Naude [3] by analyzing (5,2) and (6,3) bands. In a very extensive and detailed work, Raux et al [4] measured the position of a large number of bands and have made an accurate rotational analysis of many of them using FTIR spectroscopic technique.

4.2 EXCITATION IN NITROGEN DISCHARGE

The excitation mechanisms in a molecular gas discharge is very complex, due to the presence of a large number of radiative,
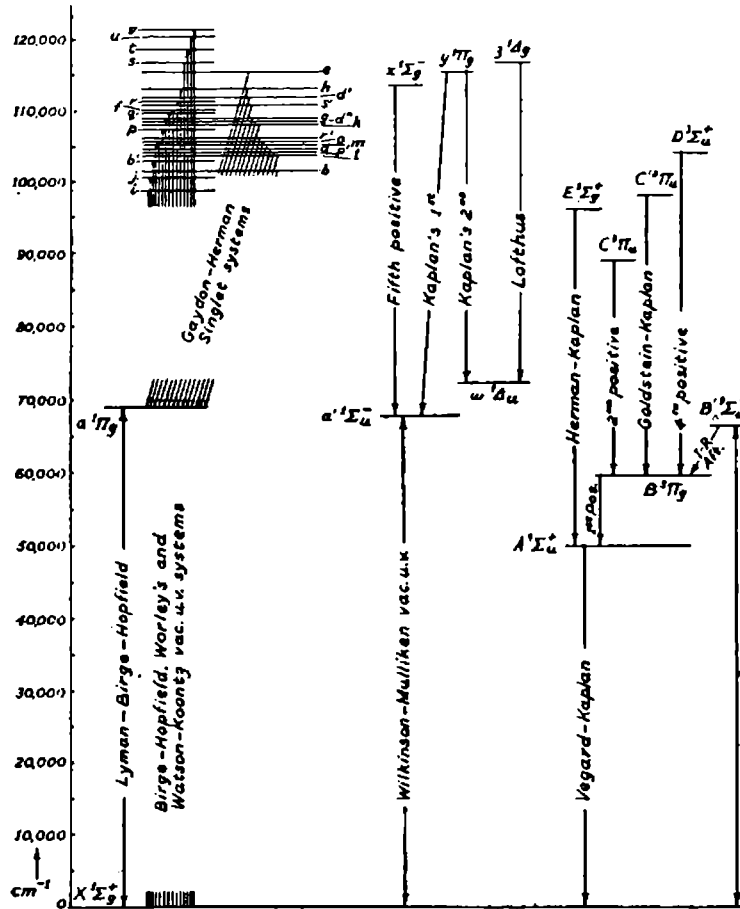
Fig 4.1 Energy level diagram of nitrogen molecule

non-radiative and collision processes involving electrons, neutral atoms, ions etc. In nitrogen, electron impact ionization of metastables (particularly the first excited level which is a metastable state ($A^3\Sigma_u^+$) whose life time is about two milli seconds) plays a very important role in maintaining the discharge. The metastable particles are created and destroyed in the discharge in a variety of collisions and the principal processes in the molecular nitrogen discharge are due to the interactions involving electrons. These are 1) Direct excitation from the ground state, 2) ionization from the ground state or excited states and 3) de-excitation of particles. Both single step and multistep collisions are involved in these processes.

The importance of a particular mechanism depends on the corresponding cross section and on the energy distribution function of electrons in the discharge. The number of transitions from state i into state j that occurs per unit volume per unit time can be written as,

$$\left\{\frac{dN_i}{dt}\right\}_{i \to j} = nN_i \langle \sigma_{ij} v \rangle \qquad (4.1)$$

$$= nN_i \int \sigma_{ij} \, f \, d^3v \qquad (4.2)$$

where n and N are the density of the electrons and atoms respectively, σ_{ij} is the cross section for this transition and f is the distribution function normalized to unity. The effectiveness of such interaction is measured by the quantity $\langle \sigma_{ij} v \rangle$, usually called the rate coefficient. The electron

distribution function may often be considered to be Maxwellian.
For most of the molecular gas discharges the effects of
excitation from the vibrational and rotational levels of
molecules by slow electrons must also be taken into account ir
order to understand the exact electron distribution. Other
processes like collision between heavy particles, de-excitatior
from various levels due to both radiative and non-radiative decay
etc. are also important in maintaining the discharge. More
details of these processes have been discussed in the literature
[5].

4.3 SPECTROSCOPY OF DIATOMIC MOLECULE

4.3.1 Band structure

Spectral details and analysis of the spectra of diatomic
molecules are described in many text books on spectroscopy [6]
This section presents an outline of the spectra of a diatomic
molecule. The total energy of a diatomic molecule is the sum of
three components, viz electronic, vibrational and rotational
energy and is given by (in cm^{-1}) [6]

$$T = T_e + G(v) + F(J) \hspace{3cm} (4.3)$$

The vibrational (G) and rotational (F) term values of the
molecule in different electronic states are given by

$$G = \omega_e(v+1) - \omega_e x_e(v+1/2)^2 + \hspace{2cm} (4.4)$$

and

$$F = B_v J(J+1) - D_v J^2 (J+1)^2 +$$

(4.5)

where ω_e and $\omega_e x_e$ are vibrational constants, B_v and D_v are rotational constants v is the vibrational quantum number and J is the rotational quantum number. The wave number of a spectral line corresponding to a transition between two electronic states is given by

$$\nu = T' - T''$$

$$= (T'_e - T''_e) + (G' - G'') + (F' - F'')$$

(4.6)

where single-primed letters refer to the upper state and the double-primed letters refer to the lower state. For a rotationless state $(F' = F'' = 0)$ the transition between different vibrational levels of the two participating electronic state is given by

$$\nu = \nu_e + [\omega'_e(v+1/2) - \omega'_e x'_e(v+1/2)^2 \quad]$$

$$- [\omega''_e(v''+1/2) + \omega''_e x''_e(v''+1/2)^2 \quad]$$

(4.7)

The rotational structure of a vibrational band in the electronic spectrum is given by

$$\nu = \nu_0 + F'(J') - F''(J'')$$

(4.8)

Here for a specific vibrational transition $\nu_0 = \nu_e + \nu_v$ is called

93

the band origin, $F'(J')$ and $F''(J'')$ are the rotational terms o
the upper and lower state respectively.

The selection rule for J is $\Delta J = J'-J'' = -1$, 0, or
corresponding to P, Q and R branches respectively. Rotationa
lines in these branches are given by

$$P(J) = \nu_0 + F'_\nu(J-1) - F''_\nu(J)$$

$$Q(J) = \nu_0 + F'_\nu(J) - F''_\nu(J) \qquad (4.9)$$

$$R(J) = \nu_0 + J'_\nu(J+1) - F''_\nu(J)$$

Graphical representation of these branches (ie J verses ν) i;
called Fortrat diagram, and can be seen that for most cases owin
to quadratic dependence of J, the branches forms a band head.

4.3.2 Combination relations

Combination relations or combination differences ar
commonly used to evaluate the rotational constants from th
observed rotational lines. This procedure yields more accurat
rotational constants for electronic bands that could be evaluate
by comparing the empirical formula or by fitting a polynomial of
J to the observed band lines.

Combination differences $\Delta_2 F'_\nu(J)$ and $\Delta_2 F''_\nu(J)$ for upper an
lower states respectively can be obtained from P and R branche:
as

$$R(J) - P(J) = F'_\nu(J+1) - F'_\nu(J-1) = \Delta_2 F'_\nu(J) \qquad (4.10)$$

and

$$R(J - 1) - P(J+1) = F''_\upsilon(J+1) - F''_\upsilon(J-1) = \Delta_2 F''_\upsilon(J) \qquad (4.11)$$

substituting for F_υ from equations (4.5) and (4.9) in these expressions we get

$$\Delta_2 F_\upsilon(J) = (4B_\upsilon - 6D_\upsilon)(J+1/2) - 8D_\upsilon(J+1/2)^3 \qquad (4.12)$$

Note that $\Delta_2 F(J)$ corresponds to separation between J^{th} and $(J+2)^{th}$ rotational levels. Using Q branch one can get following combination relations,

$$R(J) - Q(J) = Q(J+1) - P(J+1) = F'_\upsilon(J+1) - F'_\upsilon(J)$$
$$= \Delta_1 F'_\upsilon(J) \qquad (4.13)$$

$$R(J) - Q(J+1) = Q(J) - P(J+1) = F''_\upsilon(J+1) - F''_\upsilon(J)$$
$$= \Delta_1 F''_\upsilon(J) \qquad (4.14)$$

Here $\Delta_1 F(J)$ is the separation of successive rotational levels. Above combination relations may be directly obtained from the energy level diagram. The agreement of the observed combination differences in the same class provides an excellent check on the correctness of the analysis of a band. Details of the analysis of the bands using combination differences and the evaluation of the rotational constants are given by Herzberg [6].

4.3.3 Molecular quantum numbers

Spectra of each molecule exhibit numerous band systems

corresponding to transition between various molecular states. For a given value of the orbital angular momentum L, the quantum number Λ, which is the component of the electronic orbital angular momentum along the molecular axis can take values

$$\Lambda = 0,1. \quad .L \qquad (4.16)$$

Thus in the molecule for each value of L there are $L+1$ distinct states with different energy. Corresponding to $\Lambda = 0,1,2,3.$ etc. the molecular state are designated as $\Sigma, \Pi, \Delta, \Phi$ etc. respectively. The precession of the orbital angular momentum L can take place about the internuclear axis with constant component $M_L h$, where $M_L = L, L-1,.. \quad -L.$ Π, Δ, Φ states are doubly degenerate since M_L can have two values $+\Lambda$ and $-\Lambda$; Σ state are non degenerate.

The spin of the individual electron form the resultant S. The corresponding quantum number S being integral or half integral according to the total number of electrons in the molecule is even or odd. The precession of S about the field direction is given by

$$\Sigma = S, S-1.. \quad -S \qquad (4.17)$$

The total angular momentum about the internuclear axis is obtained by adding Λ and Σ ie.

$$\Omega = |\Lambda + \Sigma|$$ (4.18)

If Λ is not equal to zero, there are $2S+1$ different values of $\Lambda + \Sigma$ for a given value of Λ. Thus an electronic term (T_e) with a given $\Lambda \neq 0$ split into a multiplet term given by

$$T_e = T_o + A\Lambda\Sigma$$ (4.19)

where T_o is the term value in the absence of $\Lambda - \Sigma$ interaction and A is called the coupling constant which is a measure of the strength of such interaction.

4.3.4 Selection rules

The quantum numbers and the symmetry properties of various levels of a molecule affect the spectra through the selection rules that hold for them. The selection rule for the quantum number J of the total angular momentum is

$\Delta J = 0, \pm 1$

while symmetry selection rules are

$+ \leftrightarrow -, \; + \neq +, \; - \neq -$

ie. positive term combine only with negative and vice versa and for identical nuclei symmetric terms combine only with symmetric and anti-symmetric only with anti-symmetric. ie.,

$s \leftrightarrow s, \; a \leftrightarrow a, \; s \neq a$

In the case of a molecule with nuclei of equal charge the selection rule that even electronic states combine only with odd

ie.

$$g \leftrightarrow u, g \neq g, u \neq u$$

For the Hunds case (a) and (b) the selection rule for Λ is that $\Delta\Lambda = 0, \pm1$ and that for the resultant spin $\Delta S = 0$. More details about the molecular quantum numbers and their selection rules are extensively described by Herzberg [6]

4.4 $B^3\Pi_g - A^3\Sigma_u^+$ TRANSITION IN NITROGEN MOLECULE

The first positive system of nitrogen molecule corresponds to $B^3\Pi_g - A^3\Sigma_u^+$ transition and consists of numerous multiple headed bands degraded to shorter wavelength extending from 478 to 2531 nm. Spectral details of various bands of this system have been investigated by many workers [1-4] Bands in this system consist of three subsystems namely $^3\Pi_0(F_1) - A^3\Sigma_u^+$, $^3\Pi_1(F_2) - A^3\Sigma_u^+$ and $^3\Pi_2(F_2) - A^3\Sigma_u^+$. These transitions composed of 27 branches of which each sub-band has nine branches (three main and six satellites) [6].

For lower J values the $^3\Pi$ state is of Hund's case (a) and goes to case (b) for higher J values. In the case (a), $^3\Pi$ falls into three substates $^3\Pi_2$, $^3\Pi_1$ and $^3\Pi_0$ corresponding to $\Omega = |\Lambda+\Sigma|$ = 2,1 and 0 respectively. $^3\Pi_0$, $^3\Pi_1$ and $^3\Pi_2$ corresponds to F_1, F_2 and F_3 components of $^3\Pi$ state. The minimum values of J in these three substates are respectively 2, 1 and 0, and each level is subjected to Λ-doubling. For $^3\Pi_2$ state Λ doubling is very small, but increases in proportion to $J^2(J+1)^2$ while $^3\Pi_1$, it is not so
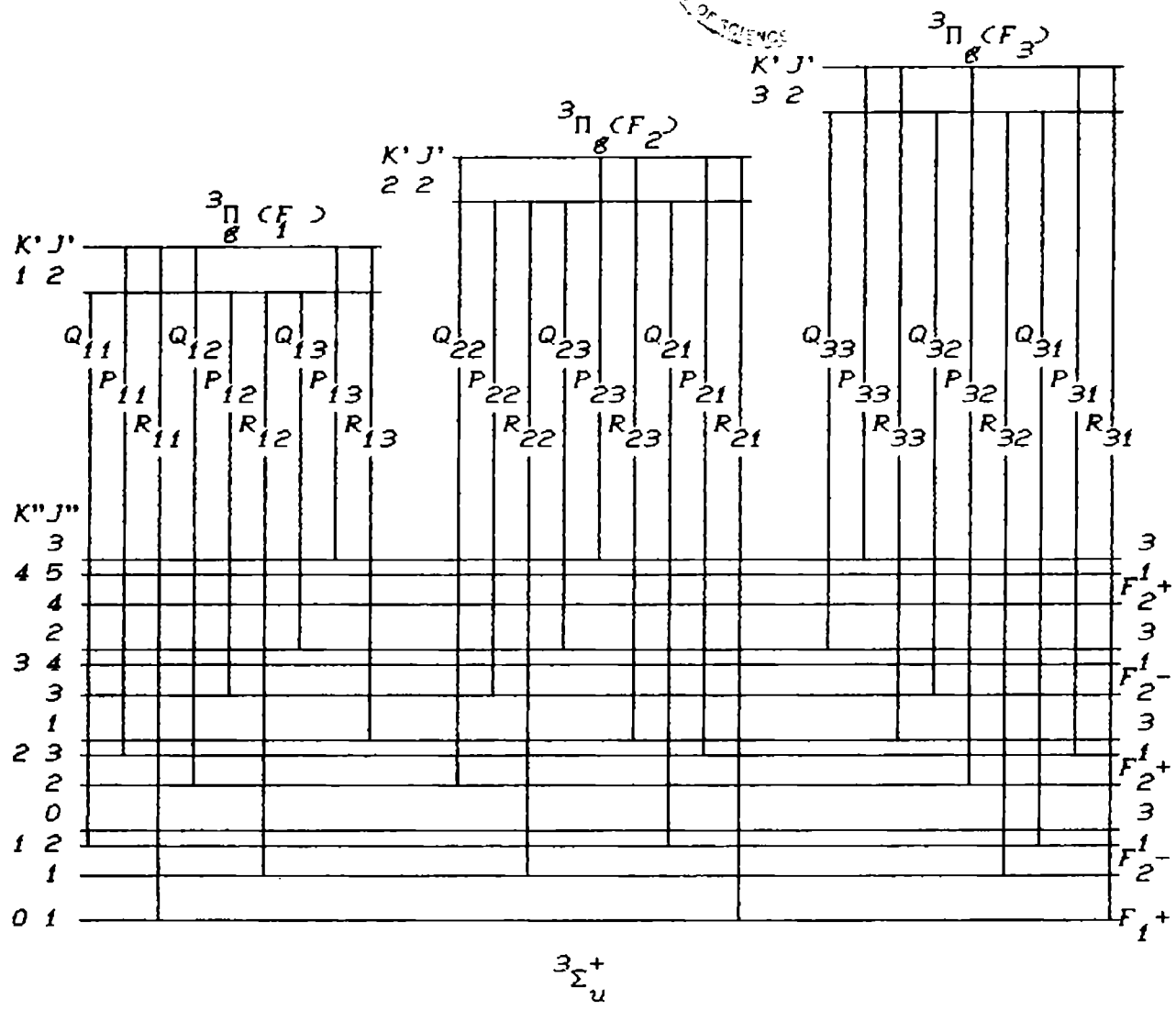
Fig 5.2 Scheme of the $B^3\Pi_g - A^3\Sigma_u^+$ transition of the N_2 molecule

small and increases with $J(J+1)$ and for $^3\Pi_0$ Λ-doubling is maximum, but is found to be approximately independent of J [6]. These differences are a convenient criterion of whether a state is normal or inverted; if it is normal $^3\Pi_2$ is above $^3\Pi_1$ and $^3\Pi_1$ above $^3\Pi_0$ and vice versa. From the Λ-type doubling it was confirmed that $^3\Pi$ state is normal. The rotational levels in $^3\Sigma$ state have three components viz. F_1, F_2 and F_3 corresponding to $J=K+1$, K and $K-1$ respectively, where K is the rotational quantum number defined in Hunds case (a) and the spin S being 1 Energy level diagram of the $B^3\Pi_g - A^3\Sigma_u^+$ band [7] is shown in the fig 4.2.

4.5 OPTOGALVANIC STUDY IN N_2 DISCHARGE

OG effect has proved to be a very effective tool for the study of energy levels and the mechanism of excitation in molecules [8,9]. Application of OGS to N_2 molecule was first reported by recording the vibrational spectra of the first positive system $(B^3\Pi_g - A^3\Sigma_u^+)$ system in the 570-610 nm spectral region [10]. Even though the spectrum was noisy, most of the vibrational bands were well developed and both positive and negative signals were generated. At low pressures (below one torr) and at high discharge voltages (above 600V), the first positive system completely disappears and the Ledbetter $(c^1\Pi_u - ^1\Sigma_g^+)$ system was observed. Ullas et al [11] have also studied the emission as well as cw and pulsed laser excited OG spectrum in a

slightly wider spectral region from 540-615nm in a hollow cathc discharge.

State selective double resonance OGS has also been report [12] in which (16,0) and (17,0) band of the $b'^1\Sigma_u^+ - a'^1\Sigma_g^+$ syst were identified by pumping from (0,0) band of the $c_4'^1\pi_u - a''^1$ system in N_2. This new method is particularly suitable identify dense spectra originating from transitions betwe excited states in radiating plasmas where the existing meth have only a limited sensitivity because of the perturbi spontaneous emission. Optogalvanic detection of rotational lir in (0,0) band of the $X^2\Sigma_g^+ - B^2\Sigma_u^+$ transition of molecul nitrogen ions (N_2^+) [13], pressure broadening and shift thallium $6^2P_{1/2} - 8^2P_{1/2,3/2}$ transition by N_2 perturbing gas [1 etc. have also been reported.

The use of rf discharge to detect Rydberg band $c_5'^1\Sigma_u^+ - a''^1$ of the N_2 molecule was first reported by Suzuki [15], and th further extended this method to investigate the well resolv rotational spectra of Ledbetter and Rydberg bands by using hi resolution spectroscopic methods [16] Laser OG effect molecules will give strong signals corresponding to electroni vibrational or rotational transitions. With a single mode las and by using high resolution spectroscopic methods such as IMOG OGDR etc. well resolved spectra of the molecules with resolution corresponding to the line width of the laser can achieved. The present chapter deals with the recording a

analysis of the OG spectrum of N_2 molecule carried out in our laboratory.

4.5.1 EXPERIMENTAL DETAILS

Since the spectral structure of molecule is complex having very dense and weak spectral lines in the OG spectrum, it is essential to operate the discharge at a low electrical noise level so as to get noise free OG spectrum. The experimental setup employed to record the OG spectrum is shown in the fig 4.3. A positive column discharge was maintained in a home made cell (fig 3.1) having stainless steel electrodes fixed at both ends of a glass tube provided with windows. The separation between the electrodes was about 5 cm and the inner diameter of the tube was about 6 mm. The cell was first cleaned and then evacuated by using a vacuum pump. Nitrogen gas is then continuously flowed through a needle valve and maintained a constant pressure by adjusting the valves provided at inlet and pumping side of the discharge cell. The discharge is produced by applying a steady dc voltage from a highly regulated power supply (Thorn EMI PM 28 B) across the electrodes. A ballast resistance of 60KΩ to limit the discharge current and a milli ammeter are connected in series with the cell. The gas pressure and the current are so adjusted to get a minimum noise level (~2 mV). The discharge noise is considerably minimized by running the discharge at high current for a long time. A capacitor (0.1μF) blocks the dc voltage and
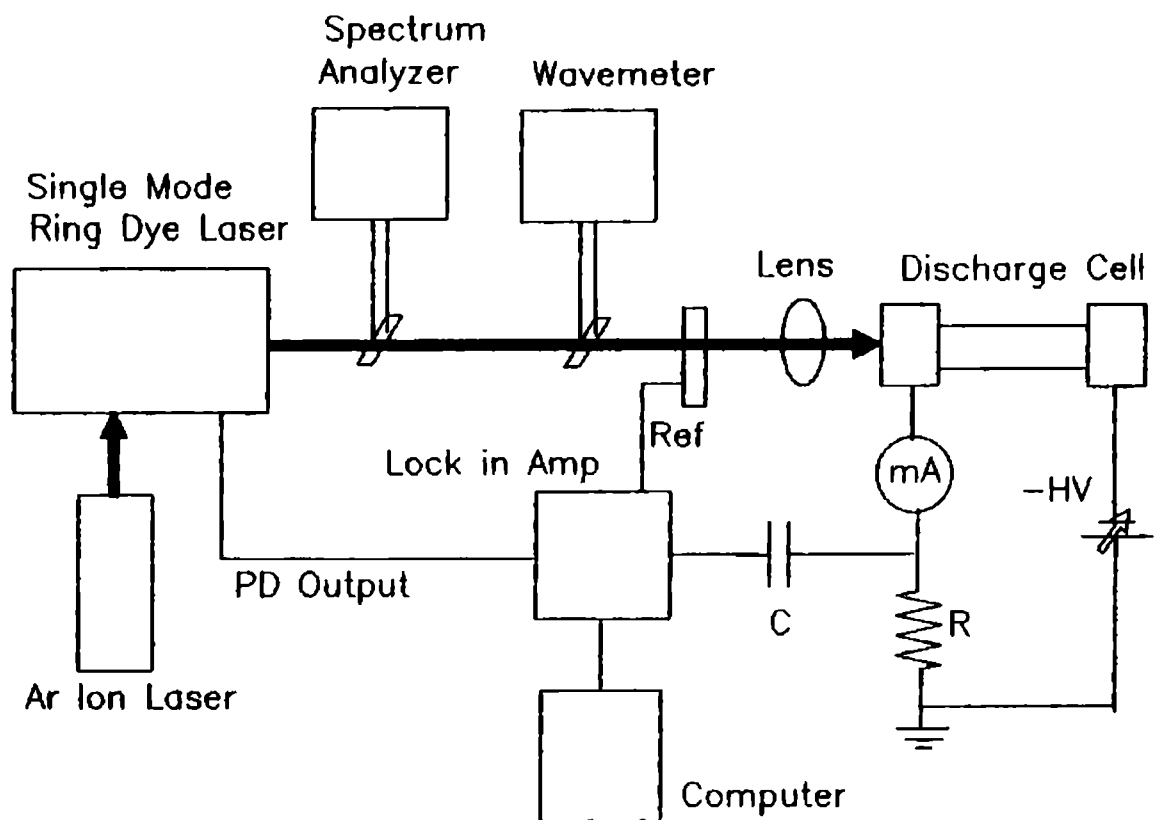
Fig 4.3 Experimental setup for Doppler limited high
resolution optogalvanic spectroscopy in nitrogen positive
column discharge

the discharge noise or the signal is displayed on the screen of an oscilloscope.

Radiation from a single mode ring dye laser (Spectra Physics 380D) operating in the Rh6G dye lasing region pumped by an argon ion laser was mechanically chopped and axially passed into the discharge column. The beam is allowed to interact without falling on the electrodes so that the background noise due to photoelectric emission is completely eliminated. Since the beam is passed axially into the discharge, the observed signal is the resultant of contributions from all parts of the interacting region of discharge with the laser beam. The broad band spectrum is recorded by scanning the dye laser and is detected using a lock-in amplifier (EG&G 5208) which was connected to a chart reorder or interfaced with a computer for data acquisition. The dye laser intensity profile variation was eliminated by normalizing the signal amplitude with a photo diode output of the dye laser. The wavelength was measured using a commercial wave meter (Burligh WA 20VI).

In high resolution experiments the spectra were recorded by scanning the dye laser in steps of 30 GHz using single mode scanning electronics. (Spectra Physics 388 & 481B). The single mode nature and wavelength calibration of the laser is checked by a spectrum analyzer (Spectra Physics 470) with free spectral range of 2 GHz. The peak position of the signal is measured within an accuracy of $0.06cm^{-1}$ The inaccuracy in determining

the wavelength of a transition was predominantly due to th

Doppler broadening of the spectral line and the frequency jitte

of the dye laser

4.5.2 LOW RESOLUTION SPECTRUM

Fig 4.4 shows a typical low resolution spectrum recorded i

the 570-600nm spectral region of the first positive system of N

molecule at a discharge current of 3.75 mA and a pressure of

mBar. As compared with the earlier studies [10,11] this has

very good signal to noise ratio. This is due to the specia

configuration of the discharge cell that is used in thi

experiment, and also the beam is allowed to interact uniforml

within the positive column region without falling on th

electrodes so that the noise due to photoelectric emission fro

the cathode surface is completely eliminated. Moreover in thi

configuration the OG signal is the resultant of the contributio

from all region of the plasma and hence there is no spatia

dependence. The vibrational bands were identified by comparin

it with the standard N_2 spectrum [2] viz (8,4), (9,5), (10,6)

(11,7) and (12,8) vibrational bands corresponding to Δv =

sequence of the first positive system.

It was observed that intensity of various bands in the O(

spectrum strongly depends on the gas pressure and the discharg

current. Fig 4.5 shows the intensity of these bands fo

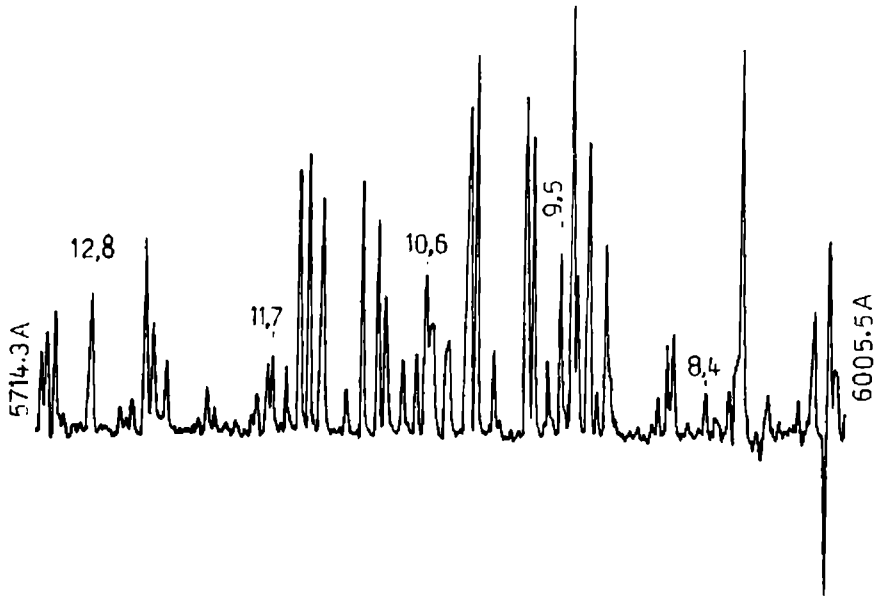different discharge conditions. All the bands were found to b

Fig 4.4 Low resolution OG spectrum of N_2 in the spectral region from 570 to 600nm with discharge current = 3.75 mA, gas pressure = 1 mBar and laser power = 300 mW

well developed at a gas pressure of 1 mBar and a discharge current of 4.5 mA while at 0.75 mBar only (8,4), (11,7) and (12,8) bands were found to be sensitive to OG phenomena. As the current is reduced, the intensity of all these bands were also found to decrease, and at a pressure below 0.5 mBar the all bands in this region of the first positive system disappeared completely. The results show that the intensity of individual bands varies in different manner with the discharge current. For example in the range of discharge current studied, the (11,7) band was found to be easily excitable exhibiting a large OG signal while the (10,6) band has the least intensity. In general, OG signal strength decreases with the decrease in pressure and current.
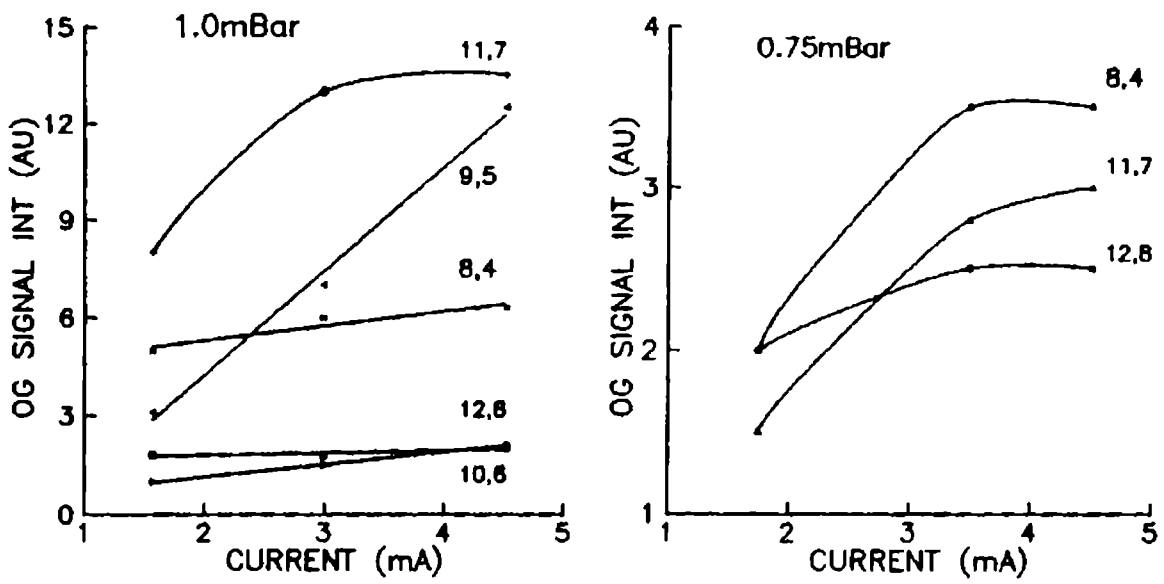
Fig 4.9 Details of the intensity of vibrational bands with pressure and current.

These variations in intensity of bands with the change in pressure and current can be understood from the collision mechanisms in the discharge system. Population of N_2 molecule in the $A^3\Sigma_u^+$ states with the decrease in gas pressure will reduce the OG signal. Another factor that affect the molecular excitation is the electronic temperature of the gas which strongly depends on the current. Thus the magnitude of the signal will reduce when the discharge current is decreased due to the reduction in electron temperature.

4.5.3 MAGNITUDE OF THE OG SIGNAL

For cw laser excitation, by considering a two level rate

equation formalism, it was shown by Erez [16] et al that, the magnitude of the OG signal, is given by the expression,

$$\Delta V = -const(a_2 T_2 - a_1 T_1)(N_1 - N_2) \qquad (4.20)$$

where a_i is related to the ionization rate in which $a_2 > a_1$, T_i is the life time and N_i is the population of the level i (i=1,2). Thus, the change in voltage can be either an increase or decrease depending on the life time of levels involved in the transitions. According to the equation (4 20), for laser excitation from a level with long life time, the OG signal is usually positive. In the case of N_2, the lower level $(A^3\Sigma_u^+)$ is a metastable state with a life time of approximately 1 9 msec and that of the upper state $(B^3\Pi_g)$ is of the order of a few micro seconds [1] Hence for all transitions the change in voltage across the discharge cell will be positive as observed here.

4.5.4 HIGH RESOLUTION OG SPECTRUM OF THE 11-7 BAND

High resolution spectrum is recorded by scanning the single mode ring dye laser in steps of 30 GHz/ 2 min. Discharge was maintained at a current of 2.8 (± 0.1) mA with nitrogen gas at a pressure of 0.8mBar and the laser beam with 225 (± 15) mW was axially passed through the cell. Typical 30 GHz spectra and a part of the OG spectrum showing the intensity of the OG signal corresponding to various rotational lines are shown in fig 4.6.
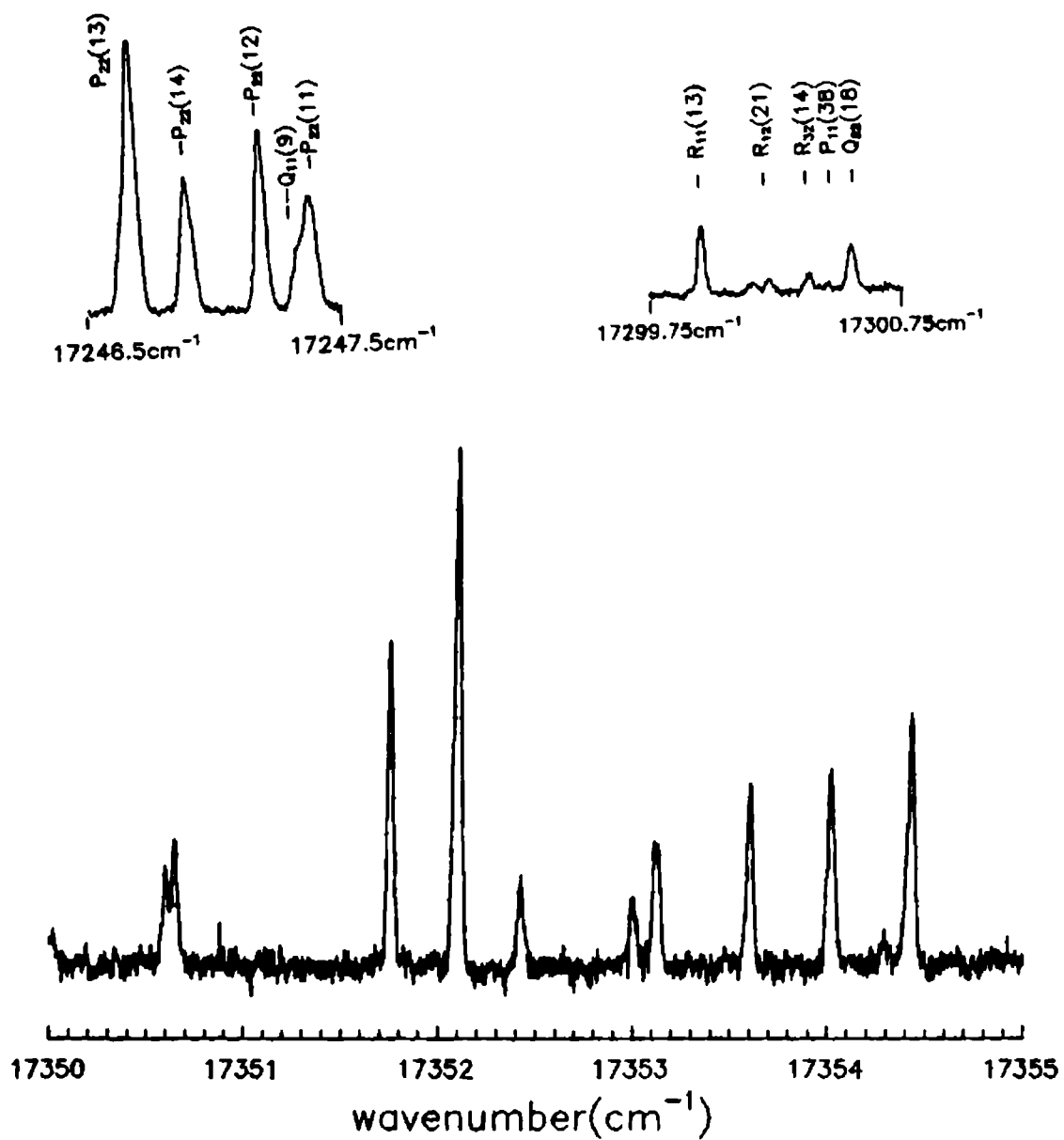
Fig 4.8 Typical examples of high resolution OG spectra in N_2

109

Fig 4.7 shows the digitized spectrum of N_2 first positive system over a spectral region from 17179 to 17376 cm^{-1} which is obtained from about four hundred such 30 GHz overlapping spectra. About 648 rotational lines have been observed and 432 of these have been identified and assigned as members of the (11,7) band of the $B^3\Pi_g$ — $A^3\Sigma_u^+$ system. Few transitions belonging to the (12,8) and (10,6) band system are also observed in this region. The identification of the OG resonances with the rotational transitions and the signal voltage are listed in the table 4.1. The correctness of the J number assignment of rotational line is tested by a number of combination relations. The rotational constant B_υ is calculated from the expression (neglecting the centrifugal distortion constant),

$$F_\upsilon(J+1) - F_\upsilon(J-1) = 4B_\upsilon(J+1/2) \qquad (4.21)$$

and from the combination relations,

$$R(J-1) - P(J+1) = F_\upsilon''(J+1) - F_\upsilon''(J-1) \qquad (4.22)$$
and
$$R(J) - P(J) = F_\upsilon'(J+1) - F_\upsilon'(J-1) \qquad (4.23)$$

respectively. The values of B_υ obtained from these combination differences are 1.41cm^{-1} and 1.313cm^{-1} for $B^3\Pi_g$ and $A^3\Sigma_u^+$ states respectively which are in agreement with the published results [4,6].
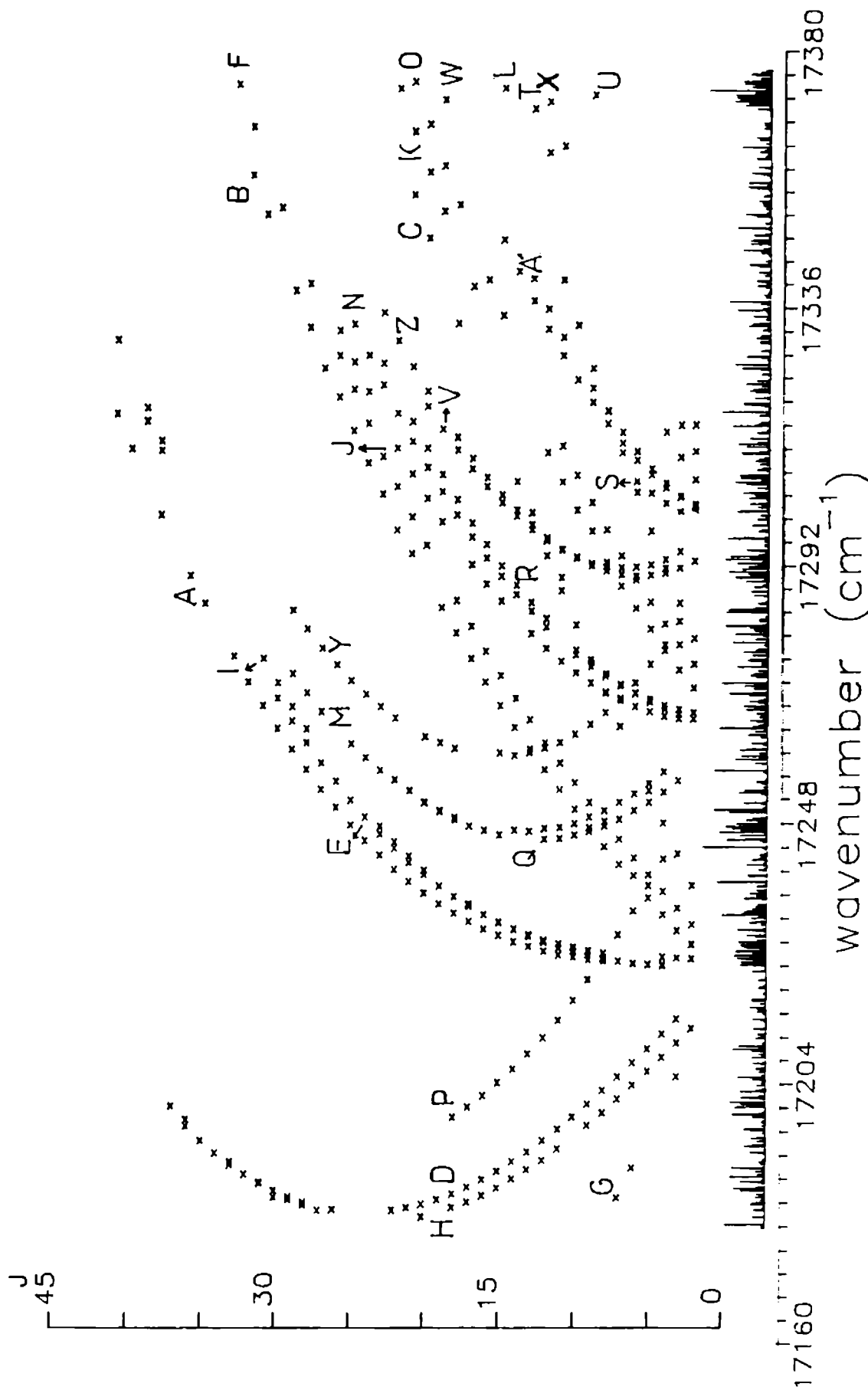
J
45

30

15

0

17160

wavenumber (cm^{-1})

17380   17336   17292   17248   17204

Fig 4.7 OG spectrum along with Fortratdiagram of the (11,7) band in the $B^3\Pi_g$ — $A^3\Sigma_u^+$ transition of N_2 from 17179 to 17376 cm^{-1} (27 branches P_{11}, Q_{11}, Q_{33} and R_{33} are indicated as A, B, Z and Z' respectively)

The $B^3\Pi_g$ state of N_2 corresponds to Hunds case(a) [6] and the multiplet structure from equation (19) ($T_e = T_o + A\Lambda\Sigma$, where A is the coupling constant, Λ and Σ corresponds to angular momentum and spin angular momentum components along the molecular axis.). In the case of $^3\Pi$ multiplets,

$$T_e(^3\Pi_0) = T_0$$
$$T_e(^3\Pi_1) = T + A$$
$$T_e(^3\Pi_2) = T_0 + 2A$$

(4.24)

The coupling constant A of the Π state can be evaluated by plotting $R_{21}(J) - R_{11}(J)$ as a function of J (fig 4.8) and extrapolating to $J = 0$. Value of A thus evaluated is 40.8 cm^{-1}, while the reported value of which is 41.5 cm^{-1} [4] The effect of Λ-doubling on the rotational levels of the $^3\Pi_0$, $^3\Pi_1$ and $^3\Pi_2$ states was evaluated from the combination defect [6] viz.

$$R(J) - Q(J) = Q(J+1) - P(J+1) + \varepsilon$$

(4.25)

and

$$R(J) - Q(J+1) = Q(J) - P(J+1) + \varepsilon$$

(4.26)

so that

$$\varepsilon/2 = (B_\upsilon^c - B_\upsilon^d)J(J+1) = qJ(J+1)$$

(4.27)

where B_υ^c, B_υ^d are rotational constants corresponding to Λ-doubling components of $B^3\Pi$ state and $q = B_\upsilon^c - B_\upsilon^d$ is the Λ-doubling
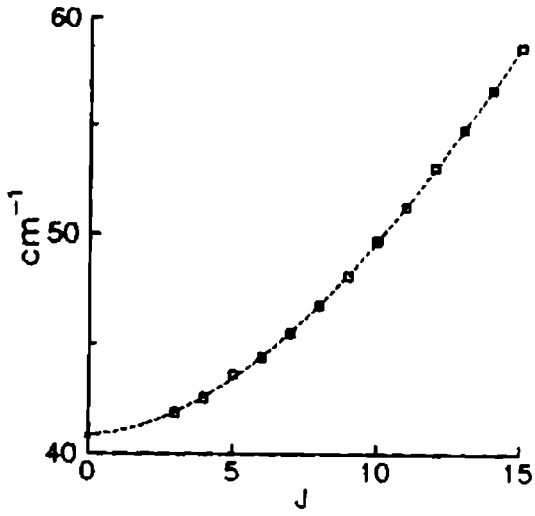
Fig 4.8

Variation of $R_{21}(J)-R_{11}(J)$
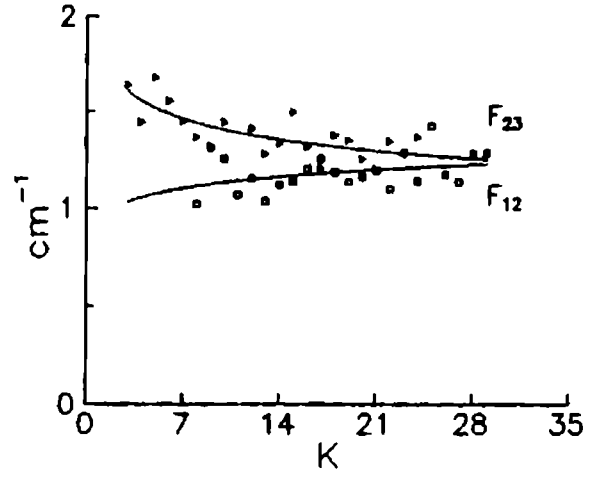as function of J to evaluate A

Fig 4.10

Spin multiplet separation
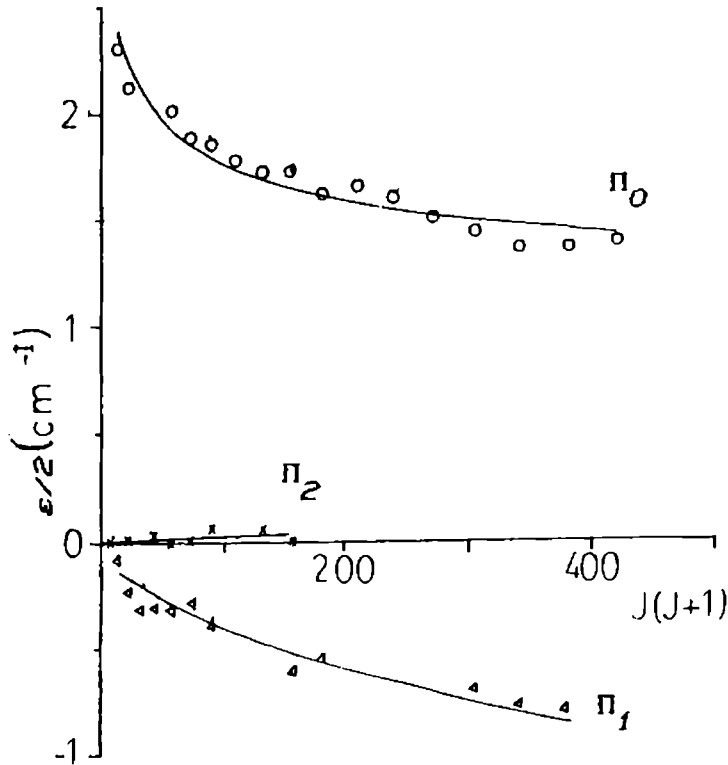for ${}^3\Sigma_u^+$ state with K

Fig 4.9 Variation of combination defect $\varepsilon/2$
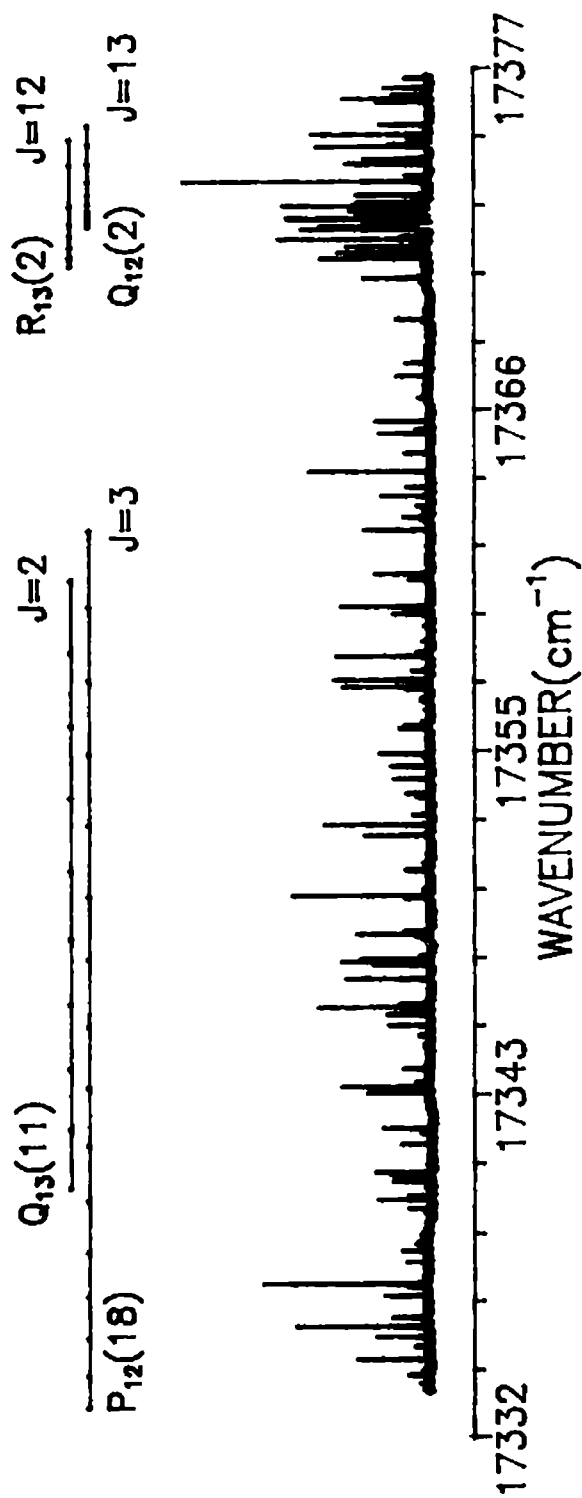as function of $J(J+1)$.
(curve shows the least square fitting)

113

Fig 4.11 Optogalvanic spectrum along with the assignment of the rotational transition of the (12,8) band.

coefficient. Fig 4.9 shows the plot of $\varepsilon/2$ as a function of $J(J+1)$. The triplet separation of the Σ state viz., $F_{12}(K)$ and $F_{23}(K)$, which is a measure of the separation of $F_1(K)$ and $F_3(K)$ levels from the $F_2(K)$ level [18,19] ($J = K+1$, K and $K-1$ corresponding to F_1, F_2 and F_3 components respectively) obtained from the data are indicated in figure 4.10.

4.5.5 HIGH RESOLUTION OG SPECTRUM OF THE 12-8 BAND

48 transitions belonging to (12-8) band are also identified in this spectral region. These transitions belong to P_{12}, P_{12}, Q_{13} and R_{13} branches corresponding to $^3\Pi_0(F_1) \longrightarrow {}^3\Sigma_u^+$ subsystems. The identification of these branches is shown in the fig 4.11 and the assignment is given in the table 4.1. It is noted that these transitions were theoretically predicted but were not experimentally observed in the work reported by Raux et al [4].

Optogalvanic spectrum of nitrogen molecule in a home made positive column discharge has been studied using cw laser The special configuration of the cell that is used in the experiment generates the OG signal with a very good signal to noise ratio and is suitable for high resolution study. OG resonances for rotational lines of (11,7), (12,8) and (10,6) bands of N_2 first positive system has been identified using Doppler limited high resolution OGS. A large number of rotational lines theoretically predicted but not experimentally observed so far were obtained by this method. The method can be extended to other wavelength

region and can also be obtained with better resolution and accuracy by adopting Doppler free techniques.

REFERENCES

1   A Lofthus and P H Krupene, J.Chem.Phys.Ref Data 6 (1977) 113

2   R W B Pearse and A G Gaydon, Identification of molecular
        spectra (Champman and Hall Ltd. , London 1965)

3   S M Naude, Proc.R.Soc.Lond. 136 (1932) 114

4   F Roux, F Michaud and J Verges, J.Mol.Spectrscopy 97 (1983)
        253

5   George Bekefi(Ed), Principle of laser plasma, (John Wiley &
        Sons NY)

6   G Herzberg, Melecular spectra and molecular structure -
        Spectra of diatomic molecules (D Van Nostrand Co.
        Princeton 1963)

7   C Effantin, C Amiot and J Verges, J.Mol.Spectroscopy 76
        (1979) 221

8   R Vasudev and R N Zare, J.Chem.Phys. 76 (1982) 5267

9   C R Webster and R T Menzies, J.Chem.Phys. 78 (1983) 2121

10 D Fedmann, Opt.Comm. 29 (1979) 67

11 G Ullas and S B Rai, Pramana-J.Phys. 36 (1991) 647

12 K Miyazaki, H Scheingraber and C R Vidal, Phys.Rev.Lett. 50
        (1983) 1046

13 R Walkup, R W Drefus and Ph Avouris, Phys.Rev.Lett. 50
        (1983) 1846

14 K Naveedullah and A S Naqvi, Opt.Comm. 56 (1985) 117

15 T Suzuki, Opt.Comm. 38 (1981) 364

16 T Suzuki and M Kakimoto, J.Mol.Spectroscopy 93 (1982) 423

17 G Erez, S Lavi and E Miron, IEER J.Quantum Electronins 15
        (1979) 1328

18 C C Jones, W Beuesch and E J Beiting, J.Mol.Spectroscopy 70
        (1978) 95

19 P K Carroll and H E Rubalcava, Proc.Phys.Soc. 76 (1960) 337

Table 4.1

Identification of OG resonances with the rotational transitions of (11,7), (12,8) and (10,6) band of N_2: $B^3\pi_g - A^3\Sigma_u^+$ system in the spectral region of 17179 to 17376 cm^{-1} ($^@$ (10,6) band, $^\#$ (12,8) band)

Wave number cm^{-1}	J-value assignment	OG signal mV
17179.85	$P_{13}(08)$	0.078
17180.22		0.069
17180.42		0.615
17181.65	$Q_{13}(20)$	0.206
17182.74	$P_{12}(22), Q_{13}(27)$	0.152
17182.85	$P_{12}(26),$ $^@R_{31}(4)$	0.185
17182.98		0.012
17183.19	$Q_{13}(18), P_{12}(21)$	0.045
17183.70	$Q_{13}(28)$	0.231
17183.76	$P_{12}(20)$	0.045
17184.04	$P_{12}(28)$	0.210
17184.12	$Q_{13}(17)$	0.020
17184.53	$P_{12}(19), Q_{13}(29)$	0.086
17184.83	$P_{13}(07)$	0.041
17185.00	$Q_{13}(30), P_{12}(29)$	0.152
17185.11	$^@Q_{11}(28)$	0.091
17185.20	$Q_{13}(18)$	0.020
17185.49	$P_{12}(18)$	0.152
17186.08	$P_{12}(30)$	0.380
17186.48	$Q_{13}(15)$	0.479

17186.64	$P_{12}(17)$	0.144
17187 33	$P_{12}(31)$	0.053
17187 47	$Q_{13}(31)$	0.111
17187.61		0.379
17187.92	$P_{12}(16)$	0.065
17187.99	$Q_{13}(14)$	0.037
17188.46		0.540
17188.70		0.012
17188.86	$P_{12}(32)$	0.132
17189.34	$P_{12}(15)$	0.157
17189.37		0.140
17189.59	$Q_{13}(13)$	0.049
17189.92	$P_{13}(06)$	0.347
17190.01		0.512
17190.47	$P_{12}(33)$	0.016
17190.72	$^@R_{31}(5)$	0.082
17191 00	$P_{12}(14), Q_{13}(33)$	0.111
17191.22	$Q_{13}(12)$	0.049
17191.39		0.041
17191.44	$^@Q_{11}(29)$	0.032
17192.49	$P_{12}(34)$	0.103
17192.60	$P_{12}(13)$	0.243
17193.13	$Q_{13}(11)$	0.032
17193.68		0.326
17193.81		0.165
17193.82		0.202
17193.84		0.202
17193.94		0.045
17194.58	$P_{12}(12), P_{12}(35)$	0.148
17195.05	$P_{13}(05)$	0.222
17195.87		0.062
17196.32		0.247
17196.52	$P_{12}(11)$	0.334

17197.09	$P_{12}(38), Q_{13}(09)$	0.070
17197.68		0.078
17197.89	$^{@}Q_{11}(30)$	0.057
17198.14	$Q_{13}(38)$	0.020
17198.55	$P_{12}(10), P_{23}(18)$	0.214
17198.91	$^{@}R_{31}(6)$	0.185
17198.95		0.214
17199.01		0.508
17199.23	$Q_{13}(08)$	0.111
17199.37		0.041
17200.21	$P_{13}(04), P_{23}(17)$	0.475
17200.42	$P_{12}(37)$	0.280
17200.67	$P_{12}(09)$	0.388
17201.05		0.546
17201.52	$Q_{13}(07)$	0.067
17201.65		0.115
17201.81		0.380
17202.11	$P_{23}(16)$	0.115
17202.68		0.037
17202.82		0.396
17202.94	$P_{12}(08)$	0.181
17203.11		0.095
17203.83	$Q_{13}(06)$	0.148
17204.26	$P_{23}(15)$	0.082
17204.46		0.045
17204.55	$^{@}Q_{11}(31)$	0.049
17204.76		0.214
17205.24	$P_{12}(07), P_{13}(03)$	0.429
17205.55		0.078
17206.10		0.127
17206.20	$Q_{13}(05)$	0.090
17206.59	$P_{23}(14)$	0.165
17206.74		0.152

17207.52	$^@R_{31}(7)$	0.099
17207.66	$P_{12}(06)$	0.217
17208.60	$Q_{13}(04)$	0.226
17208.79		0.078
17209.22	$P_{23}(13)$	0.132
17209.71		0.235
17210.08	$P_{12}(05)$	0.508
17210.39		0.115
17210.60		0.413
17211.08	$Q_{13}(03)$	0.074
17211.32	$^@Q_{11}(32)$	0.037
17211.95		0.173
17211.99	$P_{23}(12)$	0.148
17212.42		0.099
17212.63	$P_{12}(04)$	0.140
17213.47		0.103
17213.55	$Q_{13}(02)$	0.198
17214.67		0.041
17214.93	$P_{23}(11)$	0.095
17215.13	$P_{12}(03)$	0.218
17215.88		0.053
17216.02		0.062
17216.32		0.160
17216.40	$^@R_{31}(8)$	0.123
17216.76		0.144
17217 04		0.268
17217 68		0.099
17218.23	$P_{23}(10)$	0.235
17218.42		0.222
17219.42		0.049
17220.30		0 127
17220.58		0.098
17221.71	$P_{23}(09)$	0.136

120

Wavenumber	Assignment	Intensity
17223.21		0.227
17223.61		0.032
17224.01	$R_{13}(04)$	0.041
17224.21		0.404
17224.25	$P_{11}(04), R_{13}(05)$	0.251
17224.32	$P_{11}(05)$	0.371
17224.47	$R_{13}(06), P_{11}(06)$	0.193
17224.74		0.396
17224.86	$R_{13}(07), P_{11}(08)$	0.074
17225.03		0.198
17225.14	$P_{11}(09)$	0.222
17225.24	$R_{13}(08), Q_{12}(02)$	0.347
17225.38	$P_{23}(08), Q_{12}(03)$	0.454
17225.59	$Q_{12}(04), P_{11}(10)$	0.247
17225.89	$P_{11}(11), R_{13}(09)$	0.495
17226.19	$Q_{12}(08)$	0.222
17226.52	$P_{11}(12), R_{13}(10)$	0.474
17226.82	$Q_{12}(09)$	0.458
17226.97		0.099
17227.09	$R_{13}(11)$	0.218
17227.19	$Q_{12}(10)$	0.328
17227.32	$P_{11}(13)$	0.381
17227.64	$Q_{11}(02)$	0.392
17227.78	$Q_{12}(11)$	0.144
17228.09	$R_{13}(12), P_{11}(14)$	0.429
17228.24		0.075
17228.39	$Q_{12}(12)$	0.156
17229.02	$R_{13}(13)$	0.193
17229.20	$P_{11}(15)$	0.152
17229.25	$Q_{12}(13), P_{23}(07)$	0.309
17229.87		0.095
17229.97	$Q_{11}(03)$	0.193
17230.18	$R_{13}(14)$	0.454

17230.24	$Q_{12}(14), P_{11}(16)$	0.194
17230.98	$R_{12}(02)$	0.107
17231.28		0.049
17231.36	$Q_{12}(15), R_{13}(15)$	0.280
17231.51	$P_{11}(17)$	0.205
17232.12		0.256
17232.25		0.140
17232.36		0.062
17232.65	$Q_{11}(04), Q_{12}(16),$	
	$R_{13}(16)$	0.681
17232.90	$P_{11}(18)$	0.375
17233.31	$P_{23}(06)$	0.342
17233.72	$R_{12}(03)$	0.231
17234.10	$Q_{12}(17)$	0.190
17234.48	$P_{11}(19), R_{13}(17)$	0.148
17235.31	$^{@}R_{31}(10)$	0.074
17235.35		0.074
17235.42		0.347
17235.50	$Q_{11}(05)$	0.347
17235.74	$Q_{12}(18)$	0.049
17235.89		0.177
17236.31	$P_{11}(20)$	0.268
17236.59	$R_{12}(04)$	0.132
17236.85		0.169
17237.44		0.103
17237.50	$Q_{12}(19)$	0.169
17237.57	$P_{23}(05), R_{11}(02)$	0.136
17238.27	$P_{11}(21)$	0.751
17239.29	$Q_{11}(06)$	0.285
17239.41	$R_{12}(05), Q_{12}(20)$	0.301
17240.22	$R_{13}(20)$	0.086
17240.35	$P_{11}(22)$	0.148
17240.60		0.053

17241.17	$Q_{11}(07)$	0.322
17241.51	$Q_{12}(21)$	0.057
17241.75		0.041
17242.05	$P_{23}(04)$	0.247
17242.27	$R_{12}(06)$	0.140
17242.58	$R_{13}(21)$	0.057
17242.63		0.074
17242.74	$P_{11}(23)$	0.127
17242.95	$R_{11}(03)$	0.115
17243.80		0.033
17243.93	$Q_{12}(22)$	0.074
17244.18	$Q_{11}(08)$	0.966
17244.99	$R_{13}(22)$	0.086
17245.19	$P_{11}(24)$	0.121
17245.38	$Q_{23}(12),R_{12}(07)$	0.606
17245.54	$Q_{23}(11)$	0.347
17246.10	$Q_{23}(10),Q_{23}(15)$	0.422
17246.29	$Q_{12}(23)$	0.037
17246.69	$P_{22}(13),Q_{23}(09)$	0.722
17246.89	$P_{22}(14),Q_{23}(16)$	0.404
17247.19	$P_{22}(12)$	0.536
17247.34	$Q_{11}(09)$	0.198
17247.39	$P_{22}(11)$	0.334
17247.57	$R_{13}(23),Q_{23}(17),$	
	$Q_{23}(08)$	0.635
17247.78	$P_{11}(25)$	0.049
17248.03	$P_{22}(10)$	0.285
17248.07	$R_{11}(04)$	0.478
17248.36	$R_{12}(08)$	0.156
17248.54		0.165
17248.68	$Q_{23}(18),Q_{23}(07)$	0.342
17248.90		0.119
17249.00	$P_{22}(18)$	0.235

17249.07	$Q_{12}(24), P_{22}(09)$	0.082
17250.01	$P_{22}(19)$	0.586
17250.13	$Q_{23}(19), P_{22}(08),$	
	$Q_{23}(06)$	0.095
17250.40	$Q_{11}(10)$	0.801
17250.71	$P_{11}(26)$	0.074
17250.85		0.045
17251.33		0.095
17251.43	$P_{22}(20)$	0.091
17251.49	$R_{12}(09), P_{22}(07),$	
	$Q_{23}(20), Q_{23}(05)$	0.363
17251.85	$Q_{12}(25)$	0.033
17252.72		0.032
17252.95	$P_{22}(08)$	0.111
17253.24	$Q_{23}(04)$	0.437
17253.35		0.037
17253.48	$Q_{23}(21), R_{11}(05)$	0.169
17253.66	$P_{11}(27), Q_{11}(11)$	0.355
17254.18		0.070
17254.73	$P_{22}(05)$	0.078
17254.86	$R_{12}(10)$	0.103
17255.08	$Q_{12}(26)$	0.186
17255.22	$Q_{23}(03)$	0.029
17255.35	$Q_{23}(22)$	0.041
17256.74	$P_{22}(04)$	0.074
17256.98	$P_{22}(23)$	0.029
17257.06	$Q_{11}(12), P_{11}(28)$	0.788
17258.24	$R_{12}(11), Q_{12}(27)$	0.214
17258.96	$R_{11}(06)$	0.495
17259.14	$P_{22}(24)$	0.132
17259.50	$P_{33}(14)$	0.404
17259.94		0.107
17260.00	$P_{33}(15), P_{33}(13)$	0.144

17260.56	$Q_{11}(13)$, $P_{11}(29)$	0.429
17260.73	$P_{33}(18)$, $P_{33}(12)$	0.309
17261.39		0.062
17261.50	$P_{22}(25)$	0.090
17261.70	$P_{33}(11)$, $R_{12}(12)$, $P_{33}(19)$, $Q_{12}(28)$	0.255
17262.74	$P_{33}(20)$	0.127
17263.13	$P_{33}(10)$	0.309
17263.65		0.037
17263.73		0.210
17264.05	$R_{13}(28)$	0.049
17264.10	$P_{11}(30)$	0.049
17264.27	$Q_{11}(14)$	0.726
17264.50	$R_{11}(07)$	0.248
17264.74		0.160
17264.82	$P_{33}(09)$	0.136
17265.38	$Q_{12}(29)$	0.185
17265.57	$R_{12}(13)$	0.276
17265.68	$R_{23}(02)$	0.049
17265.78	$P_{21}(03)$	0.078
17265.88	$P_{33}(22)$	0.078
17266.16	$P_{21}(04)$	0.144
17266.39		0.123
17266.54	$R_{23}(03)$	0.032
17266.75	$Q_{22}(02)$	0.198
17266.82	$P_{33}(08)$	0.074
17266.95	$P_{22}(27)$, $P_{21}(05)$	0.045
17267.24		0.049
17267.31	$Q_{22}(03)$	0.024
17267.41	$R_{23}(04)$	0.350
17267.68		0.041
17267.79	$R_{13}(29)$, $P_{21}(08)$, $P_{33}(23)$	0.235

17267.93	$P_{11}(31)$	0.078
17267.98	$Q_{22}(04), Q_{11}(15)$	0.384
17268.25		0.041
17268.59	$R_{23}(05)$	0.161
17268.88	$P_{21}(07)$	0.289
17269.08	$Q_{22}(05)$	0.127
17269.21	$R_{12}(14), Q_{12}(30),$	
	$P_{33}(07)$	0.082
17269.83		0.301
17269.93	$P_{33}(24)$	0.285
17270.01	$R_{23}(06)$	0.136
17270.15	$Q_{22}(06), R_{11}(08),$	
	$P_{22}(28)$	0.586
17270.30	$P_{21}(08)$	0.243
17271.00	$Q_{21}(02)$	0.247
17271.46	$Q_{22}(07)$	0.371
17271.60	$R_{23}(07)$	0.177
17271.88	$P_{21}(09), P_{33}(06),$	
	$R_{13}(30)$	0.219
17271.98	$Q_{11}(16), P_{11}(32)$	0.698
17272.23	$P_{33}(25)$	0.024
17272.96	$Q_{22}(08)$	0.210
17273.13	$R_{12}(15)$	0.127
17273.35		0.284
17273.41	$R_{23}(08), P_{22}(29)$	0.078
17273.58	$P_{21}(10)$	0.231
17273.86		0.065
17274.06	$Q_{21}(03)$	0.177
17274.73	$Q_{22}(09)$	0.474
17274.87		0.061
17274.97	$P_{33}(26)$	0.098
17275.06	$R_{22}(02), P_{33}(05)$	0.040
17275.30	$R_{23}(09)$	0.115

126

17275.59	$P_{21}(11)$	0.115
17275.85	$R_{11}(09)$	0.322
17276.03	$Q_{11}(17), R_{13}(31)$	0.280
17276.40	$P_{11}(33)$	0.024
17276.74	$Q_{22}(10)$	0.280
17277.25		0.065
17277.31	$R_{12}(16)$	0.383
17277.41	$Q_{21}(04)$	0.012
17277.57	$R_{23}(10)$	0.202
17277.76	$P_{21}(12), P_{33}(27)$	0.181
17278.34		0.078
17278.41	$P_{33}(04), R_{22}(03)$	0.078
17278.90		0.540
17279.47	$R_{21}(02)$	0.222
17279.99	$R_{23}(11)$	0.103
17280.23	$P_{21}(13)$	0.090
17280.31	$Q_{11}(18)$	0.503
17280.76	$P_{11}(34)$	0.214
17281.00	$P_{33}(28), Q_{21}(05)$	0.239
17281.40	$Q_{22}(12)$	0.301
17281.51	$R_{12}(17)$	0.090
17281.72	$R_{11}(10)$	0.648
17281.89	$R_{22}(04)$	0.090
17282.33	$P_{33}(03)$	0.028
17282.61		0.169
17282.80	$R_{23}(12)$	0.152
17283.16		0.049
17283.26		0.041
17283.28		0.045
17283.36		0.028
17284.08	$Q_{22}(13)$	0.640
17284.22	$P_{33}(29)$	0.070
17284.47		0.603

17284.59	$Q_{21}(06)$	0.037
17284.72	$Q_{11}(19)$	0.243
17284.83	$P_{22}(32)$	0.037
17285.38	$P_{11}(35)$	0.152
17285.51	$R_{21}(03)$	0.111
17285.59	$R_{23}(13)$	0.177
17285.68	$R_{22}(05)$	0.078
17285.82	$P_{21}(15)$	0.045
17285.91	$R_{12}(18)$	0.041
17286.58		0.020
17286.92	$Q_{22}(14)$	0.239
17287.63	$R_{11}(11)$	0.280
17288.43	$Q_{21}(07)$	0.235
17288.61	$R_{23}(14)$	0.103
17288.79	$P_{21}(16), P_{22}(33)$	0.103
17289.32	$Q_{11}(20)$	0.359
17289.52	$R_{22}(06)$	0.103
17290.01	$R_{13}(34)$	0.454
17290.11	$Q_{22}(15)$	0.508
17290.18	$Q_{33}(06), P_{11}(36)$	0.214
17290.35	$Q_{33}(05)$	0.280
17290.45	$Q_{33}(07)$	0.049
17290.66	$Q_{33}(04), R_{12}(19)$	0.330
17291.08	$Q_{33}(08)$	0.611
17291.55	$R_{21}(04), Q_{31}(03)$	0.421
17291.69	$P_{32}(07)$	0.082
17291.81	$P_{32}(06), P_{32}(08)$	0.095
17291.98	$R_{23}(15), Q_{33}(09)$	0.330
17292.17	$P_{21}(17), P_{32}(05)$	0.119
17292.45	$P_{32}(09)$	0.181
17292.55	$Q_{21}(08)$	0.487
17292.76	$Q_{33}(02)$	0.119
17293.08	$P_{32}(04)$	0.053

17293.20		0.660
17293.30	$Q_{33}(10)$, $Q_{22}(16)$	0.235
17293.40	$P_{22}(34)$	0.049
17293.50	$P_{32}(10)$	0.024
17293.68	$R_{22}(07)$	0.285
17293.72	$R_{11}(12)$	0.588
17294.02	$Q_{11}(21)$	0.174
17294.39	$P_{32}(03)$	0.057
17294.64	$P_{32}(11)$	0.181
17294.80	$Q_{33}(11)$	0.351
17295.25	$P_{11}(37)$	0.024
17295.45	$R_{12}(20)$	0.081
17295.62	$R_{23}(16)$	0.077
17296.22	$P_{32}(12)$	0.082
17296.71	$Q_{33}(12)$	0.623
17296.83	$Q_{22}(17)$	0.536
17297.90	$R_{21}(05)$, $Q_{21}(09)$	0.173
17298.02	$P_{22}(35)$, $Q_{11}(22)$	0.148
17298.09	$R_{22}(08)$, $P_{32}(13)$	0.114
17298.93	$Q_{33}(13)$	0.280
17298.98		0.247
17299.21	$R_{23}(17)$	0.037
17299.43	$P_{21}(19)$	0.041
17299.96	$R_{11}(13)$	0.202
17300.16		0.037
17300.23	$R_{12}(21)$	0.045
17300.39	$R_{13}(36)$, $P_{32}(14)$	0.057
17300.49	$P_{11}(38)$	0.041
17300.59	$Q_{22}(18)$	0.148
17301.31	$P_{31}(02)$	0.487
17301.40	$Q_{21}(10)$, $Q_{33}(14)$	0.437
17301.99	$R_{33}(02)$	0.198
17302.31	$Q_{32}(02)$	0.111

17302.58	$P_{31}(03)$	0.309
17302.67	$P_{32}(15), R_{22}(09)$	0.090
17303.21	$R_{23}(18)$	0.045
17303.39	$P_{21}(20)$	0.049
17303.60	$Q_{32}(03)$	0.322
17303.79	$R_{33}(03)$	0.156
17304.04	$Q_{33}(15)$	0.243
17304.11	$Q_{11}(23)$	0.107
17304.25	$P_{31}(04)$	0.032
17304.46	$R_{21}(06)$	0.404
17304.56	$Q_{22}(19)$	0.301
17305.32	$Q_{32}(04)$	0.198
17305.41	$P_{32}(16), R_{12}(22)$	0.049
17305.97	$R_{33}(04), P_{11}(39)$	0.367
17306.23	$Q_{21}(11)$	0.243
17306.33	$R_{11}(14), P_{31}(05)$	0.524
17306.67	$Q_{31}(02)$	0.144
17307.07	$Q_{33}(16)$	0.445
17307.42	$R_{22}(10)$	0.206
17307.49	$Q_{32}(05), R_{23}(19)$	0.462
17307.58	$P_{21}(21)$	0.363
17308.38		0.074
17308.47	$P_{32}(17), R_{33}(05)$	0.210
17308.75	$Q_{22}(20)$	0.136
17309.40		0.177
17309.48	$Q_{11}(24)$	0.144
17309.99	$Q_{32}(06)$	0.231
17310.31	$Q_{33}(17)$	0.185
17310.51	$Q_{31}(03)$	0.099
17310.60	$R_{12}(23)$	0.002
17311.23		0.421
17311.27	$R_{21}(07), Q_{21}(12)$	0.206
17311.42		0.445

17311.49	$R_{33}(08), R_{13}(38),$	
	$R_{32}(02)$	0.190
17311.71	$P_{32}(18)$	0.057
17311.77	$P_{11}(40)$	0.041
17311.97	$P_{21}(22), R_{23}(20)$	0.032
17312.41	$R_{22}(11)$	0.367
17312.89	$Q_{32}(07), R_{11}(15)$	0.487
17313.17	$Q_{22}(21), P_{22}(38)$	0.209
17313.60		0.037
17313.85	$Q_{33}(18)$	0.317
17314.30		0.020
17314.72	$Q_{31}(04), R_{33}(07)$	0.218
17314.81		0.157
17314.93	$Q_{11}(25)$	0.074
17315.19	$P_{32}(19)$	0.049
17315.91	$R_{31}(02), R_{32}(03)$	0.573
17316.13	$Q_{32}(08), R_{12}(24)$	0.222
17316.45	$R_{13}(39), Q_{21}(13),$	
	$R_{23}(21)$	0.165
17317.58	$R_{22}(12)$	0.160
17317.62	$P_{11}(41)$	0.181
17317.80	$Q_{22}(22)$	0.086
17318.26	$R_{21}(08), R_{33}(08)$	0.726
17318.48		0.037
17318.66	$P_{22}(39)$	0.024
17318.78		0.016
17318.99	$P_{32}(20)$	0.024
17319.25		0.164
17319.50	$Q_{31}(05), R_{11}(16)$	0.404
17319.67	$Q_{32}(09)$	0.417
17320.58	$Q_{11}(26)$	0.148
17320.62	$R_{32}(04)$	0.247
17321.50	$P_{21}(24)$	0.032

17321.59	$Q_{33}(20)$	0.239
17321.88	$R_{12}(25)$, $Q_{21}(14)$	0.317
17322.15	$R_{33}(09)$	0.260
17322.27		0.037
17322.41		0.020
17322.65	$Q_{22}(23)$	0.152
17322.77	$R_{31}(03)$	0.111
17322.95		0.037
17323.06	$R_{22}(13)$	0.371
17323.56	$R_{13}(40)$, $Q_{32}(10)$	0.214
17323.82	$P_{11}(42)$	0.024
17324.66	$Q_{31}(06)$	0.144
17325.53	$Q_{11}(27)$, $R_{21}(09)$	0.173
17325.74	$R_{32}(05)$	0.437
17325.80	$Q_{33}(21)$	0.103
17326.32	$R_{11}(17)$	0.210
17326.39	$R_{23}(23)$	0.536
17326.59	$P_{21}(25)$	0.032
17327.11		0.061
17327.55	$Q_{21}(15)$	0.144
17327.68	$R_{12}(26)$	0.065
17327.75	$Q_{32}(11)$, $Q_{22}(24)$	0.375
17328.73	$R_{22}(14)$	0.157
17330.05	$P_{11}(43)$	0.169
17330.10	$Q_{31}(07)$, $R_{31}(04)$	0.070
17330.29	$Q_{33}(22)$, $P_{22}(41)$	0.169
17330.48		0.032
17330.89	$R_{33}(11)$	0.231
17331.28	$R_{32}(06)$	0.169
17331.41		0.016
17331.98	$P_{21}(26)$	0.020
17332.12		0.053
17332.27	$Q_{32}(12)$	0.132

17332.47	$Q_{11}(28)$		0.062
17332.97	$R_{21}(10)$		0.342
17333.05	$Q_{22}(25)$	$^{\#}P_{12}(18)$	0.049
17333.26	$R_{11}(18)$		0.288
17333.40			0.198
17334.09		$^{\#}P_{12}(17)$	0.086
17334.27			0.020
17334.62	$R_{22}(15)$		0.272
17335.03	$Q_{33}(23)$		0.053
17335.20			0.012
17335.32		$^{\#}P_{12}(16)$	0.082
17335.69	$R_{33}(12)$		0.503
17335.98	$Q_{31}(08)$		0.136
17336.70		$^{\#}P_{12}(15)$	0.173
17336.98			0.086
17337 10	$Q_{32}(13)$		0.627
17337.82	$R_{31}(05)$		0.090
17338.19		$^{\#}P_{12}(14)$	0.107
17338.42			0.049
17338.48		$^{\#}Q_{13}(12)$	0.049
17338.72	$Q_{11}(29)$		0.029
17339.56	$Q_{21}(17)$		0.099
17339.83		$^{\#}P_{12}(13)$	0.218
17339.96	$R_{12}(28)$		0.095
17340.23		$^{\#}Q_{13}(11)$	0.029
17340.44	$R_{11}(19)$		0.140
17340.62			0.161
17340.69	$R_{21}(11)$		0.169
17340.73	$R_{22}(18)$		0.227
17340.90	$R_{33}(13)$		0.024
17341.64		$^{\#}P_{12}(12)$	0.111
17341.97			0.041
17342.16	$Q_{32}(14)$	$^{\#}Q_{13}(10)$	

	$Q_{31}(09)$		0.194
17343.28	$R_{32}(08)$		0.222
17343.40			0.012
17343.51		$^{\#}P_{12}(11)$	0.339
17343.66			0.049
17344.12		$^{\#}Q_{13}(9)$	0.103
17344.83			0.028
17345.00			0.029
17345.16	$Q_{11}(30)$		0.049
17345.52		$^{\#}P_{12}(10)$	0.165
17345.87			0.173
17345.91	$Q_{21}(18)$		0.165
17345.93	$R_{31}(06)$		0.429
17346.25	$R_{12}(29)$	$^{\#}Q_{13}(8)$	0.127
17347.07	$R_{22}(17)$		0.326
17347 50	$Q_{32}(15)$		0.214
17347 62			0.326
17347.73		$^{\#}P_{12}(9)$	0.272
17347.84	$R_{11}(20)$		0.053
17348.40		$^{\#}Q_{13}(7)$	0.049
17348.54	$R_{21}(12)$		0.280
17348.71	$Q_{31}(10)$		0.107
17349.62			0.107
17349.80	$R_{32}(09)$	$^{\#}P_{12}(8)$	0.528
17350.01			0.032
17350.60			0.082
17350.64		$^{\#}Q_{13}(6)$	0.107
17351.77	$Q_{11}(31)$		0.243
17352.11		$^{\#}P_{12}(7)$	0.408
17352.42	$Q_{21}(19)$		0.088
17352.97	$R_{12}(30)$		0.057
17353.01		$^{\#}Q_{13}(5)$	0.037
17353.12	$Q_{32}(16)$		0.095

134

17353.61	$R_{22}(18)$		0.144
17354.02			0.152
17354.25			0.024
17354.43	$R_{31}(07)$	$^{\#}P_{12}(6)$	0.198
17355.24	$R_{11}(21)$		0.123
17355.37		$^{\#}Q_{13}(4)$	0.111
17355.52	$Q_{31}(11)$		0.045
17356.14			0.045
17356.24			0.037
17356.53			0.103
17356.63	$R_{21}(13)$		0.317
17356.84		$^{\#}P_{12}(5)$	0.371
17357.12			0.086
17357.62			0.363
17357.76		$^{\#}Q_{13}(3)$	0.053
17358.62	$Q_{11}(32)$		0.037
17359.01	$Q_{32}(17)$		0.144
17359.20	$Q_{21}(20)$		0.115
17359.29		$^{\#}P_{12}(4)$	0.322
17360.17		$^{\#}Q_{13}(2)$	0.078
17360.34	$R_{22}(19)$		0.214
17361.79		$^{\#}P_{12}(3)$	0.251
17362.13			0.037
17362.21			0.115
17362.46			0.032
17362.59	$Q_{31}(12)$		0.066
17362.92			0.198
17363.23	$R_{31}(08)$		0.127
17363.75	$R_{32}(11)$		0.462
17364.34			0.103
17364.98	$R_{21}(14)$		0.202
17365.11	$Q_{32}(18)$		0.057
17365.37			0.247

17366.17	$Q_{21}(21)$		0.037
17366.89	$R_{12}(32)$		0.129
17367.37	$R_{22}(20)$		0.119
17367 79			0.127
17369.03			0.024
17369.98	$Q_{31}(13)$		0.028
17370.13		$^{\#}R_{13}(2)$	0.239
17370.40			0.020
17370.54		$^{\#}R_{13}(3)$	0.032
17370.77		$^{\#}R_{13}(4)$	0.416
17370.82		$^{\#}R_{13}(5)$	0.280
17370.98			0.342
17371.17	$R_{32}(12)$	$^{\#}R_{13}(6)$	0.362
17371.41			0.573
17371.56	$Q_{32}(19)$	$^{\#}R_{13}(7)$	0.111
17371.75			0.491
17371.83		$^{\#}Q_{12}(2)$	0.421
17371.85			0.289
17371.93		$^{\#}R_{13}(8)$	
		$^{\#}Q_{12}(3)$	0.252
17372.06		$^{\#}Q_{12}(4)$	0.536
17372.12			0.540
17372.23		$^{\#}Q_{12}(5)$	0.280
17372.35	$R_{31}(09)$	$^{\#}Q_{12}(6)$	0.309
17372.51		$^{\#}R_{13}(9)$	0.561
17372.60		$^{\#}Q_{12}(7)$	0.276
17372.88		$^{\#}Q_{12}(8)$	0.272
17373.07			0.024
17373.32		$^{\#}Q_{12}(9)$	0.937
17373.39	$Q_{21}(22)$		0.066
17373.52	$R_{21}(15)$		0.090
17373.85		$^{\#}R_{13}(11)$	0.285
17373.88		$^{\#}Q_{12}(10)$	0.326

17374.03	$R_{12}(33)$	0.284
17374.44		0.429
17374.52	$^{\#}Q_{12}(11)$	0.160
17374.56	$R_{22}(21)$	0.032
17374.67		0.020
17374.70	$^{\#}R_{13}(12)$	0.086
17374.84		0.445
17375.16	$^{\#}Q_{12}(12)$	0.190
17375.32		0.194
17375.95		0.218
17376.02		0.330
17376.15	$^{\#}Q_{12}(13)$	0.157
17376.38		0.177
17376.70		0.103

SIMULTANEOUS INVESTIGATIONS ON LASER-INDUCED FLUORESCENCE AND OPTOGALVANIC EFFECT IN NEON DISCHARGE

5.1 INTRODUCTION

Even though, in recent years OG effect has been widely used as a powerful technique for several spectroscopic and analytical applications [1,2], a detailed understanding of the processes governing OG mechanism is restricted only to a very few cases. Quantitative understanding of this effect in a variety of discharges and experimental conditions has improved the potentiality of this detection technique and made it an important tool for the diagnostics of the plasma. The effect, as described in earlier chapters, is produced when a gas discharge is irradiated with light which is resonant with one of the transitions in atoms, molecules or ions present in the discharge. Most of the theoretical models of OG phenomenon reported in the literature are designed for a particular type of discharge and for the specific conditions existing therein [3,5]. The main difficulty in developing a more general model is the existence of a large number of different processes that characterize the discharge system.

The interaction of a laser beam with discharge is a complex process and depends on the balance between all excitations and de-excitations of various species present in the medium.

Optogalvanic effect is basically a change in electrical properties of a gas discharge due to modifications in the population of states caused by the absorption of radiation. It gives information on changes in the population distribution as a result of selective laser excitation.

The interaction of laser with discharge will generate variations in the temperature, population etc. and the combination of OG spectroscopy with other techniques such as absorption, photoacoustics, fluorescence etc. can be utilized to get more detailed informations regarding various processes in the discharge that result into OG effect. The simultaneous investigations of OG effect and absorption can be used to get line shape of spectral lines which reveal the collision process in the discharge while the monitoring of OG effect with photoacoustic effect can be utilized to study the non-radiative decay path in the discharge. Fluorescence emission is another phenomenon which represents a well established technique for obtaining informations on radiative de-excitation path between various energy levels. Variations in emission characteristics is another important consequence generated by interaction of laser beam with the discharge medium. This occurs as a result of modifications in the population of states; resulting in both increase and decrease in emission intensities of certain lines as compared to that without irradiating the discharge. Hence, simultaneous investigations of OG effect and emission

characteristics provide a sensitive method to study the population of states in a discharge and the various factors which influences in generating the OG effect. Simultaneous monitoring of OG effect and other effects like photo acoustic effect [6-8], and optical absorption [9] have been reported to gather information about the laser-discharge interaction in a positive column discharge. However, only limited studies on simultaneous monitoring of OG and fluorescence phenomena have been carried out [10,11]. De Marinus et al [12] have studied the spatial dependence of the fluorescence intensity in a neon negative glow discharge and Dreez et al [13] have studied the change in temperature by monitoring the emission intensity before and after laser illumination of uranium transitions in a hollow cathode discharge. The present chapter deals with the studies on simultaneous monitoring of OG effect for $1s_5 \rightarrow 2p_2$ and $1s_5 \rightarrow 2p_4$ transitions of neon and the laser induced emission spectrum.

5.2 EXPERIMENTAL DETAILS

A frequency stabilized ring dye laser (Spectra Physics-380D) pumped by argon ion laser (Spectra Physics - 171) was used as the excitation source. Wavelength of the laser was exactly tuned on the line centre of the neon transition (at 5882 Å and 5945 Å corresponding to $1s_5 \rightarrow 2p_2$ and $1s_5 \rightarrow 2p_4$ transitions of neon respectively) where the OG signal amplitude is a maximum. The wavelength of the laser was fixed with an accuracy of $\pm 0.01 cm^{-1}$
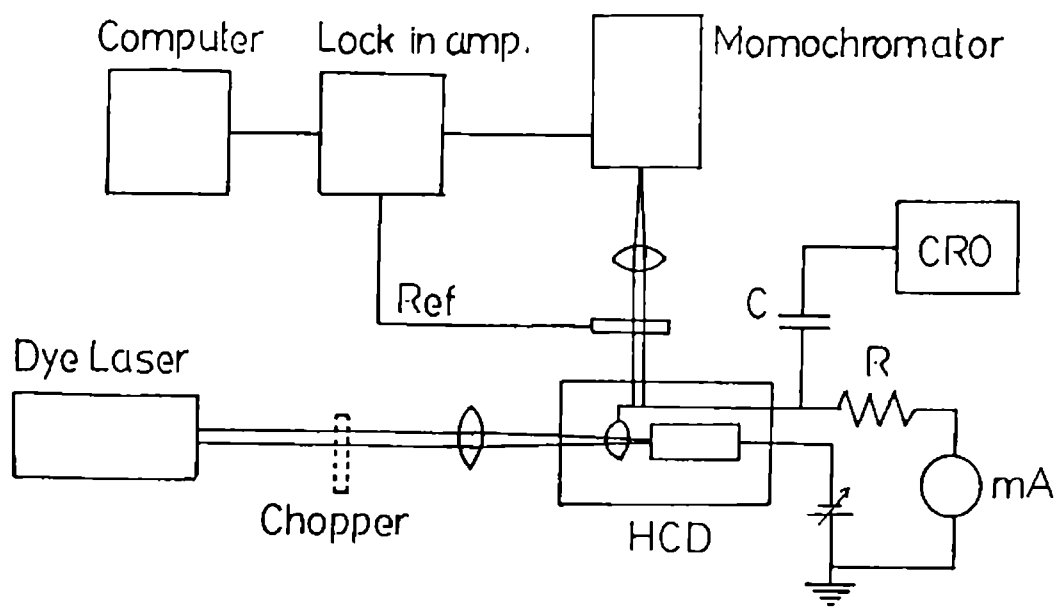
Fig 5.1 Experimental setup.

of the transition. A commercial Ne/Mo hollow cathode lamp with a gas pressure of 10 Torr (Cathodean UK) was used as the discharge source and the laser beam was focused into it. The cell is operated with glow discharge region in the voltage-current characteristics. A 0.5m monochromator (Jarrell Ash) was used for recording the emission spectrum of the discharge with and without laser excitation for various discharge currents up to 5mA. The PMT output was processed by a lock-in amplifier and a computer was used for data acquisition. Since the

range of current used for the operation of the discharge was very low, molybdenum (Mo) atomic lines were not observed in the emission spectrum. The neon transitions within the scanning range of the monochromator were identified in all cases. The OG signal corresponding to an increase in the discharge impedance during laser excitation, was measured using an oscilloscope. A schematic of the experimental setup is shown in fig 5.1.
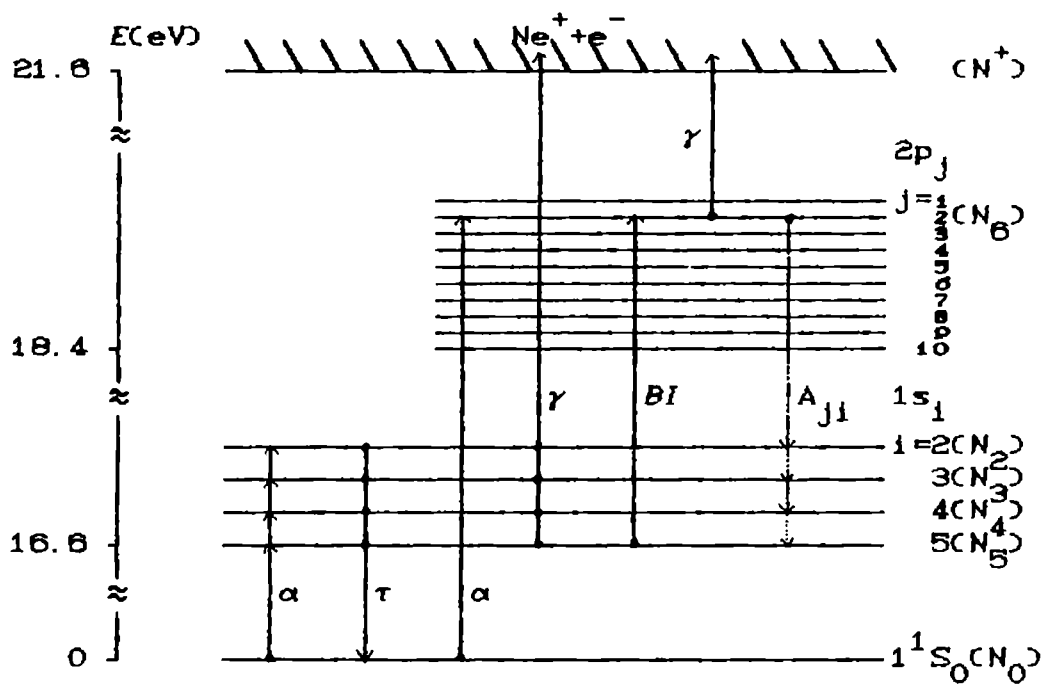
Fig 2.2 Simplified energy level scheme showing the coupling between levels included in the rate equation analysis.

5.3 ENERGY LEVEL DIAGRAM OF NEON

The first excited state configuration of neon $(2p^5 3s)$ has four components denoted as $1s_i$ $(i=2,3,4$ and $5)$. Two of these viz. $1s_3$ and $1s_5$ are metastable states with a long life time [14,15] while $1s_2$ and $1s_4$ states have strong radiative coupling with the ground state $(^1S_0)$. The decay rate of the $1s_5$ and $1s_3$ levels due to diffusion to the walls are substantially smaller than the decay rate of the $1s_4$ and $1s_2$ states as a result of the escape of the trapped radiation. The next excited state configuration is $2p^5 3p$ giving rise to ten states represented as $2p_j$ $(j = 1$ to $10)$ which are also coupled radiatively to the $1s_i$ states. We have used a simplified energy level diagram in which the ground state, four $1s_i$ levels and the ionized state are considered independently while only the prominent effects from $2p_2$ state due to radiative processes are included (fig 5.2).

5.4 LASER EXCITATION OF $1s_5 \rightarrow 2p_2$ TRANSITION $(5882 \overset{o}{A})$

a) Laser induced fluorescence spectrum

Laser excitation corresponding to $1s_5 \rightarrow 2p_2$ transition of neon will perturb the population density of $2p_2$ state and the monitoring of fluorescence from $2p_j$ to $1s_i$ levels will give information on the upper state population. The discharge tube and the monochromator were adjusted as so to minimize the effect of scattered laser beam at $5882 \overset{o}{A}$ in the spectrum. The emission and the laser induced fluorescence spectrum of the neon hollow
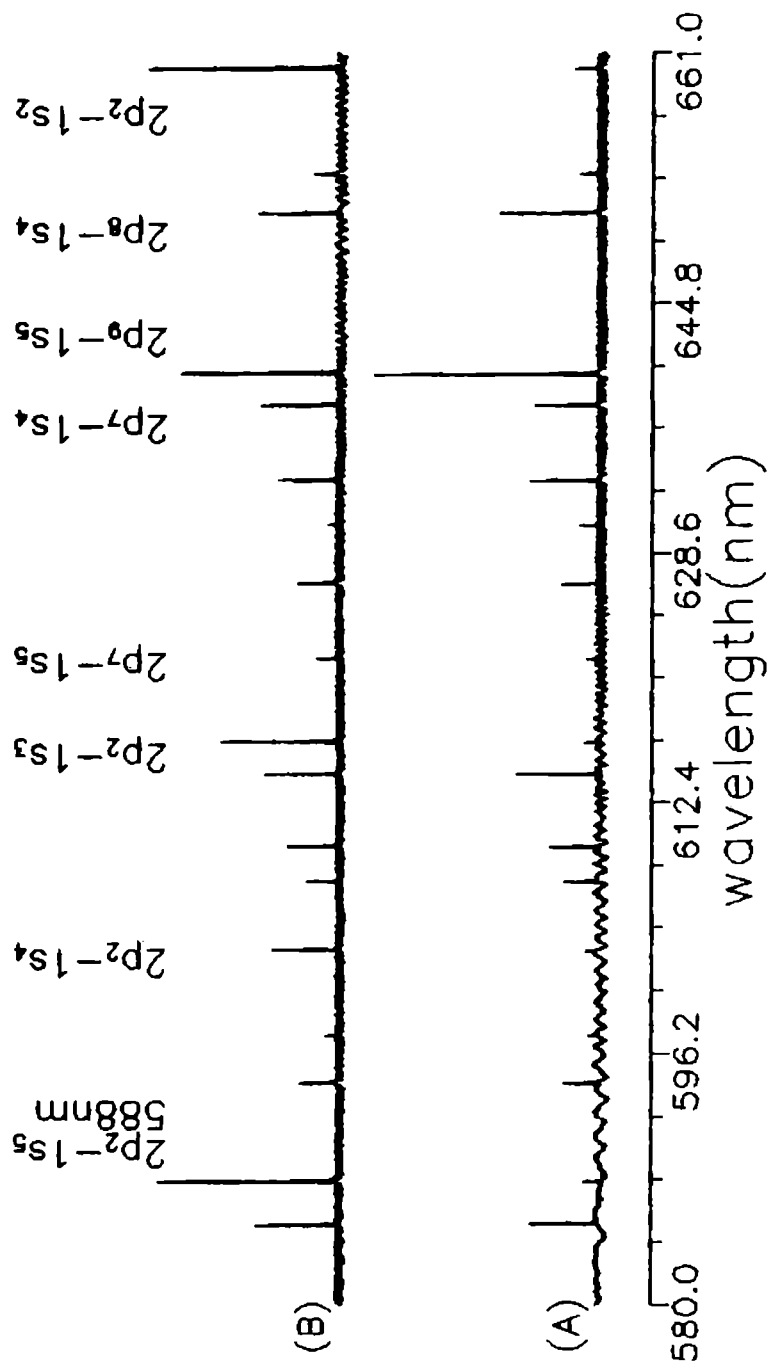
Fig 5.3 A) Emission spectrum of neon discharge at 5mA and B) the same under laser irradiation at 5882 Å, laser power 250 mW.

144

cathode at a discharge current of 5mA by laser excitation of $1s_5$ $\rightarrow$ $2p_2$ transition in neon are shown in fig 5.3. This shows that laser absorption produces a noticeable change in the emission characteristics of the discharge. These changes are mainly due to modifications in the population of $2p_2$ state and non-radiative decay from $2p_2$ state to $2p_j$ ($j \neq 2$) state and also depends on the coupling of these levels to the ground state. Measurements of variation in emission intensity of $2p_2$ $\rightarrow$ $1s_i$ ($i = 2,3,4$ and 5) transitions as a function of the discharge current (fig 5.4a,b,c,d) show that in presence of laser beam, the emission intensities are non-linear functions of current while in the absence of laser excitation they have a linear dependence. The enhancement in the intensity of these transitions during laser excitation indicates that the population of the $2p_2$ state increases considerably. The emission intensity of $2p_1 \rightarrow 1s_2$ also shows slight increase (fig 5.4e) under laser irradiation due to collisional excitation of atoms from $2p_2$ to $2p_1$ level. The emission intensity for transitions $2p_3 \rightarrow 1s_4$, $2p_4 \rightarrow 1s_4$ and $2p_4$ $\rightarrow$ $1s_5$ (fig 5.4 f,g,h) shows a slight increase during laser excitation while in the case of $2p_5 \rightarrow 1s_3$ and $2p_5 \rightarrow 1s_5$ (fig 5.4i,j) transitions it is approximately equal with and without laser excitation. It has been established that such collisional excitation or de-excitation cross section between two levels with energy difference ΔE varies as $\exp(-\Delta E/k_b T)$ [11]. This implies that atoms in $2p_2$ level can de-excite to nearby sub levels

Continued

g) $2p_4-1s_4$

h) $2p_4-1s_3$

i) $2p_5-1s_3$

j) $2p_3-1s_5$

k) $2p_6-1s_4$

l) $2p_8-1s_3$
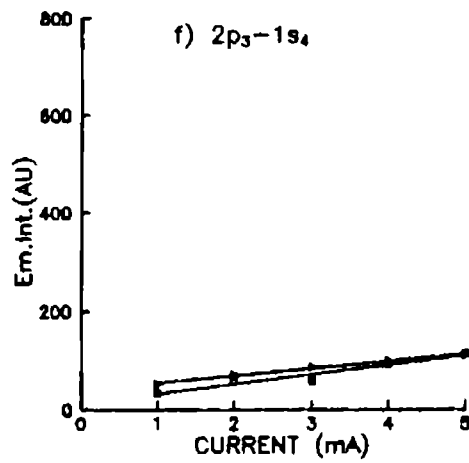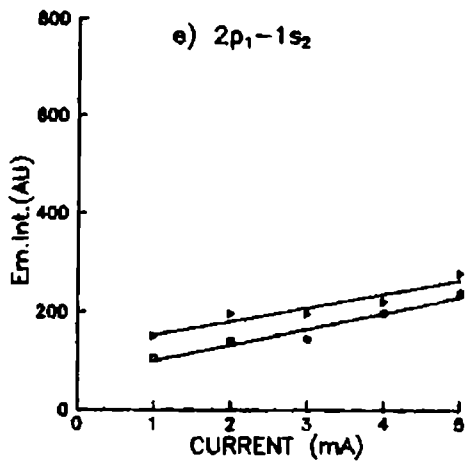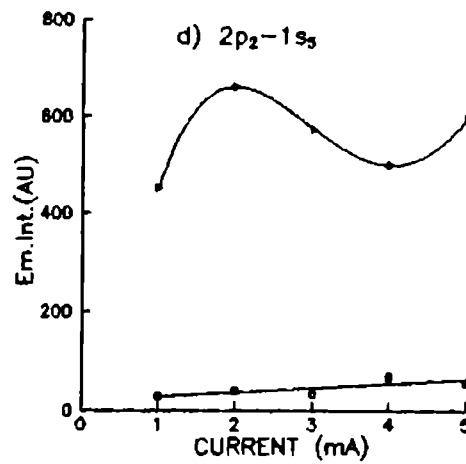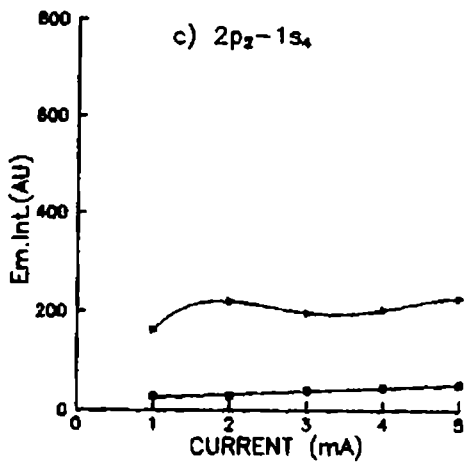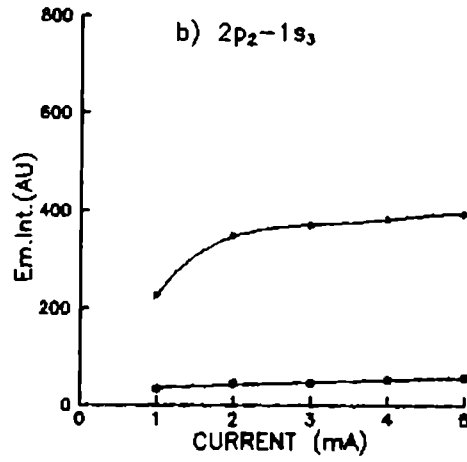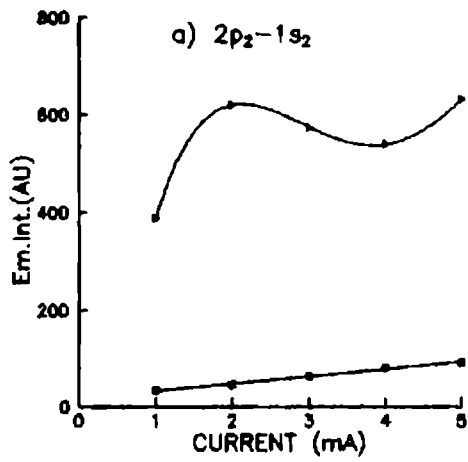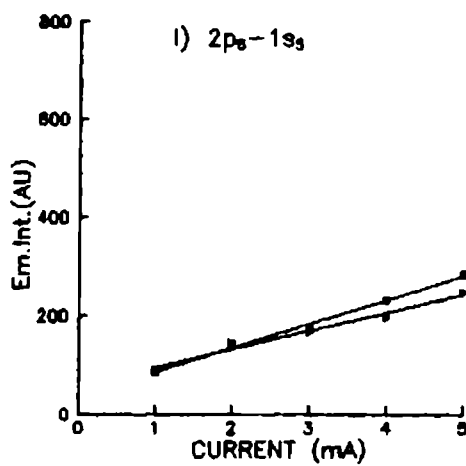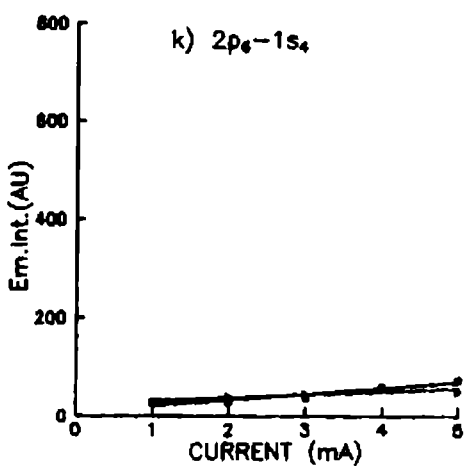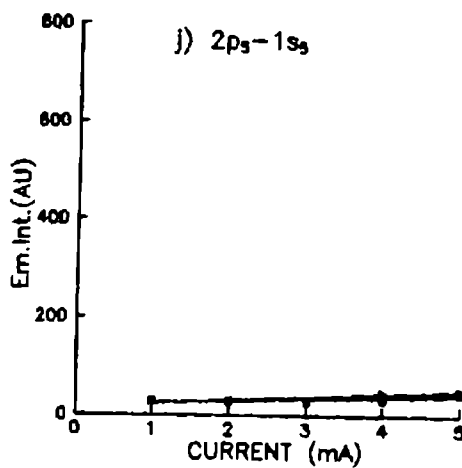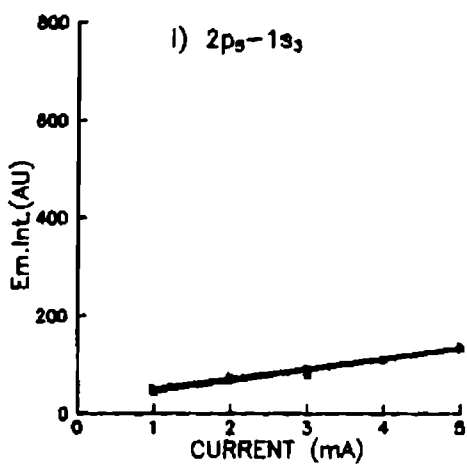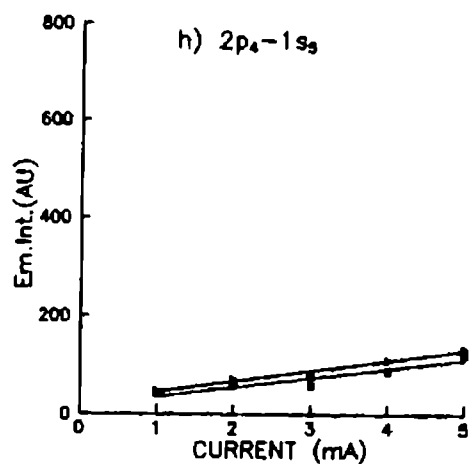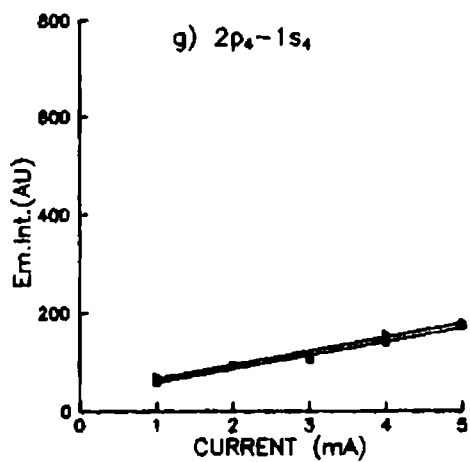
Continued
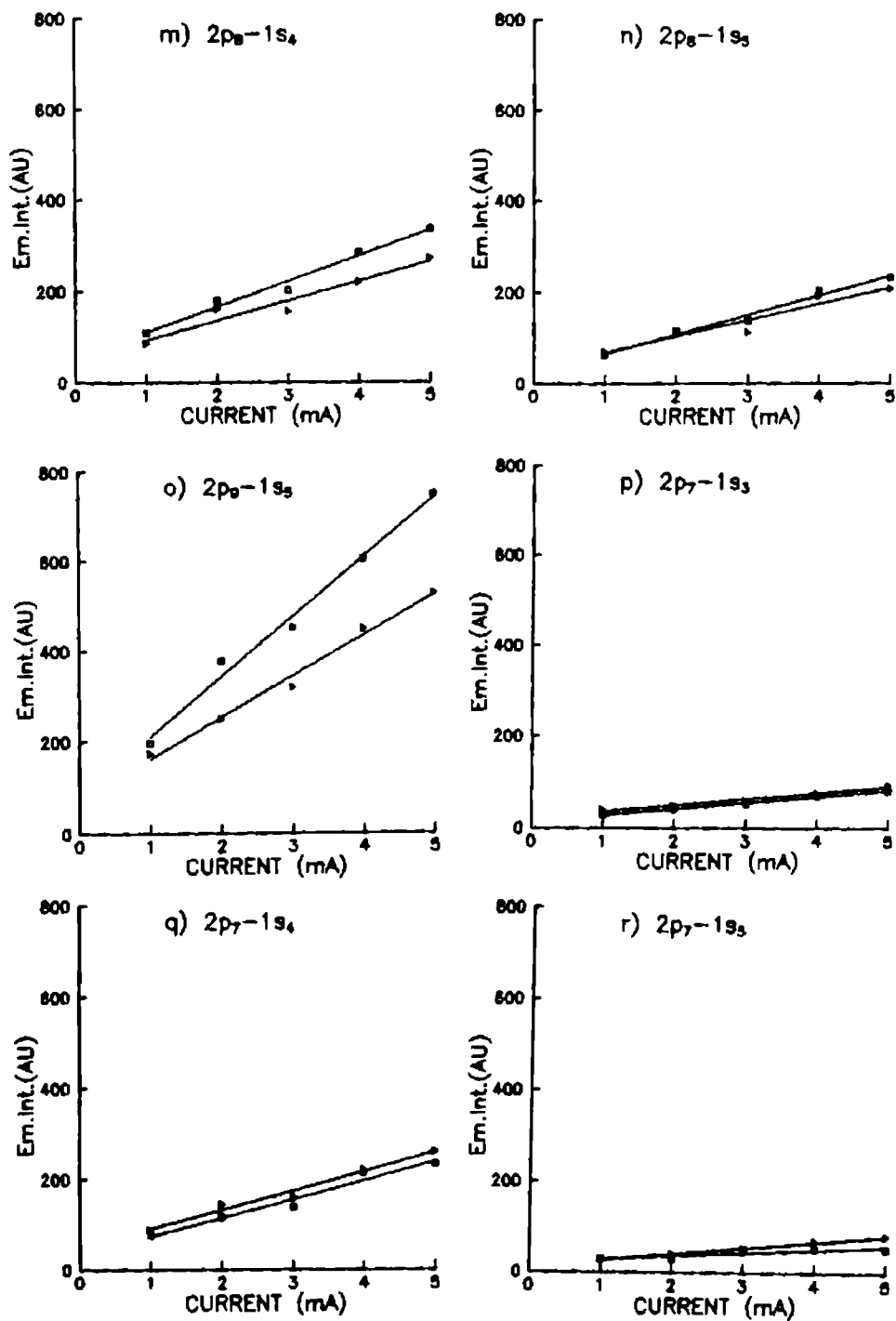
Fig 5.4 Dependence of the emission intensity for $2p_j \rightarrow 1s_i$ as function of discharge current ($\square$ - without laser, $\triangle$- with laser at 5882 Å)

(j=3,4,5) while such collisional de-excitations to $2p_j$ levels with j = 6,7,8,9,10 will be less probable. It should be noted that population of $1s_5$ level will decrease due to absorption of laser light and hence the $2p_j$ manifolds arising through electron collision from 1s level viz,

$$Ne~(1s_5) + e^- \rightarrow Ne~(2p_j) + e^-$$

will diminish. In presence of laser irradiation for $2p_6 \rightarrow 1s_4$, $2p_6 \rightarrow 1s_5$, $2p_8 \rightarrow 1s_4$, $2p_8 \rightarrow 1s_5$, and $2p_9 \rightarrow 1s_5$ transitions (fig 5.4 k,l,m,n,o) decrease in intensity is observed, where a reduction in the population of $2p_j$ manifolds due to above process is large as compared to collissional de-excitation from $2p_2$ to these states. This decrease in intensity under laser excitation is predominant in the case of $2p_8 \rightarrow 1s_4$ and $2p_9 \rightarrow 1s_5$ transitions (fig 5.4m,o). However such decrease in population density in $2p_j$ levels (j = 1,3,4,5) will be compensated by non-radiative transitions from $2p_2$ state. This fact is in support of the observations that the emission intensity for transitions from $2p_j$ levels (j = 1,3,4,5) do not have any decrease under laser excitation. An exception is observed in the case of $2p_7 \rightarrow 1s_3$, $2p_7 \rightarrow 1s_4$ and $2p_7 \rightarrow 1s_5$ transitions where there is an enhancement in intensity at higher current (fig 5.4p,q,r). Observed emission lines along with their transitions and the change in intensity under laser excitation are given in table 5.1.

b) Optogalvanic signal of $1s_5 \longrightarrow 2p_2$ transition in neon

In the absence of any external source of excitation, the primary pathway for ionization goes directly through the metastable levels. The radiative relaxation paths of a state diminish the probability for their involvement in ionization. It is well known that the nature of OG signal is determined mainly by the metastable concentrations. In general, the impedance of a neon discharge increases with resonant excitation of transitions starting from $1s_3$ and $1s_5$ levels due to the depletion of these metastables and consequently the electron density and the impedance decreases in the case of transitions from $1s_2$ and $1s_4$ states which may decay radiatively to the ground state [15,16].
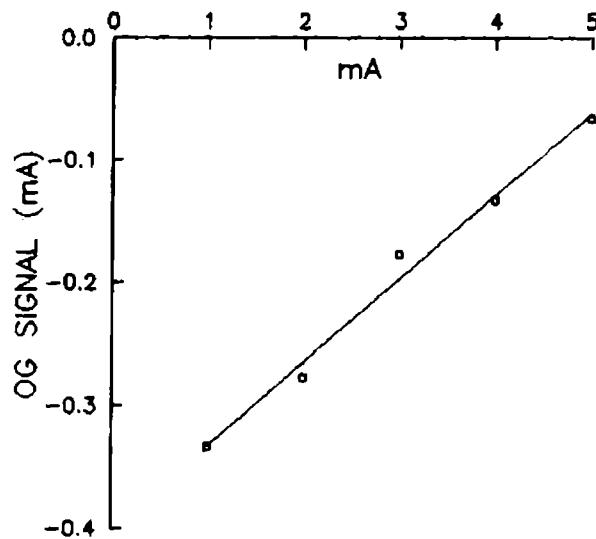
Fig 5.5 OG signal variation with current
for $1s_5 \longrightarrow 2p_2$ transition

OG spectra of Ne is well known and available in the literature [2]. Excitation at 5882 $\mathring{A}$ corresponds to $1s_5 \rightarrow 2p_2$ and transition in which the lower state $(1s_5)$ is a metastable and hence the OG signal of this transition corresponds to an increase in the discharge impedance or an equivalent decrease in current in the circuit. The observed OG signal for this transition as a function of the discharge current is shown in the fig 5.5.

5.5 LASER EXCITATION OF $1s_5 \rightarrow 2p_4$ TRANSITION (5945 $\mathring{A}$)

a) laser induced fluorescence spectrum

The emission and the laser induced fluorescence spectrum of neon discharge in the wavelength range from 5800 to 6700 $\mathring{A}$ at a discharge current of 5 mA are shown in fig 5.6. The emission intensity for both conditions varies linearly with the discharge current for all the observed transitions within this spectral region. The transitions having considerable change in emission intensities during laser-on and laser-off conditions are shown in the fig 5.7. Laser excitation at 5945 $\mathring{A}$ $(1s_5 \rightarrow 2p_4)$ modifies the emission characteristics of transitions from $2p_4 \rightarrow 1s_i$ $(i = 2,4$ and 5) which is obviously due to a large increase in the population of $2p_4$ (fig 5.7a,b,c). For $2p_3 \rightarrow 1s_4$, $2p_5 \rightarrow 1s_3$ and $2p_7 \rightarrow 1s_4$ transitions also the same behaviour is observed (fig 5.7 d,e,f) while for $2p_8 \rightarrow 1s_4$, and $2p_9 \rightarrow 1s_5$ the emission intensity during laser excitation is less than that of the unperturbed discharge (fig 5.7 g,h) For other transitions,
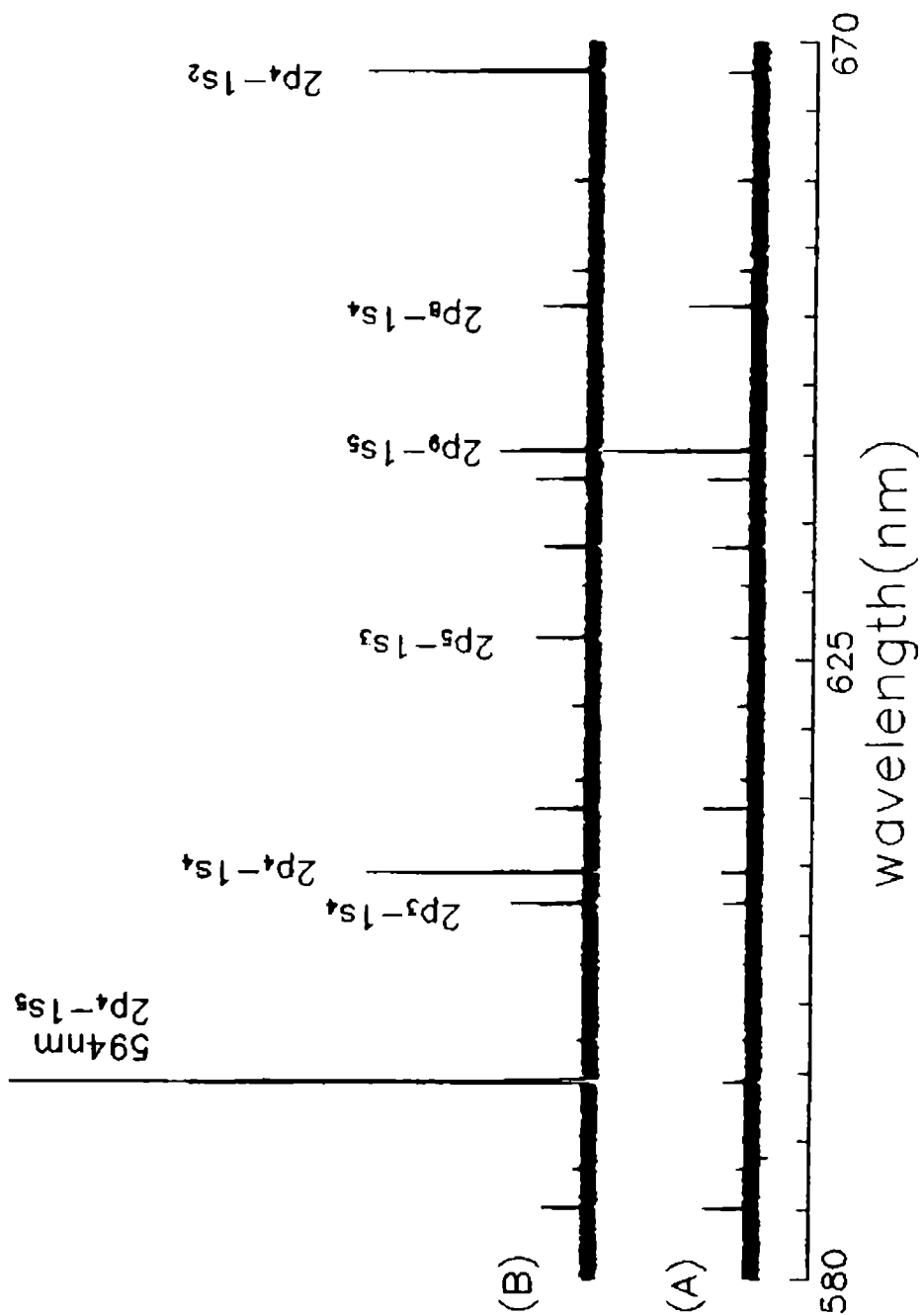
Fig 5.6 A) Emission spectrum of neon discharge at 5mA and
B) the same under laser irradiation at 5945 Å

$2p_4-1s_2$

$2p_8-1s_4$

$2p_9-1s_5$

$2p_5-1s_3$

$2p_4-1s_4$

$2p_3-1s_4$

$2p_4-1s_5$
594nm

(B)

(A)

670

625

580

wavelength(nm)

152

a) $2p_4-1s_2$

b) $2p_4-1s_4$

c) $2p_4-1s_5$

d) $2p_3-1s_4$

e) $2p_5-1s_3$

f) $2p_7-1s_4$

Continued

153
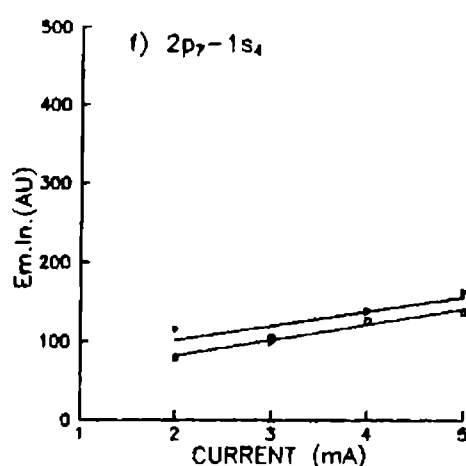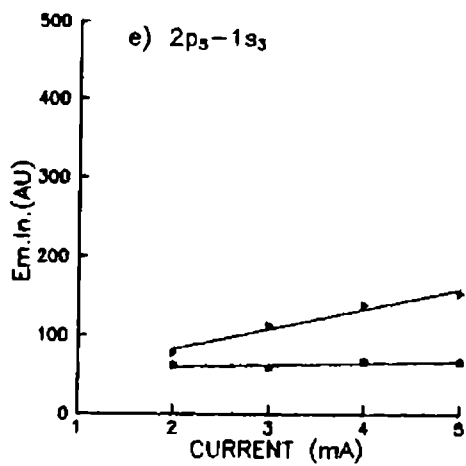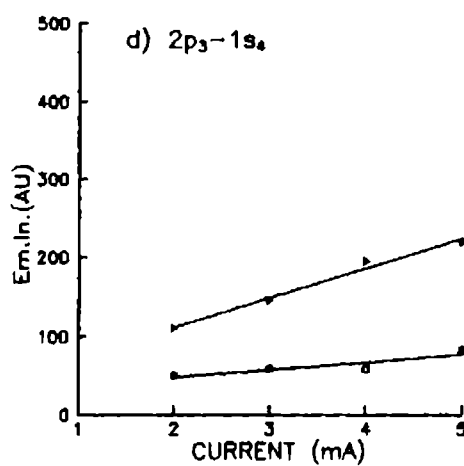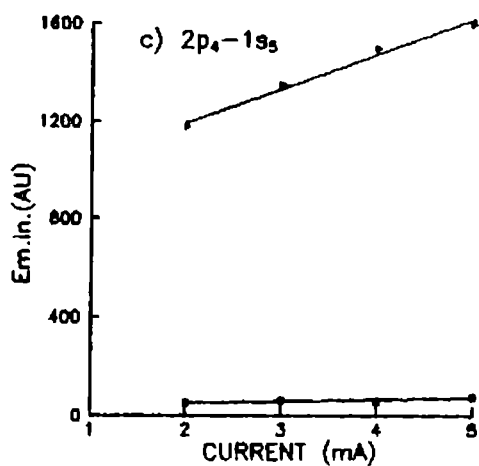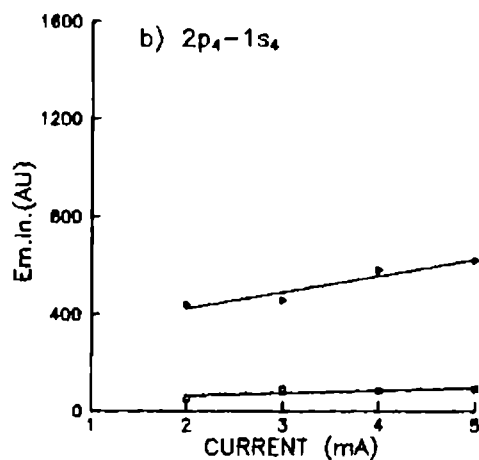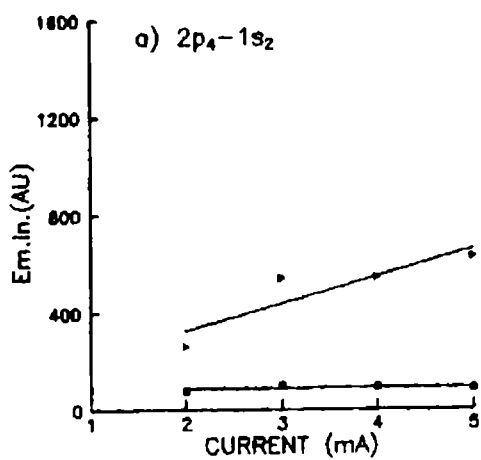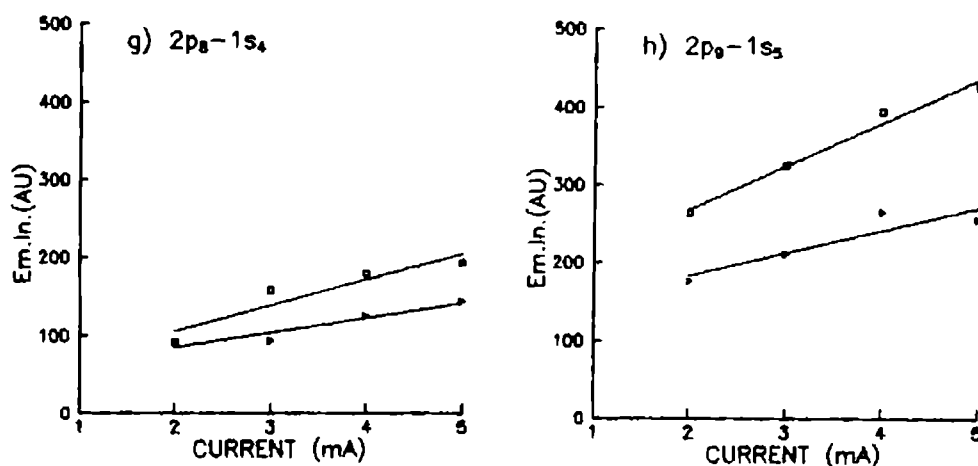
Fig 5.7 Dependence of the emission intensity for $2p_j \rightarrow 1s_i$ as function of discharge current (□ - without laser, △ - with laser at 5945 Å)

intensities under both the conditions are more or less the same, while for a few transitions change in emission intensity is observed only at higher currents. In this case also for transitions starting from states close to $2p_4$ the emission intensity increases while for those are not close to $2p_4$ shows a decrease in emission intensity (table 5.1). This indicates that, for both cases, processes like the collisional mixing between the 2p states and electron impact excitation of $1s_i$ states alters the population of 2p states resulting into the variation in the emission intensity during laser excitation. These changes for $2p_j \rightarrow 1s_i$, $j \neq 4$, are mainly arising from the modifications in the population of these states due to non-radiative decay from the $2p_4$ states and the collisional mixing between various $2p_j$ states.

Table 5.1. Change in emission intensities under laser excitation

at 588.2nm and 594.5 nm with a discharge current of 5mA

Wavelength nm	Transition	$(I_L - I)/I$ [#]	
		$1s_5 \rightarrow 2p_2$ [$]	$1s_5 \rightarrow 2p_4$ [*]
585.2	$2p_1 \rightarrow 1s_2$	0.17	~ 0
588.2	$2p_2 \rightarrow 1s_5$	9.23 [@]	0.23
594.5	$2p_4 \rightarrow 1s_5$	0.09	22.0 [@]
597.5	$2p_5 \rightarrow 1s_5$	0.12	0.17
603.0	$2p_2 \rightarrow 1s_4$	3.33	~ 0
607.4	$2p_3 \rightarrow 1s_4$	-0.03	1.50
609.6	$2p_4 \rightarrow 1s_4$	0.03	5.06
614.3	$2p_6 \rightarrow 1s_5$	-0.12	0.07
616.3	$2p_2 \rightarrow 1s_3$	5.79	~ 0
621.7	$2p_7 \rightarrow 1s_5$	0.55	0.02
626.6	$2p_5 \rightarrow 1s_3$	0.04	1.09
630.4	$2p_6 \rightarrow 1s_4$	-0.30	-0.16
633.4	$2p_8 \rightarrow 1s_5$	-0.10	0.06
638.3	$2p_7 \rightarrow 1s_4$	0.18	0.21
640.2	$2p_9 \rightarrow 1s_5$	-0.29	-0.53
650.6	$2p_8 \rightarrow 1s_4$	-0.18	-0.39
653.2	$2p_7 \rightarrow 1s_3$	0.14	-0.04
659.9	$2p_2 \rightarrow 1s_2$	5.85	~ 0
667.8	$2p_4 \rightarrow 1s_2$		6.12

[#] I_L and I are emission intensities with and without laser irradiation.

[$] 10 μm and [*] 5 μm - slit width of the monochromator used for recording the spectrum

[@] Intensity includes scattered radiation from the exciting laser at these wavelengths.
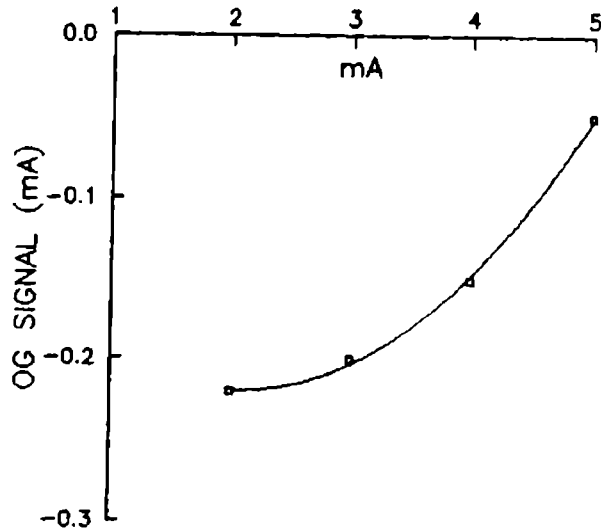
Fig 5.8 OG signal variation with current
for $1s_5 \rightarrow 2p_4$ transition

b) optogalvanic signal of $1s_5 \rightarrow 2p_4$ transition in neon

Transition at 5945 $\overset{\circ}{A}$ corresponds to $1s_5 \rightarrow 2p_4$ in which $1s_5$ is a metatstable state and hence the OG effect at this wavelength will cause an increase in the discharge impedance or will be an equivalent decrease in current in the circuit. Fig 5.8 shows the variation of the OG signal as a function of the discharge current.

5.8 POPULATION DENSITY IN THE DISCHARGE

A rate equation approach, by considering the prominent excitation and de-excitation processes, can be used to determine the perturbations in the population of states by resonant laser excitation and is useful to explain qualitatively some important

processes in the discharge that lead to optogalvanic effect. A number of papers based on the rate equation formalism have been published, for certain transitions in neon positive column discharges [11,12,14,15,17]. In these models, terms corresponding to multistep ionization, various collisional excitation and decay processes were included to give a correct description of the experimental findings. Van Velhuizen et al [18] have used, the rate equation approach to explain the observed OG signal for certain transitions in a neon hollow cathode discharge (hcd) lamp. In this section we make use of the rate equation approach to explain the OG effect for $1s_5 \rightarrow 2p_2$ transition.

The excitation and decay processes along with their rate constants are shown in the energy level diagram (fig 5.2). Various rate constants included in the model are as follows.

1. Direct excitation

$$Ne(^1S_0) + e^- \rightarrow Ne^* + e^-$$
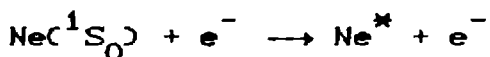
This represents the excitation of the ground state atoms by direct electron impact with a rate constant α_m. The rate constant is a strong function of E/N_o where E is the field and N_o is the density of the ground state atoms.

2. Direct ionization

$$Ne^* + e^- \rightarrow Ne^+ + 2e^-$$
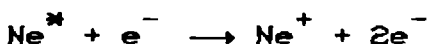
This is the ionization by collision of excited atoms and electrons with a rate constant γ_m. This process depends on both the direct electron impact ionization of metastables/excited

state and the indirect processes involving electron excitation of higher levels followed by radiative decay to the lower excited state.

3. Spontaneous emission on allowed radiative transitions with a rate coefficients A_{ij}.

4. Stimulated absorption of $1s_5 \longrightarrow 2p_2$ transition with a rate coefficient BI, where I is the intensity of the laser radiation

5. The diffusion to the wall with a reciprocal life time τ.

Loss process of the main metastable atom is by diffusion to the tube walls. The loss rate is calculated from the relations [19].

$$\tau_{3,5} = \frac{D_m}{N_0} \left(\frac{2.4}{r} \right)^2 \qquad (5.1)$$

$$\text{where } D_m = 7.6 \times 10^{18} [m^{-1}(sec)^{-1}] \; T^{0.73} \qquad (5.2)$$

and N_0 and T are the ground state atom density and the temperature respectively. The gas temperature is assumed to be 300 K throughout. The wall loss of the $1s_2$ and $1s_4$ atoms were taken from ref. *Sasso et al* [11] and *Daughty et al* [14] respectively.

The population of $2p_2$ is denoted by N_6 and that of $1s_1$ states are denoted as N_i ($i=2$ to 5). The steady state populations of the $2p_2$ and $1s_1$ levels can be obtained from the rate equations,

$$\frac{dN_6}{dt} = \alpha_6 N_0 n - \gamma_{67} N_6 n - \sum_{i=2}^{5} A_{6i} N_6 + BI\left[N_5 - \frac{g_5}{g_6} N_6\right] \qquad (5.3)$$

$$\frac{dN_5}{dt} = \alpha_5 N_0 n - \gamma_{57} N_5 n + A_{65} N_6 + BI\left[\frac{g_5}{g_6} N_6 - N_5\right] - \tau_5 N_5 \qquad (5.4)$$

$$\frac{dN_4}{dt} = \alpha_4 N_0 n - \gamma_{47} N_4 n + A_{64} N_6 - \tau_4 N_4 \qquad (5.5)$$

$$\frac{dN_3}{dt} = \alpha_3 N_0 n - \gamma_{37} N_3 n + A_{63} N_6 - \tau_3 N_3 \qquad (5.6)$$

$$\frac{dN_2}{dt} = \alpha_2 N_0 n - \gamma_{27} N_2 n + A_{62} N_6 - \tau_2 N_2 \qquad (5.7)$$

Contribution of terms due to metastable-metastable collision are neglected in these calculations.

The electron density n, in the discharge with (n_{on}) and without (n_{off}) laser excitation were calculated from the relation [11]

$$i = 2h_0 e\pi r^2 v_d n \qquad (5.8)$$

where i is the tube current, r is the radius of the discharge plasma and $2h_0$ is the Tongs-Langmuir constant, which is for a cylindrical cell, varies from 0.42 to 1 depending on the mean free path. In our calculations $2h_0$ is approximately taken as one [20]. The drift velocity v_d for different discharge conditions were evaluated from the reported data [21].

The change in the discharge current due to the perturbations in the electron density by laser excitations is given by,

$$\Delta i = e\pi r^2 v_d \Delta n \qquad (5.9)$$

$$\Delta n = n_{on} - n_{off} \qquad (5.10)$$

Fig 5.9 shows the variation of the change in the electron density as a function of the discharge current, during laser excitation at 5882 Å.

The steady state equations $(dN_m/dt = 0)$ are solved for laser-off and laser-on conditions and N_m are calculated for both conditions. The values of various rate constants used in the calculations are listed in the table 5.2.
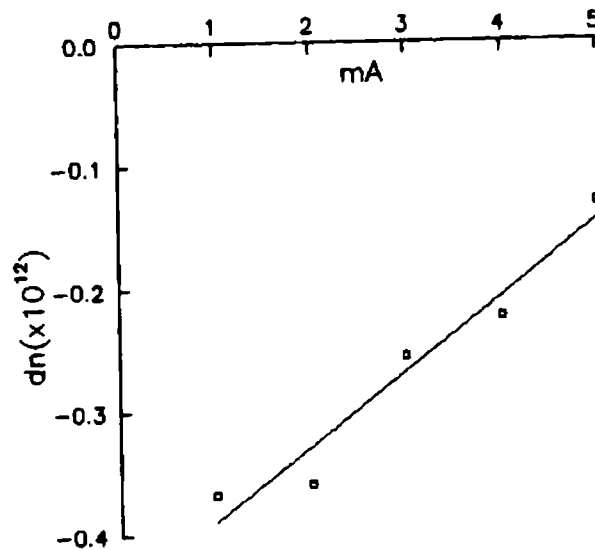
Fig 5.9 Change in electron density with current during laser excitation at 5882 Å

Table 5.2

$$\alpha_3 \simeq \alpha_5 = 1\times10^{-11} \; cm^3/sec \qquad [15]$$

$$\alpha_2 \simeq \alpha_4 = 5\times10^{-12} \; cm^3/sec$$

$$\alpha_6 = 1\times10^{-12} \; cm^3/sec$$

$$\gamma_{67} = 2\times10^{-8} \; cm^3/sec$$

$$\gamma_{27} = \gamma_{37} = \gamma_{47} = \gamma_{57} = 6\times10^{-9} cm^3/sec$$

$$A_{62} = 2.32\times10^7 \; sec^{-1}$$

$$A_{63} = 1.46\times10^7 \; sec^{-1}$$

$$A_{64} = 0.56\times10^7 \; sec^{-1}$$

$$A_{65} = 1.15\times10^7 \; sec^{-1}$$

$$\tau_3 = \tau_5 = 350 \; sec^{-1} \qquad [19]$$

$$\tau_2 = 1.65\times10^6 \; sec^{-1} \qquad [8]$$

$$\tau_4 = 1\times10^5 \; sec^{-1} \qquad [14]$$

$$BI = 1.446\times10^5 sec^{-1}$$

$$N_0 = 3.218\times10^{17} \; atoms/cm^3$$

$$r = 0.25 \; cm$$

5.7 MECHANISM OF OG EFFECT

Calculations show that, laser excitation of $1s_5 \rightarrow 2p_2$ transition, increases the population of the upper level at least by a factor of ten (fig 5.10a). This can also be seen from the experimental observations (fig 5.4a) in which the laser induced emission intensity enhances 5-8 times depending on the discharge

current. Laser irradiation causes an increase in the $1s_2$, $1s_3$ and $1s_4$ states which is due to the radiative decay from various $2p_j$ states (fig 5.10). $1s_2$ and $1s_4$ levels are radiatively coupled to the ground state ($^1S_0$) and are supposed to have least contribution to the OG effect. The changes for metastable population are much higher than that of $1s_2$ and $1s_4$ states. In the absence of laser excitation, the population of the $1s_3$ and $1s_5$ metastables in the discharge vary slightly with the current. Laser excitation causes considerable decrease in the $1s_5$ density, which was maximum at the low current. In the positive column discharges under laser excitation of the same transition, Kane [15] observed that the population of $1s_5$ is significantly depleted and for all other $1s_i$ levels the population is increased.

These observations indicate that the major factor that influences the generation of the OG signal is the modifications in the ionization processes as a result of the perturbations in the populations of states. The laser excitations at the above wavelength (λ = 5882 $\mathring{A}$) results an in increase in the population of $2p_2$, $2s_2$ and $1s_4$ levels while it decreases in the case of $1s_5$ state.

In the case of $1s_5 \longrightarrow 2p_2$ laser excitation, contributions to OG effect due to $1s_2$, $1s_4$ and $2p_2$ states, which are radiatively coupled to the lower states, are negligible where as the role of $1s_3$ and $1s_5$ metastables are prominent. Even though, the $2p_2$
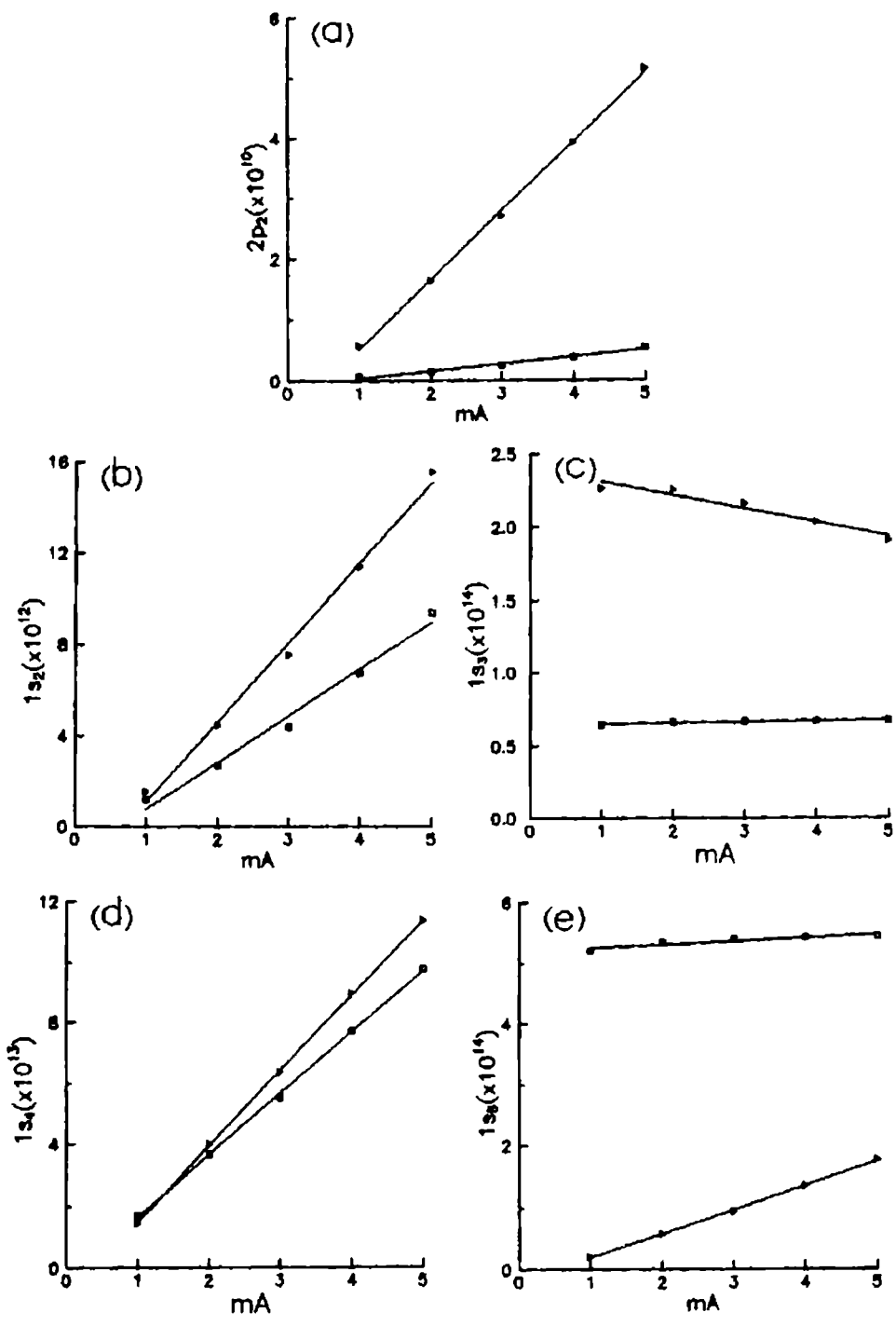
Fig 10 Population density of $2p_2$ and $1s_i$ ($i=2,3,4,5$) states
($\square$ - without laser, Δ - with laser at 5882 Å)

163

state population increases considerably, strong radiative coupling of this state to $1s_1$ levels and non radiative decay to $2p_j$ ($j\neq 2$) levels will enhance the laser induced fluorescence phenomenon and reduce its contribution to ionization. In the range of current studied, the change in the $1s_3$ state density is almost independent of current and will support the ionization processes. Thus, overall depletion in the metastables will reduce the ionization and hence increases the impedance of the discharge during laser excitation of $1s_5 \longrightarrow 2p_2$ transition in neon is expected.

It is noted from the calculations that the density of $2p_2$ state vary linearly during laser excitation (fig 5.10), while that for all $2p_2 \longrightarrow 1s_1$ transitions in the presence of laser irradiation the emission intensities are actually non-linear function of the discharge current as shown by experimental observations (fig 5.4). This observation necessitates the modification of the rate equations, and requires the consideration of all the 2p states separately along with the inclusion of all the laser perturbed collisions, radiative and non-radiative processes [11].

The observations described above clearly indicate that the major factors which influences the OG signal are the modifications in the ionization processes as a result of the perturbations in the populations of states. As shown in fig 5.7 and fig 5.8 the current dependence of OG signal corresponding to

5882 Å and 5945 Å excitations differ widely. This indicates that apart from the metastable nature of the lower level, there exists other processes which will affect magnitude of the OG signal. One such process is due to the change in ionization rate as a result of collisional mixing between $2p_j$ states followed by laser irradiation which is different for these two transitions.

Modifications in the emission characteristics of a neon hollow cathode discharge due to resonant absorption of $1s_5 \rightarrow 2p_2$ and $1s_3 \rightarrow 2p_4$ transitions are investigated. In both cases, the emission properties are found to be altered significantly as a result of changes in the population of $2p$ states by radiative and non-radiative processes. The qualitative analysis of a set of simplified rate equations of states indicate that the OG effect for $1s_5 \rightarrow 2p_2$ transition in neon hollow cathode is generated as a result of decrease in the ionization due to the depletion of metastable states. Electron impact ionization, population mixing between $2p$ states and their decay path to $1s_1$ states significantly affect the magnitude of the OG signal.

REFERENCES

1   R B Green, R A Keller, G G Luther, P K Schenck and J C Travis
        Appl. Phys. Lett. 29 (1978) 727
2   J E M Goldsmith and J E Lawler Contemp. Phys. 22 (1981) 235
3   J E Lawler Phys. Rev A 22 (1980) 1025
4   M Meada, Y Nomiyama and Y Miyazoe Opt. Comm. 39 (1981) 64

5   W H Richardson, L Maleki and E Garmire Phys.Rev.A 36 (1987)
    5713

6   E Arimondo, M G DiVito and K Ernst and M Inguscio Opt.Lett. 9
    (1984) 530

7   V Sofonea and I I Popescu Opt.Comm. 60 (1986) 302

8   A Sasso, M G Di Vito and E Arimondo Opt.Comm.68 (1988) 270

9   H A Bachor, P J Manson and R J Sandeman Opt.Comm. 43 (1982)
    337

10 E F Zalewski, R A Keller and R Engleman Jr. J.Chem.Phys.70
    (1979) 1015

11 A Sasso, M Ciocca and E Arimonto J.Opt.Soc.Am.B 5 (1988)
    1484

12 E De Marinus and A Sasso J.Appl.Phys. 63 (1988) 649

13 C Dreze, Y DEmers and J M Gagne J.Opt.Soc.Am. 72 (1982) 912

14 D K Daughty and J E Lawler Phys.Rev.A 28 (1983) 773

15 D M Kane J.Appl.Phys. 56 (1984) 1267

16 G Erez, S Lavi and E Miron, IEEE J.Quantum Electron. 15
    (1979) 1328

17 D M Kane Opt.Comm. 47 (1983) 317

18 E M van Veldhuizen, F J de Hoog and D C Schram J.Appl.Phys.
    56 (1984) 2047

19 R S Stewart, K W Mc Knight and K I Hamad Phys.D:Appl.Phys.
    23 (1990) 832

20 L Tonks and I Langmuir Phy.Rev. 34 (1929) 876

21 C Brown Basic Data on Plasma Physics (Wiley, New York, 1959)
    p65

SPECTRAL PROFILE OF OPTOGALVANIC SIGNAL

6.1 INTRODUCTION

The spectral profile of any atomic or molecular transition is associated with a finite spread of energy levels involved in the transitions. Three different processes that contribute to the finite width of a spectral line are natural broadening, Doppler broadening and interaction with neighboring particles caused by external effects like pressure broadening [1,2]. Line shape may be studied experimentally either by emission or absorption methods using instruments having negligible instrumental line width. The resultant shape of a spectral line depends on various line broadening processes and the magnitude of broadening is measured in terms of full width at half maximum.

The width and shape of spectral lines are of interest since they can provide information about temperature, density and composition existing in the source. Further, a detailed calculation of interactions involving radiation and atoms require an accurate knowledge of the spectral profile. Broadening in electrical discharges is mainly associated with temperature and collision effects which are commonly known as Doppler and pressure broadening respectively.

6.2 DOPPLER BROADENING

Doppler broadening arises as a result of Doppler effect

which is the apparent shift in wavelength of signal from a source moving towards or away from an observer. Due to Doppler effect, the resonance frequency of the atom is shifted such that $\omega = \omega'(1 \pm v/c)$ where ω' is the resonant frequency and v is the velocity of atoms in the direction towards or away from the direction of the electromagnetic field. Since the atoms are in random thermal motion with a Maxwellian velocity distribution the Doppler broadened line profile will have a Gaussian shape [2] viz.,

$$g(\omega) = \frac{2}{\Delta\omega_D} \left(\frac{\log 2}{\pi}\right)^{1/2} exp\left[-4\log 2 \frac{(\omega - \omega')^2}{(\Delta\omega_D)^2}\right]$$

(8.1)

where ω' is the resonant frequency. The width of a Doppler broadened spectral line is given by the expression,

$$\Delta\omega_D = 2\frac{\omega}{c} \left(\frac{2k_b T}{M} \log 2\right)^{1/2}$$

(8.2)

where M is the atomic or molecular weight. The Doppler width can be considerably minimized by operating the discharges at very low current or by cooling the source to very low temperature.

8.3 PRESSURE BROADENING

In discharges, the atoms are subjected to interactions with the neighbouring atoms, ions or electrons which will perturb the

states of the radiating atom and lead to the broadening of spectral line [3]. Since the line width is a function of the density of the perturbing species, this is generally known as pressure broadening. According to the theory of impact approximation, the interaction with the nearest perturbing particles at a distance r from the atom leads to a frequency shift given by

$$\Delta \nu = \frac{C_n}{r^n} \qquad\qquad (6.3)$$

where n is a whole number and C_n is a constant which depends on the excited level involved and also on the perturbing species. The case $n = 3$ gives rise to stark effect of energy levels which hold good for hydrogen and hydrogenic ions while $n = 5$ lead to quadratic stark effect which holds good for non hydrogenic systems. $n = 2$ applies to the case of resonance dipole-dipole interactions and the long-range attractive Van der Waal dipole-dipole interaction is described by $n = 6$. The first two interactions are important for highly ionized gases where as in the case of low current discharges the resonance and the Van der Waal interactions are the most significant for line broadening. The spectral distribution corresponding to pressure broadening is Lorentzian [3] with FWHM given by

$$\Delta \omega_{1/2} = \gamma + 1/\tau_c \qquad\qquad (6.4)$$

where $1/\tau_c$ is the mean number of collisions per unit time and γ is the radiative decay rate.

6.4 OG SPECTRAL PROFILE

In recent years, high resolution laser spectroscopic study in electrical discharges, especially in negative glow discharges have attracted considerable interest. In particular, OG effect has been greatly used for a large number of high resolution spectral studies of both atomic and molecular species. The change in electrical behavior of gas discharges as a result of resonant absorption by atoms in a particular state is a complex process, that depends on the microscopic processes like optical absorption and the macroscopic effect of changes in the plasma current. OG line profile for transitions in calcium, lithium, sodium [4], neon [5], etc. were reported. Bechor et al [6] have compared the line profile obtained from absorption and OG methods and showed that both techniques yield the same result for certain conditions of the plasma. At low currents the profile for both methods were identical where as at higher currents some profile were distorted and sign reversal were also observed. Since the local plasma parameters and the geometry of the plasma are current dependent, these distortions are due to the summation of individual local line profile along the optical path which is also a complex function of current. As an alternative to conventional methods, collision processes in discharges can be

investigated using laser optogalvanic spectroscopy [7-9].

The signal to noise ratio of the OG signal is better than that of the absorption method so that it is possible to record profile in situations where the peak absorption is very small. Moreover, in a discharge, the atoms are in excited state so that higher energy levels of the atom can be easily studied. Another advantage of the method is that scattered/background radiation or the apparatus profile will not affect the line width and measurements up to the line width of the dye laser can be achieved without much difficulty. When the OG effect is linear with the laser intensity, so that no saturation or distortion occurs in the profile, OG detection can be used as quantitative method for line profile spectroscopy such as the determination of line broadening effects [7,8]. This method has also been used for the accurate measurement of gas temperature in cathode fall region of neon discharge [5,10], the determination of isotope concentration [11], collision cross section [8] and shift of spectral line [7].

We have studied the OG spectral profile of certain transitions in a sealed neon hollow cathode as well as in a glow discharge and in a continuous gas flow nitrogen positive column discharge. The experimental setup employed is same as in fig 4.3. The wavelength of the single mode ring dye laser is tuned through the absorption profile with a speed of 15GHz/min and the OG signal is recorded using a lock-in amplifier. Fig 6.1 shows the
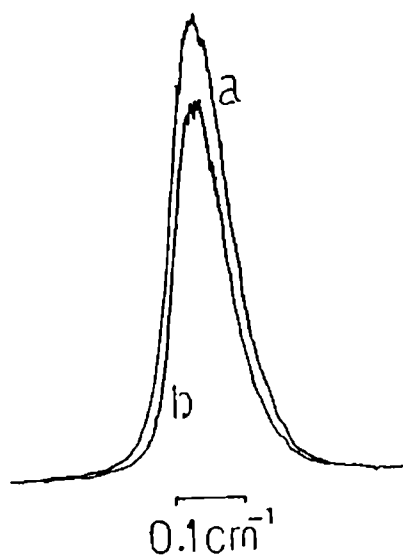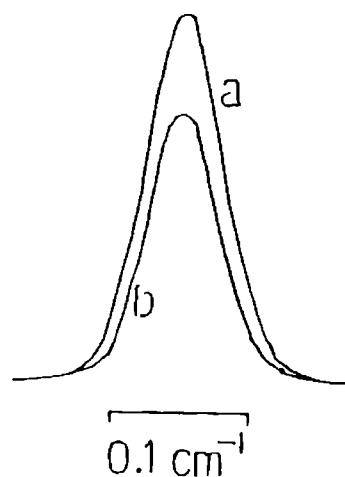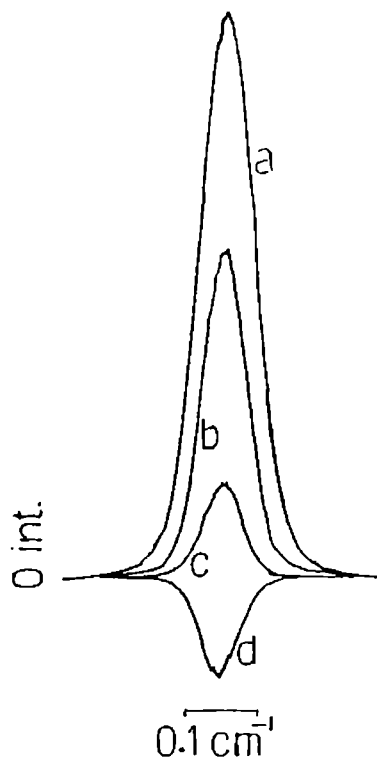
Fig 6.1

OG Spectral profile in Neon

$(R=33K$ and laser power 350 mW$)$.

A$)$ $1s_2 \to 2p_2$ a$)$ 15mA, b$)$ 12mA

B$)$ $2p_8 \to 4d_4$ a$)$ 3mA b$)$ 1mA and

C$)$ $2p_9 \to 4d_4$ a$)$ 15mA, b$)$ 8mA,

              c$)$ 4mA d$)$ 3mA

OG spectral profile for $1s_2 \rightarrow 2p_2$, $2p_8 \rightarrow 4d_4$ and $2p_9 \rightarrow 4d_4$ transitions of neon at 5852A, 5820A and 5764A respectively. These are from higher energy states of neon with following configurations viz. $2p_8$ and $2p_9$ belonging to $2p^5 3p$ configuration, $1s_2$ in $2p^5 3s$ and $4d_4$ in $2p^5 4d$ configurations. Note that the ground state configuration is $1s^2 2s^2 2p^6$ In the case of $2p_9 \rightarrow 4d_4$ transition both positive and negative voltage changes are observed (fig 6.1c) in OG signal.

When the ballast resistance in the circuit is increased the OG signal amplitude increases but the FWHM was always same for all resistances at constant current and laser power, which indicates that there is no influence of ballast resistance in broadening of OG profile (fig 6.2). The spectral profile for $R_{12}(6)$ rotational transition of (12,8) band of the first positive system of nitrogen molecule at 17388.7cm^{-1} is also recorded.

It is observed that the FWHM (γ in cm^{-1}) depends linearly on the discharge current (i) according to the relation

$$\gamma = \gamma_o + \alpha i \qquad\qquad (6.5)$$

where α is the slope of the γ-i plot. The behavior of this equation indicates that an enhancement in the discharge current produces an an increase in FWHM. The experimental data and the least square linear fit for $1s_2 \rightarrow 2p_2$, $2p_8 \rightarrow 4d_4$ and $2p_9 \rightarrow 4d_4$ transitions of neon are shown in the fig 6.3. The pressure of

Fig 6.4 Variation of FWHM with current for $R_{12}(8)$ transition of (12,8) band in the $B^3\Pi_g - A^3\Sigma_u^+$ system of N_2.
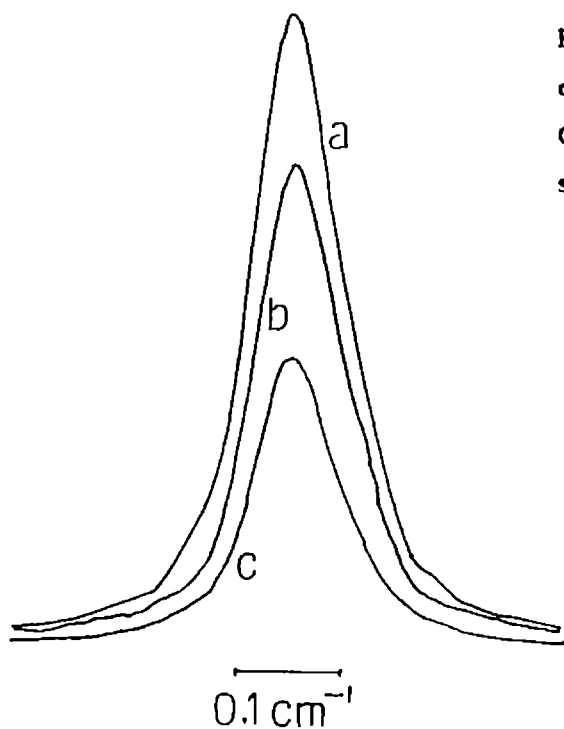
Fig 6.2 OG spectral profile for $1s_5 \to 2p_2$ transition of neon for various resistances a) 75 KΩ, b) 45 KΩ and c)10 KΩ (current 0.28mA and laser power 225mW).
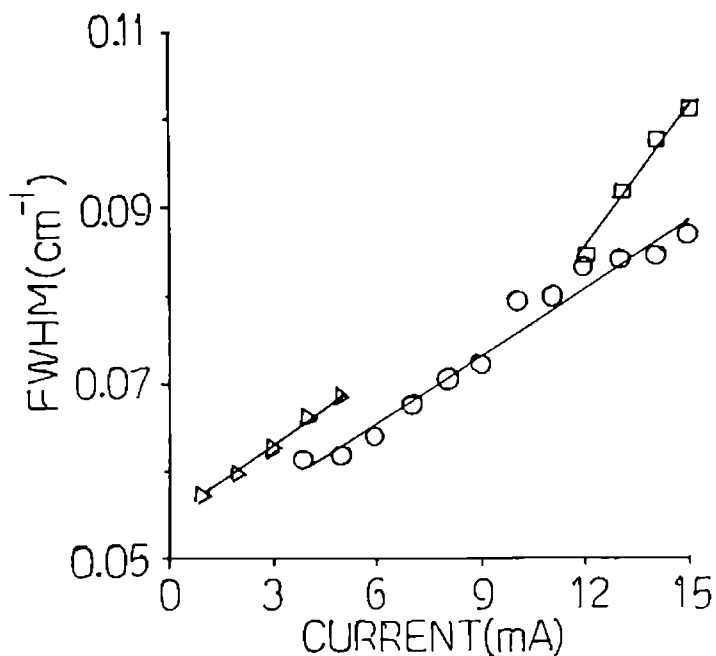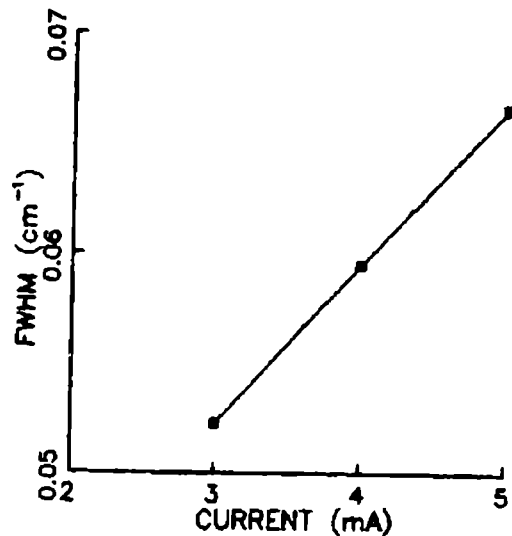
Fig 6.3 Variation of FWHM with current for neon transitions in hcd A) $2p_8 \to 4d_4$, o) $1s_2 \to 2p_2$ and O) $2p_9 \to 4d_4$.

the gas in the hollow cathode lamp was about 10 Torr which corresponds to a concentration(N) of 3.218×10^{17} atoms/cm^3 at room temperature. The the collision broadening coefficient is given by α/N.

In low pressure and low current discharges, the width is determined mainly by Doppler and pressure broadened mechanisms. Assuming the Doppler effect is the dominant line broadening process, the temperature (T) can be evaluated from the line width of the measured OG signal profile using the relation [12] as

$$\Delta\nu = 2\frac{\nu}{c}(\ \frac{2RT}{M}\ \log\ 2)^{1/2} \qquad\qquad (6.6)$$

Here $\Delta\nu$ is the FWHM in Hz and ν is the frequency at the line centre, M is the atomic or molecular weight and R is the gas constant.

According to the theory of impact approximation, the various interactions present in the discharge (with the neighboring atoms, excited states, ions, electrons etc.) will perturb the states of the radiating atoms, which will result into broadening of line according to

$$\beta = 2\sigma\nu \qquad\qquad (6.7)$$

where β is the broadening coefficient in angular frequency units, σ is the collision cross section and $\nu = (16kT/\pi m)^{1/2}$ is the

average velocity of the absorbing atom of mass m. The average temperature calculated at 5mA was about 800K with corresponding v is 1.021×10^5 cm/sec. The value of broadening coefficient and collision cross sections evaluated are listed in the table 6.1.

In the case of N_2 for $R_{12}(6)$ transition of (12,8) band in the first positive system at 17388.7cm^{-1} at 3 torr ($N = 9.65 \times 10^{16}$ molecules/cm^3 at room temperature), the value of slope γ is 0.0068 cm^{-1}/mA (fig 6.4). At 5mA, the average temperature is about 800K and v is 1.096×10^5 cm/sec. The broadening coefficient and collision cross sections evaluated from this data are also listed in the table 6.1.

TABLE 6.1

	transition	wavelength	broadening coefficient (cm^{-1}/atoms cm^{-3})	cross section (cm^2)
Ne	$1s_2 \rightarrow 2p_2$	5852 (Å)	17.34×10^{-21}	15.99×10^{-15}
	$2p_8 \rightarrow 4d_4$	5820	9.23×10^{-21}	8.52×10^{-15}
	$2p_9 \rightarrow 4d_4$	5764	7.74×10^{-21}	7.14×10^{-15}
N_2	(12,8), $R_{12}(6)$	17388.7cm^{-1}	7.05×10^{-20}	6.06×10^{-14}

6.5 DISTORTION IN THE OG LINE PROFILE

We have observed distortions in the line shape while studying the OG signal in a discharge of neon indicator lamp. A well developed dip at the line centre was observed as shown in

Fig 6.5

Distorted OG profile of $1s_5 \rightarrow 2p_2$ transition of neon in indicator lamp glow discharge. a) 0.6mA, b) 0.55 mA, c) 0.4mA, d) 0.3mA and e) 0.25mA (laser power 300mW).

$\overline{0.1\,cm^{-1}}$
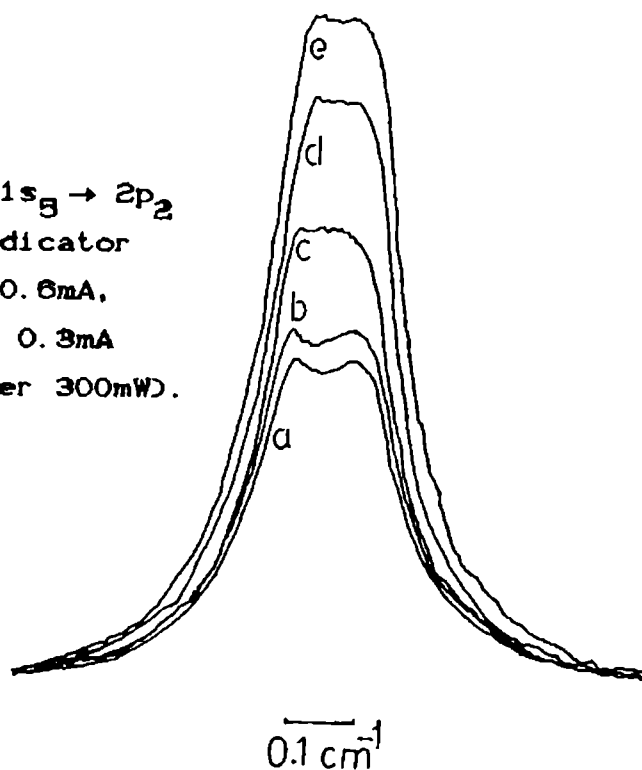
fig 6.5. The line shape of a transition as stated earlier, depends on the perturbation due to neutral and the charged particle collisions. The dip reflects the non-linear properties of the gaseous medium, which in general consists of information associated with the interaction of atoms with the laser and the neighboring atoms. Two distinct collision processes that influence the line profile are thermal velocity changing collisions (VCC) and quenching collisions (QC) [13-15]. The VCC leads to a broad background superimposed on the narrow homogeneously broadened resonance line, where as QC causes a decrease in the life time of levels. These collision processes also depend on the discharge conditions like current, pressure

etc. A detailed study of reasons for the occurrence of this distortion has not been carried out do to the experimental constraints.

6.6 SPATIAL DEPENDENCE OF THE OG EFFECT

Two important features of the OG effect are positive/negative behavior of the signal and the spatial dependence of the signal. The spatial dependence implies that amplitude and sign of the signal depend on the region within the discharge where the laser beam interacts with the plasma. Positive as well as negative signal were also reported depending on the position of the irradiating beam with in the discharge at various discharge currents [5].

In this work the spatial dependence of the OG effect is studied in a neon indicator lamp, with glow discharge formed in between a disc shaped cathode and a ring anode placed at a separation of about 2.5mm using 5882 $\overset{o}{A}$ (corresponding to resonant absorption of $1s_5 \longrightarrow 2p_2$ transition of neon) radiation from a ring dye laser. The cell is mounted on a micro positioner and the OG signal amplitude is measured for different spatial positions of the discharge glow in steps of 0.01mm at different discharge currents using a lock in amplifier. The OG signal is found to have a small amplitude for very close to the cathode (fig 6.6). As the position of irradiation is varied towards the anode, the signal becomes a positive maximum. This is the

negative glow region where there is an abundance of neon species. As the distance from the cathode is further increased, the signal become a negative maximum and then return to zero.

According to equation (2.10), magnitude of the OG signal depends on the lower state population and the sign depends on their average life time. Hence, the spatial dependence of the OG signal measures the density of species present at various region with in the discharge. Very close to the cathode, the electrons emitted from its surface have a small velocities and will recombine with ions to produce neon atoms. When the position of irradiation is slowly changed towards the anode side, the signal reaches a positive maximum. This corresponds to the region where the density of neon species is maximum and also the velocity of electrons in this region does not affect the life time appreciably. The life time of $1s_5$ metastables mainly influenced by collision between positive ions, metastables and the excited states. The collision processes make the effective life time to decrease there by causing the $1s_5$ state to loose its metastable character progressively and a condition is reached where the OG signal is negative [5]. With the increase in current the magnitude of the signal decreases due to the depletion of metastable population as a result of electron impact excitation.

The maximum positive signal obtained for different current at the same spatial position of irradiation indicates that the density of $1s_5$ state is maximum in this region which does not
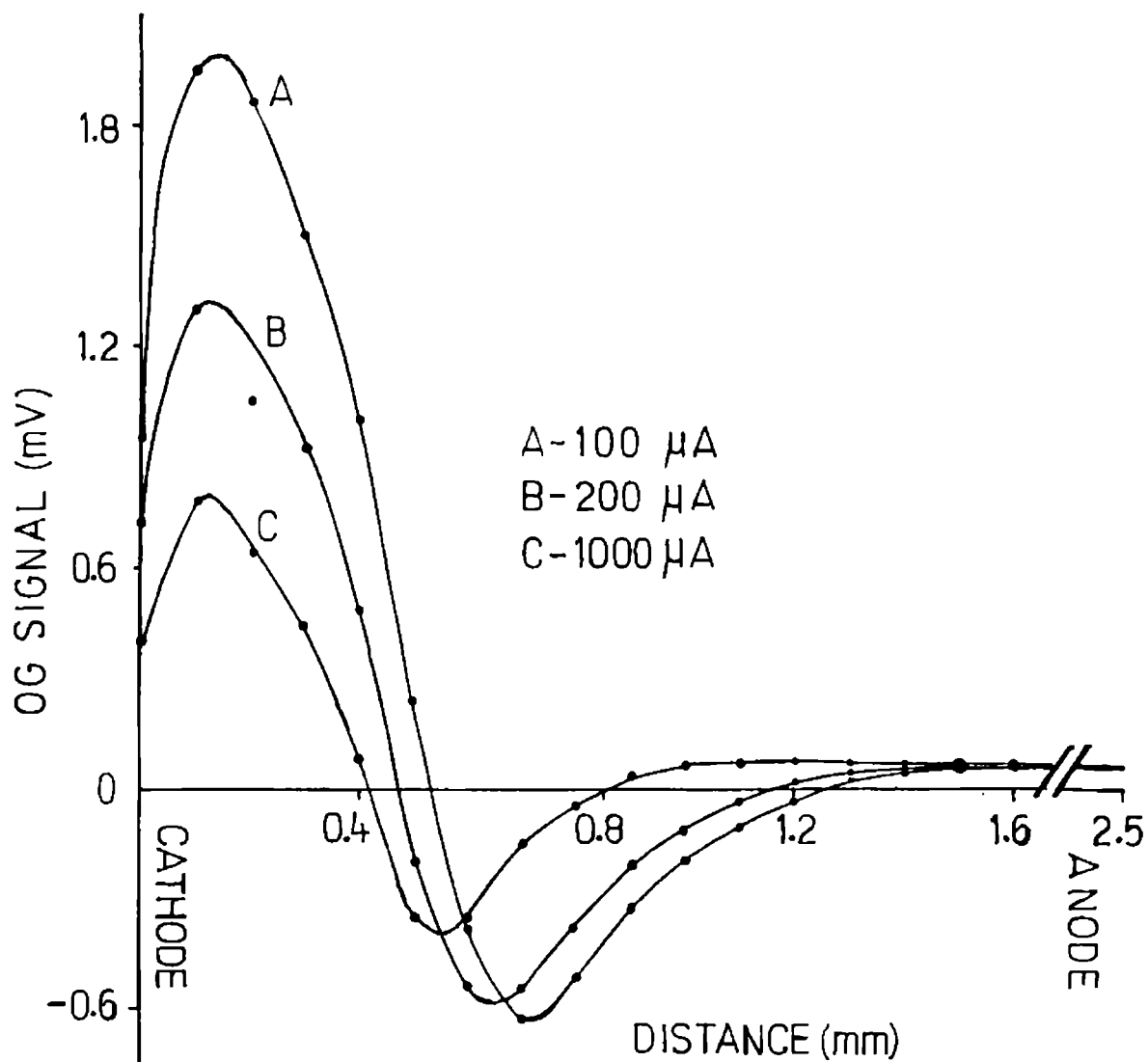
Fig 8.8 Spatial dependence of OG effect in a neon indicator lamp glow discharge for $1s_5 \rightarrow 2p_2$ transition

change considerably with the discharge current (fig 6.6).
However the increase in current shifts the region of maximum
negative OG signal towards the cathode.

In conclusion the broadening of spectral lines for certain
transitions have been studied by high resolution optogalvanic
line profile spectroscopy. Positive/negative signals with
distorted profile were recorded. The spatial dependence of the
OG signal which gives the spacewise distribution of $1s_5$ state in
a neon discharge is also investigated.

REFERENCES

1 O Svelto, Principles of lasers, (Plenum Press, New York, 1979)
2 K Thyagarajan and A K Ghatak, Lasers-Theory and applications
           (Plenum Publishing Corporation, New York 1981)
3 Alan Corney, Atomic and laser spectroscopy (Oxford University
           Press, Oxford, 1977)
4 R G Green, R A Keller, G G Luther, P K Schenck and J C Travis
           Appl.Phys.Lett. 29 (1976) 727
5 E H van Veldhuizen, F J de Hoog and D C Schram J.Appl.Phys.
           56 (1984) 2047
6 H A Bachor, P J Manson and R J Sandeman Opt.Comm. 43 (1982) 337
7 T Masaki, Y Adachi and C Hirose Appl.Spectrosco. 42 (1988) 54
8 K Naveedullah and A S Naqvi Opt.Comm. 56 (1985) 117
9 A S Naqvi and K Naveedullah, 55 (1985) 61
10 D K Doughty, J E Lawler Appl.Phys.Lett. 45 (1984) 611
11 P Pianarosa, Y Demers and J M Gagne J.Opt.Soc.Am.B 1 (1984)
           704
12 A C G Mitchell and M W Zemansky, Resonance radiation and
           excited atoms (University Press, Cambridge, 1961)
13 R H Cordover and P A Bonczyk, Phy.Rev. 188 (1969) 696

14 D M Kane and M H Dunn, Opt.Comm. 50 1984) 219

15 D S Gough and P Hannaford, Opt.Comm. 55 (1985) 91

LASER INDUCED PHOTOEMISSION OPTOGALVANIC EFFECT

7.1 INTRODUCTION

In recent years there has been growing interest in the study of photoelectric (PE) effect due to its importance in both fundamental and applied fields. In PE effect, the electrons in the solid are first optically excited into state of higher energy and then they move to the surface with or without scattering and subsequently escape from the surface. The practical applications of this effect were recognized at the beginning of this century and exploited by means of photocells, photo multipliers etc. which lead to an increase in experimental and theoretical interest. Understanding of the physics of photoemission process provides an extremely sensitive method for detailed analysis of the electronic properties of atoms, molecules, condensed matter, surface properties etc. [1]. An important aspect of PE effect is its surface sensitivity, ie. features of the emitted electrons (viz velocity, density spectral features etc.) are related to the properties of solid as defined by the outermost layers of atoms in the emitter. Hence, PE process is intrinsically influenced by surface conditions and external parameters such as photon energy, angle/region of incidence, applied voltage etc. As compared with other methods, laser driven photoelectron emission can produce intense, short duration beam with very high current density [2].

7.2 PHOTOELECTRIC EFFECT

Photoelectric effect consists in the liberation of electrons when a monochromatic radiation falls on the surface of a solid. If the energy $\hbar\omega$ of a photon exceeds the work function (ϕ) of the material, electrons of mass m will leave from the surface with an energy

$$\frac{1}{2}mv^2 = \hbar\omega - \phi \qquad (7.1)$$

Thus, the photoelectric effect will be observed if, the frequency of radiation

$$\omega \geq \frac{\phi}{\hbar} \qquad (7.2)$$

In presence of intense laser source, density of photon is so high that an electron could be eject by absorbing simultaneously two or more photons. The law of PE effect for N photon absorption is then

$$\frac{1}{2}mv^2 = N\hbar\omega - \phi \qquad (7.3)$$

and the PE effect can be observed if the condition

$$\omega \geq \phi/N\hbar \qquad (7.4)$$

is satisfied. This gives the threshold frequency $\omega_{th} = \phi/N\hbar$. The photoelectric effect therefore depends on both frequency and intensity of radiation. This N photon process is generally known

as multi photon photoelectric effect and for $N=2$ it is known as two photon photoelectric effect. Quantum theory of two photon PE effect has been described in many text books [3,4].

7.3 PHOTOEMISSION OPTOGALVANIC EFFECT

Study of PE effect in presence of discharge has importance in understanding various characteristics of the discharge plasma. The photoelectrons emitted from the cathode may excite or ionize some of the atoms on their way to the anode and produce more secondary electrons by collision. The energy absorbed by the species present in the discharge alters the charge density in the plasma and produces a measurable impedance change. Then, the total current under laser irradiation will be resultant of the original plasma current without laser irradiation and that caused by the interaction of photoelectrons emitted from the cathode surface with the plasma medium. The accelerating electric field effectively convert the low energy photoelectrons into those with sufficient energy to produce ionization in the plasma. The amplification of photoelectron burst by the plasma observed as optogalvanic signal is extremely sensitive to the discharge conditions. Thus, the optogalvanic effect produced by injecting electrons into the discharge via photoelectron emission from the cathode surface by laser irradiation is usually known as photoemission optogalvanic (POG) effect [5].

There are a few differences between OG and POG effects. OG

process is due to resonant absorption of light energy by atoms, ions or molecules of the gaseous medium or the electrode material present in the discharge which occurs only at resonant wavelength and can produce an increase or decrease in current depending on the life time of levels involved in the transitions [6,7]. POG effect is a non-resonant process where the impedance change occurs as a result of interaction of the photoelectrons emitted from the cathode surface with the discharge medium. Here, the essential condition is that the energy of radiation is required to be greater than the photoelectric threshold. Usually the interaction of photoelectrons with plasma will produce more secondary electrons which will increase the current in the circuit so that if we measure the signal across the resistance, voltage change across the resistance will be an increase (which we call as positive POG signal). However, negative change can also be generated under certain conditions of the discharge when the electron-ion recombination is a predominant process. Observation of POG effect caused by single photon absorption under various discharge conditions and its application for plasma surface characterization [5], real time monitoring of metal or semiconductor surfaces [8], diagnostics of electrodes in a discharge lamp [9] etc. have been reported.

7.4 PHOTOCURRENT UNDER PULSED LASER EXCITATION

The electron emission from solid targets irradiated by high

power laser pulses are due to either photoelectric effect or thermionic emission produced by laser induced temperature rise. For sufficiently strong electromagnetic fields, these photoemission effect may originate either by single or by multi photon process. Observation of multiphoton photoemission has more recently been observed by the use of high power, ultra short laser pulses. These lasers can produce sufficiently high irradiation necessary for the multi photon emission and because of very short duration, photoelectron emission processes are very much pronounced than the thermionic electron emission. Multi photon emission from tungsten by pulsed laser excitation has been experimentally observed by Yen et al [10].

According to generalized Fowler-Dubridge theory [11] the total electron current density is composed of partial currents given by

$$J(r,t) = \sum_{N=0}^{\infty} J_N(r,t) \qquad (7.5)$$

The quantity J_0 is due to thermionic emission and J_N is N photon photoemission photocurrent density given by

$$J_N(r,t) = a_N \left(\frac{e}{\hbar\nu}\right)^N A(1-R)^N P^N(r,t) T^2(r,t) F\left(\frac{N\hbar\nu-\phi}{k_b T(r,t)}\right) \qquad (7.6)$$

Here e is the electron charge, R is the surface reflectivity, A

is the theoretical Richardson coefficient $(120A/cm^2K^2)$, ν is th

frequency, ϕ is the work function, k_b is the Boltzman constant,

is the incident laser intensity, T is the absolute temperature o

the surface and a_N is a sample dependent constant. The functio

$F(x)$ is called Fowler function and is given by [10]

$$F(x) = \begin{cases} \sum\limits_{m=1}^{\infty} (-1)^{m+1} e^{mx}/m^2 & \text{for } x \leq 0 \\ \dfrac{\pi^2}{6} + \dfrac{x^2}{2} - \sum\limits_{m=1}^{\infty} (-1)^{m+1} e^{-mx}/m^2 & \text{for } x \geq 0 \end{cases}$$ (7.7)

Equation 7.6 indicates an important feature of the two photo:

absorption; the probability of absorption and hence th

photocurrent is proportional to the square of the incident ligh

intensity.

7.5 TWO PHOTON PHOTOEMISSION OPTOGALVANIC EFFECT

7.5.1 Experimental set up

The output radiation from a pulsed dye laser (Quanta Ray PDI

2) pumped by the second harmonic of a Q switched Nd:YAG lasei

(Quanta Ray DCR-11) was used as the excitation source. Thi

discharge was maintained in a glass tube having an inner diametei

of ~ 1 cm and length ~ 15 cm and is provided with tungstei

electrodes at a separation of about ~ 1 cm (fig 3.2). Provisioi

for continuous flow of gas into the cell at rotary vacuum ha:

also been provided. The discharge was produced by dc excitatioi

by applying a stable dc voltage. A ballast resistance i:
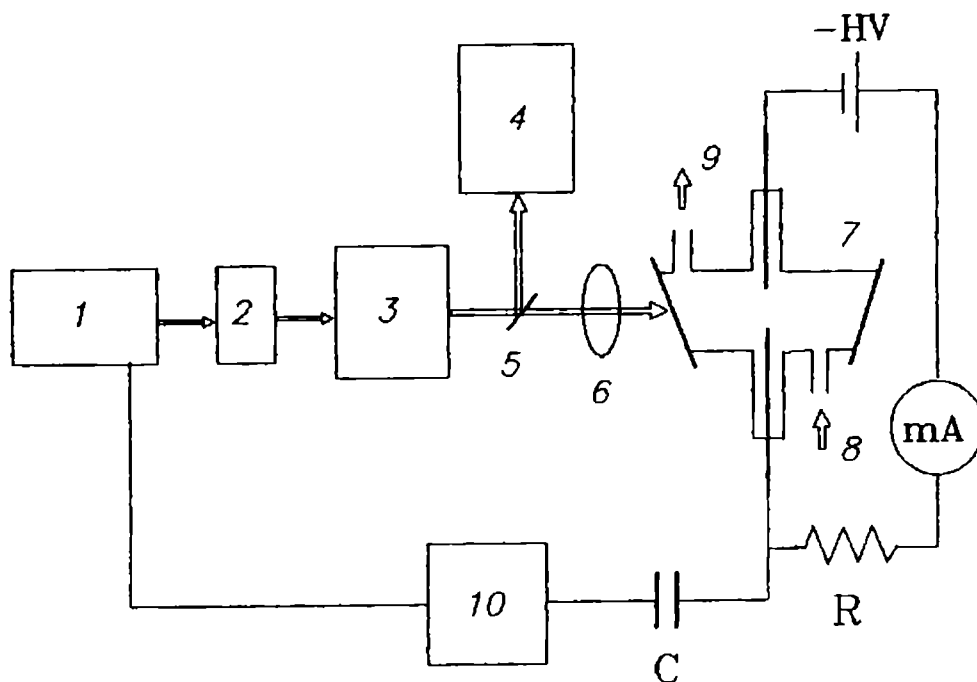
Fig 7.1 Schematic diagram of the experimental set up for pulsed POG effect. (1 Nd YAG laser, 2 Second harmonic generator,3 Dye laser, 4 Power meter, 5 Beam splitter, 6 Lens, 7 Discharge cell, 8 Gas inlet, 9 Gas outlet 10 CRO)

connected in series with the cell to limit the current in the circuit. Gases like N_2, NO_2 and Ar at a few torrs of pressure have been used in the discharge cell and the discharge conditions are adjusted so as to get a minimum discharge noise. Pulsed dye laser was focused in to the cathode using a lens. The POG signal obtained with a ~ 10 nsec pulse at 564nm radiation from the dye laser is taken out via a capacitor (0.1 μF) and the signal strength is measured using a CRO. The amplitude of the signal was measured by varying the laser energy, discharge current and the gas pressure. The strength of the signal strongly depends on

the laser power and the discharge conditions.   Fig 7.1 shows the experimental setup employed to observe the POG signal.

7.5.2 Two photon POG effect

It has been reported that both emission-limited and space-charge limited signals are observed in the POG effect [5]. At higher pulse energies, transition from emission-limited to space-charge limited current occurs so that a greater portion of the photoemission current is space charge limited.   The work function of the electrode material (tungsten) is 4.3 eV [12] which approximately coincides with twice the photon energy of the laser at 564nm. Least square fitting of the experimental observation show that the signal amplitude (S) can be represented as a quadratic function of the laser energy E as

$$S = aE + bE^2 \qquad\qquad (7.8)$$

Where a and b are fitting coefficients which are sensitive to the discharge conditions.

Fig 7.2a shows the variation of POG signal with laser power at a gas pressure of 7 torr.   The least square fitting of the experimental data confirms that the strength of the POG signal can be fitted into a quadratic function of pulse energy according to equation (7.8).   Log-log plot of the signal strength verses laser energy has a slope 2, which clearly indicate the two photon
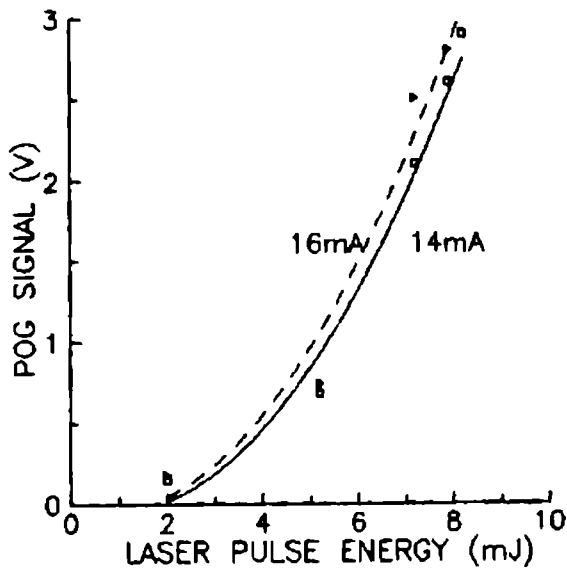
Fig 7.2a
POG signal verses laser
pulse energy for N_2 at
7 Torr.
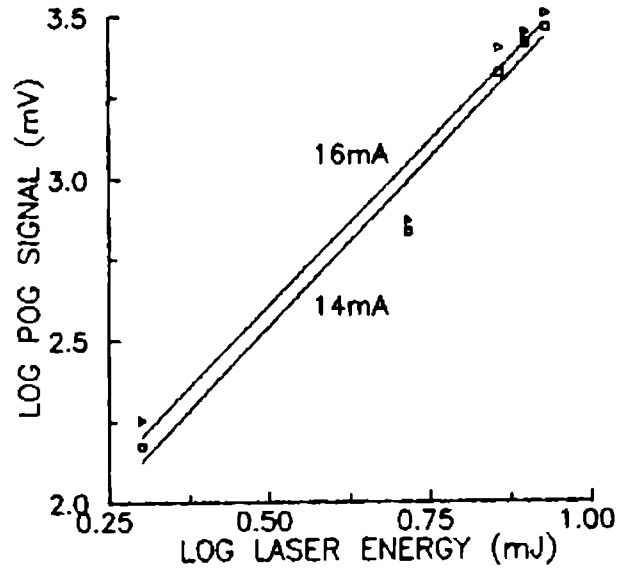
Fig 7.2b
log-log plot of POG
signal verses laser
pulse energy for
N_2 at7 Torr.

(TP) absorption (fig 7.2b). When the gas pressure is 5 torr, again the signal have a quadratic dependence with a slope about 1.5, indicating the presence of one photon (OP) as well as two photon process (fig 7.3) The TP is obvious from the work function matching condition, which is by simultaneously absorbing two photons at 584nm radiation and the presence of one photon process

is due to OG signal arises from the excitation of gas molecules. Laser induced impedance changes can also be generated by thermionic processes due to instantaneous heating of the target in presence of laser pulse.
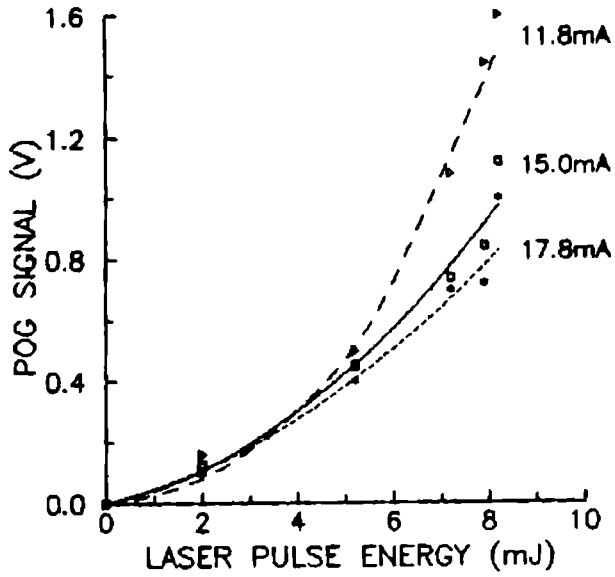
Fig 7. 3a
POG signal verses
laser pulse energy
for N_2 at 5 Torr.
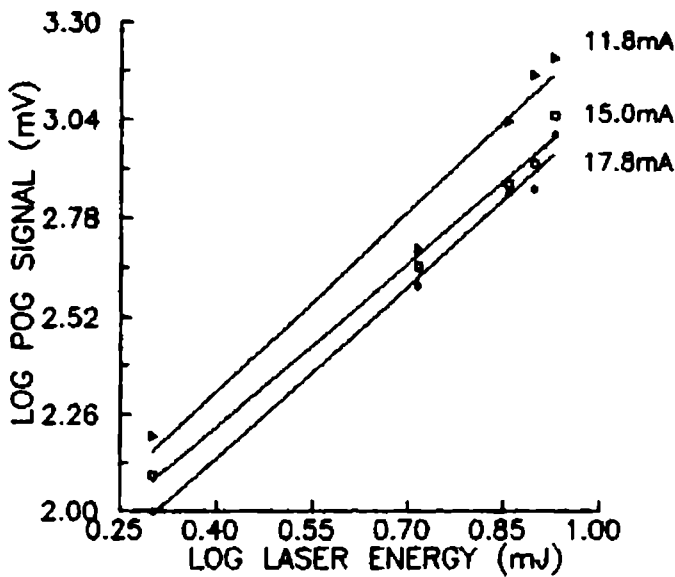
Fig 7 3b
log-log plot of POG
signal verses laser
pulse energy for
N_2 at 5 Torr.

In the case with for Ar and NO_2 gases in the cell also, O and TP process are observed (fig 7.4). Hoverer the contributio due to OP is larger in these cases. A threshold laser energy i required for generating TP absorption below which, the change i impedance is due to the direct absorption of radiation of th species present in the discharge. This change can be positive o negative depending on the life time of levels involved in th transition [7]. It is noted that N_2, NO_2 and Ar gases hav absorption at this wavelength [13-15] which will give rise to O signal corresponding to the absorption of these transitions These results indicates that in addition to the property of th cathode material, nature of the experimental gas and th discharge conditions considerably influences the POG signal. detailed study on the dependence of POG signal on discharg current and gas pressure under pulsed laser excitation has bee presented in a previous work [16].

Fig 7.4

POG signal verses laser pulse energy for N_2(15mA), NO_2(15.4mA) and Ar(15.5mA)
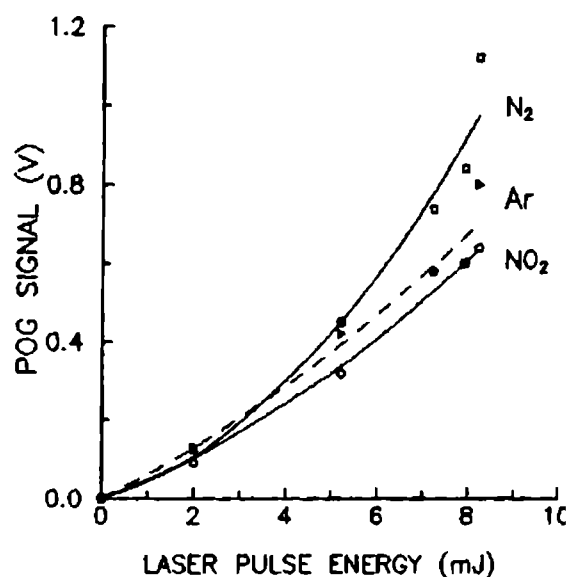
7.6 POG EFFECT UNDER CW LASER EXCITATION

7.6.1 Introduction

The POG effect can also be generated by cw laser excitatio where the time profile of the signal will follow that of th modulating beam. This section presents results of studies o voltage and laser power dependence of PE and POG effect generated in a Neodymium hollow cathode using cw lase excitation. A highly stable dc voltage (Thorn EMI), is applie to a commercial hollow cathode in which Nd is taken as th cathode material and neon gas as the buffer gas (Cathodeon UK) The discharge is operated in negative glow region of th discharge. A resistance of 66 KΩ and a milli ammeter ar

HCD
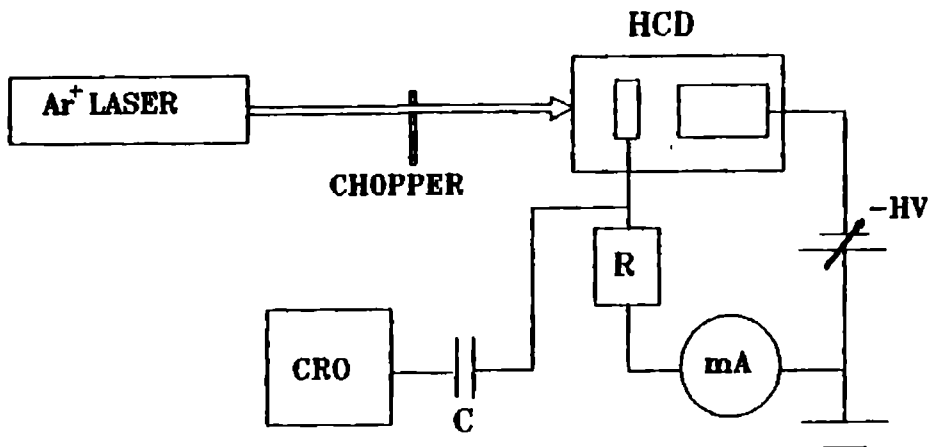
Fig 7.5 Schematic diagram of the experimental set up for cw POG effect.

connected in series with the cell (fig 7.5). Radiation from an argon ion laser, with multiline mirror is mechanically chopped and is allowed to fall on to the cathode. The discharge was very stable with a noise level less than 2 mV. When the laser beam is not falling on the cathode there is no signal, confirming that no resonant OG effect by the plasma medium itself. The strength of the PE signal generated after two averages is measured using a storage oscilloscope (Iwatsu) as a function of the applied voltage and the laser power. The current is both photon emission limited as well as field emission limited and the field at which the current becomes photon emission limited also depends on the laser power. The signal voltage across the resistance under following processes have been investigated separately;

1) PE effect   before striking the discharge

2) POG effect and

3) Negative POG signal; region of discharge instability

7.6.2 PE effect

The quantum yield of a photo electric emitter depends upon three basic processes - viz. photo excitation, transport of electrons to the emitter surface and the escape over the surface barrier - and is given by [17]

$$Y(\hbar\omega - E) = c\int_{0}^{\hbar\omega-E} N_i(-E')(\hbar\omega - E - E')dE' \qquad (7.9)$$

where $N(-E')$ represents the energy distribution of electrons and E is the barrier energy of the cathode. Y depends on both frequency and power of the radiation. According to equation (7.9), if the field is increased the barrier height will decrease and hence the yield and the strength of the photo current will increase. The photo current (I) and the quantum yield (Y) are related by

$$I = \frac{PY}{\hbar\omega}$$

(7 10)

where P is the absorbed light power and $\hbar\omega$ is the photon energy in electron volts. Thus

$$I = A(\hbar\omega, P) \int_0^{\hbar\omega - E} N_i(-E')(\hbar\omega - E - E')dE'$$

(7.11)

where A is a constant depends on the photon energy $\hbar\omega$ and the laser power P. The mechanism responsible for the field dependent-barrier lowering depends on processes like the image force lowering and the field penetration through the electrodes, as given by

$$E = E(V) = E_0 - KV^{1/2}$$

(7.12)

where V is the applied voltage and K is the barrier-lowering constant in units of $eV/V^{1/2}$ This phenomenon of barrier-lowering is same as Schotty effect [18]. Thus from

equations (7.11) and (7.12) the voltage dependence of the photo current can be written as

$$I = A \int_0^{\hbar\omega - E_0 + KV^{1/2}} N_i(-E') (\hbar\omega - E_0 + KV^{1/2} - E') dE' \qquad (7.13)$$

Functional form of the photocurrent for various electron energy distributions applicable to many cases has been described by Powel [17]. For example, the electron energy distribution from metal at $0^\circ C$ with the step corresponding to the Fermi energy can be described by a step function and a linear ramp distribution should be expected to apply to many semiconductors. The emission from Fermi tail in metals and degenerate semiconductors can be expressed by an exponential distribution. The energy distribution of electrons can be expressed in the form

$$N_i(-E') \propto \exp(E'/k_b T) \qquad (7.14)$$

where T is the temperature. Hence the functional form of the photo current is obtained from the equations (7.13) and (7.14) as,

$$I \propto A(k_b T)^2 \left[\exp\left\{ \frac{\hbar\omega - E_0 + KV^{1/2}}{k_b T} \right\} + \left\{ \frac{\hbar\omega - E_0 + KV^{1/2}}{k_b T} \right\} - 1 \right] \qquad (7.15)$$

for $(\hbar\omega - E_0 + KV^{1/2})/k_b T$ large enough, this expression reduced to

$$I = A(k_b T^2)exp\ ((\hbar\omega - E_0 + KV^{1/2})/k_b T) \hspace{3cm} (7.18)$$

According to this equation the strength of the photocurrent depends on the photon energy, applied voltage, work function of the cathode material and the temperature. The increase in voltage will modify the surface work function according to equation (7.12) and will show an increase in the photocurrent. The parameter K also depends on the dielectric constant of the medium and the inter electrode separation [17]. Taking the logarithm of equation (7.18) can be seen that a plot of log I verses $V^{1/2}$ will be a straight line with a slope $K/k_b T$.

The work function of the cathode (Nd) material is 2.95eV [19] and the energy of the laser radiation used lies in the range of 2.4eV to 2.6eV. Even though there is a mismatch between the photon energy and the work function, even at the minimum voltage, the PE signal is observed. The work function of a material depends on the state of the surface viz, its contamination, roughness, temperature etc. [8]. Thus, due to Schotty affected field electron emission and Schotty affected thermionic processes, a less photon energy threshold is sufficient to generate the PE effect. Surface enhanced ionization, in which the interaction of radiation with positive ions of the metal surface can also lower the work function sufficiently to allow efficient generation of photoelectron by the photon flux. In this mechanism initially a positive ion layer is formed on the

metal surface and subsequently photoemission occur from the modified surface. Both processes take place during the laser irradiation and after the adsorbed molecule has been excited its effective ionization potential is lower than the surface work function. Multiphoton ionization enhanced by the metal surface due to the amplification of the electromagnetic field by the surface can also reduce the effective surface work function [20].

Before striking the discharge the PE signal increases (fig 7.8a) with voltage and it becomes maximum at a laser power of about 2W, above which it begins to decrease. There is no dependence of the PE signal on the chopping frequency at low
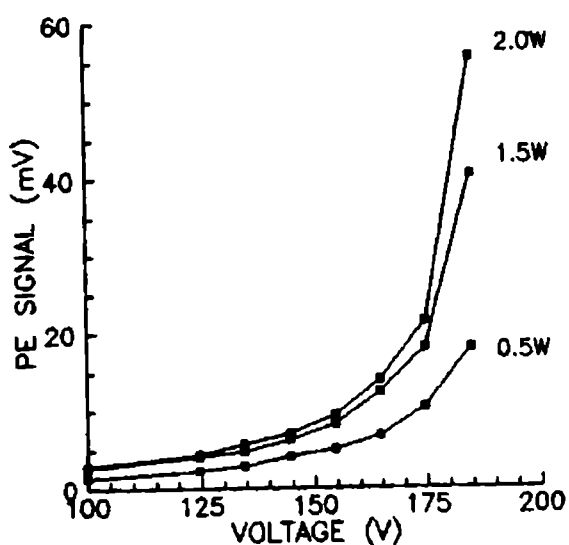
Fig 7.8a
Voltage dependence
of the PE signal.
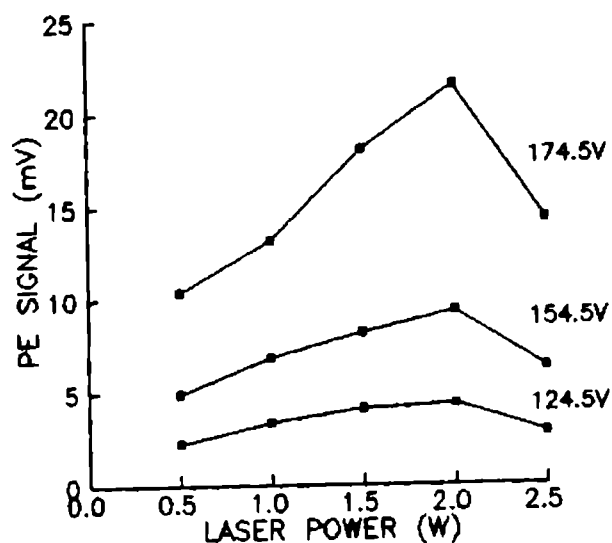
Fig 7.8b
laser power dependence
of the PE signal.

frequency indicating the absence of thermionic process. At higher laser powers non-linearities in laser-target interactions reduces the PE effect (fig 7.6b). The laser power(P) dependence of the PE signal ($\Delta V_{PE}=IR$) can be fitted into a quadratic equation,

$$\Delta V_{PE} = aP - bP^2 \qquad\qquad (7.17)$$

The coefficients a and b depend on the discharge voltage and also the temperature near the irradiated region on the cathode. It is observed that a and b increase with the voltage. From the slope of the log I verses $V^{1/2}$ plot (fig 7.7) the value of the barrier lowering constant K evaluated is 0.019. In this calculations we have assumed an average temperature of 300K. The value of K obtained from the exponential fitting (fig 7.8) of the experimental values was 0.018 which is in close agreement with the former. This indicates that $E(V) < E_0$, so that, the voltage

Fig 7.7
log PE signal
verses $V^{1/2}$ plot.
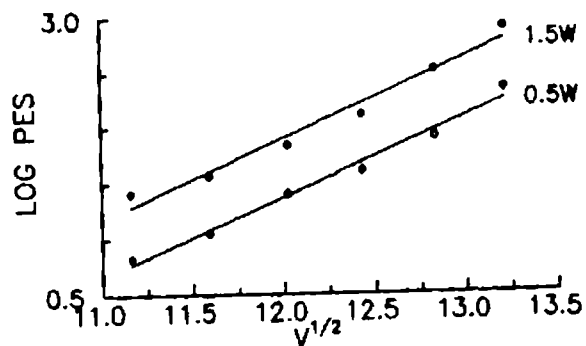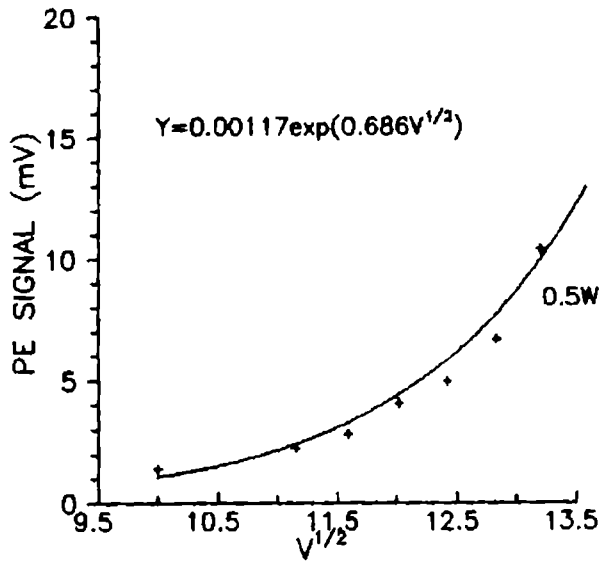
Fig 7.8
Exponential curve fit for
experimental data of the
PE signal amplitude with $V^{1/2}$

applied between the electrodes reduces the barrier energy of the cathode surface according to the equation (7.12).

7.6.3 Quantum efficiency

The effective quantum efficiency (Y_e), which is the ratio between the number of photo electrons (n) and the number of absorbed photons (N), can be written as

$$Y_e = n/N \; \infty \; \frac{I\hbar\omega}{P}$$
(7.18)

The number of photoelectrons generated is given by $n = It/e$ where t is the time and I is the photocurrent. At low voltages the electron generation is predominantly by photoemission limited
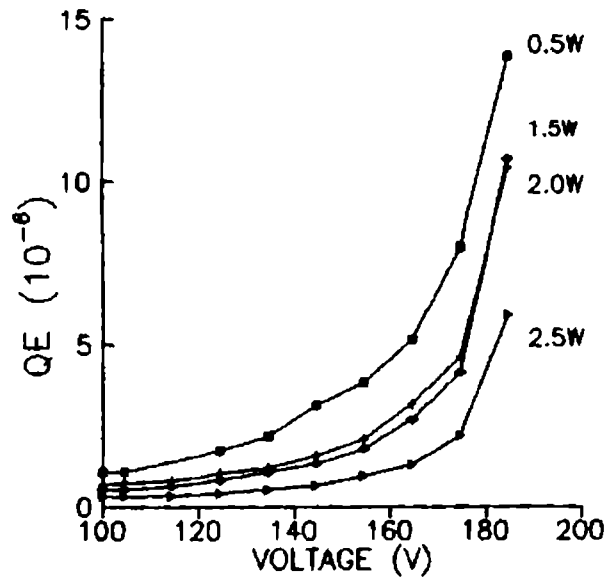
Fig 7.9 Variation of quantum efficiency
for PE effect

while as the voltage increases both photoemission and space
charge effects take part in the process. The calculated value of
Y_e is in the range of 10^{-7} to 10^{-6} electrons per photon depending
on the experimental conditions (fig 7.9) which is comparable with
that obtained by Ivri et al[2] using pulsed laser excitation.

7.6.4 POG effect

The magnitude of the POG signal strongly depends on the
escape depth of the photo electrons through the surface of the
cathode and also on the plasma characteristics. The dependence
of signal on the discharge voltage and the laser power are shown
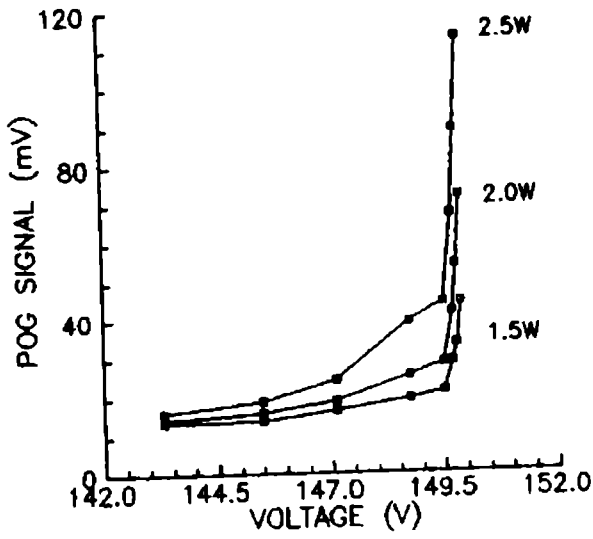
Fig 7.10a

POG signal verses
discharge voltage.
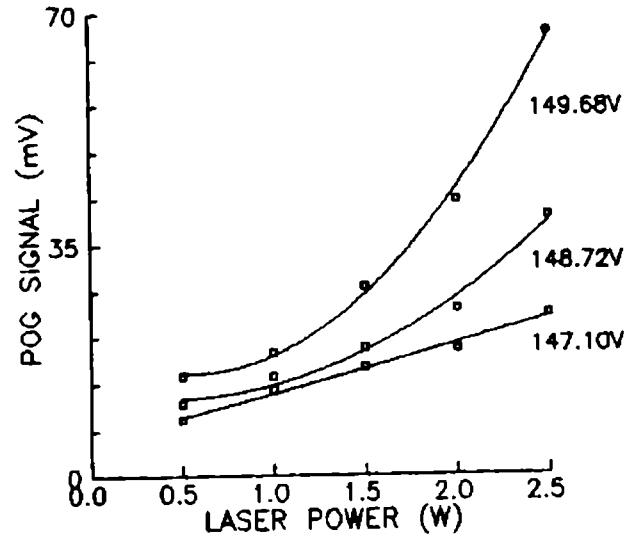
Fig 7.10b

POG signal verses
laser power.
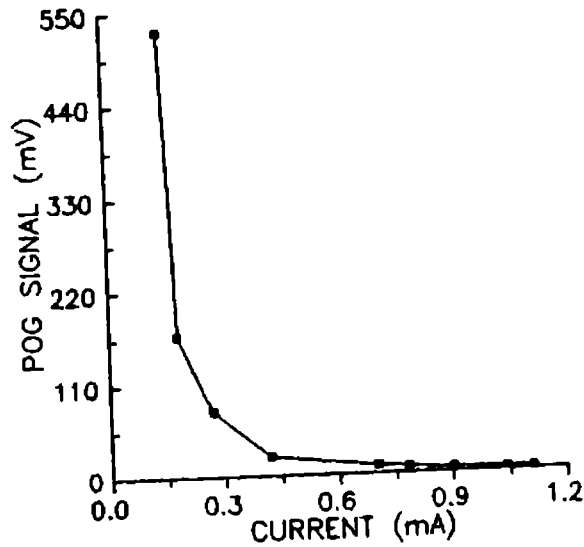
Fig 7.11 Variation of the POG signal with current
below the striking voltage in presence of the discharge.

203

in fig 7.10. Another noticeable observation is that after striking the discharge if the tube current is reduced, the POG signal is found to increase reaching a maximum value at the point where the discharge is turned off (fig 7.11).

The electrons emitted from the cathode on its way to the anode are multiplied producing a large number of secondary electrons. Thus, if the multiplication factor, given by

$$\alpha(V) = \frac{\Delta V_{POG}}{\Delta V_{PE}} \qquad (7.19)$$

is greater than one, current increases and the POG signal (ΔV_{POG}) will be greater than that of the PE signal (ΔV_{PE}). In general, the QE in the plasma is larger than that in the vacuum [5] due to the collisionally produced secondary electrons as a result of ionizing collisions with neon atoms on their way from cathode to anode. The dependence of the multiplication factor on the laser power and the voltage are shown in the fig 7.12. In presence of discharge under certain conditions also log I verses $V^{1/2}$ plot (fig 7.13) is a straight line. In this case photocurrent can be obtained from equation (7.16) by replacing K as the effective barrier lowering constant as K_d, where

$$K_d = \alpha K \qquad (7.20)$$

As the laser power is increased the value of K_d increases showing an intensity dependence. In presence of discharge the quantum
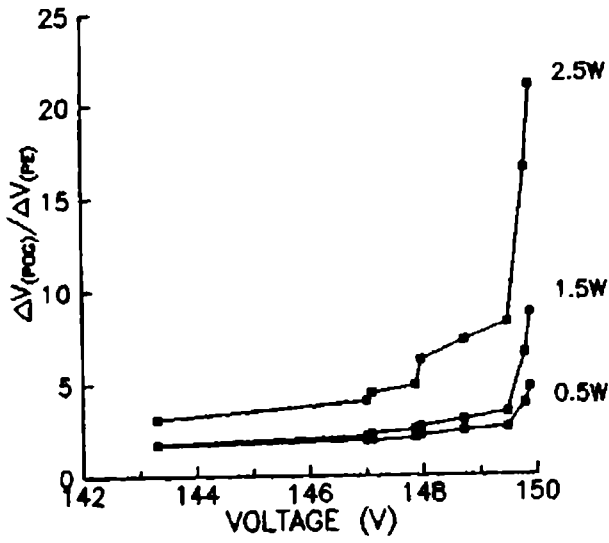
Fig 7.12a

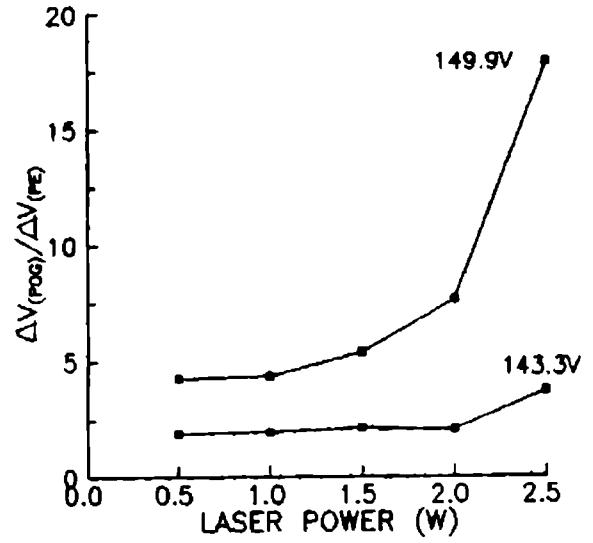The dependence of the
electron multiplication
factor with voltage

Fig 7.12b

The dependence of the
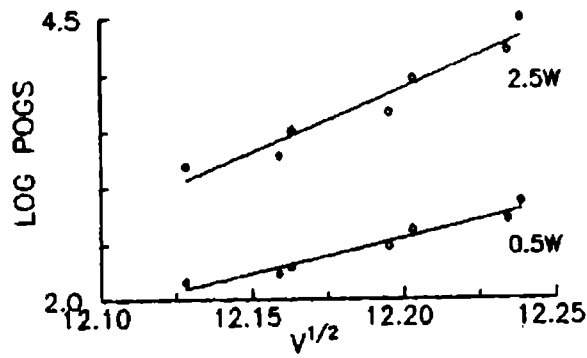electron multiplication
factor with laser power

Fig 7.13 Log POG signal verses $V^{1/2}$ plot

efficiency is approximately α times to that without discharge conditions.

7.7 INVESTIGATION OF DISCHARGE INSTABILITY USING POG EFFECT

It has been shown that under certain discharge conditions plasma becomes unstable showing complex nature [18]. The application of POG effect to investigate such instabilities in a gas discharge is described in this section. Near the instability, the POG signal is negative and shows growth and decay of about a few minutes. OG effect can be positive or negative depending on the life time of levels involved in the transition, where as in POG effect, since the photo electron emission will produce more secondary electrons by collision with atoms as the electrons move from cathode to anode will produce an increase in the current. However, we have observed an increase as well as decrease in the POG signal depending on the discharge conditions. The region where the POG signal decreases show some kind of instabilities and the amplitude of the signal has some noticeable changes even if all the experimental parameters were kept constant. Here a number of peculiar properties such as self sustaining oscillations, irregularity in the discharge noise etc. are also generated in the discharge and have observed that this can easily be investigated by monitoring the POG effect. The discharge noise pattern, amplitude and phase of the POG signal are measured using a 200 MHz digital storage scope (Iwatzu) and

lock-in amplifier respectively (EG&G 5208). Another lock-in (SR 850) is used to record the POG signal at the instability point of the discharge.

In presence of discharge, as the electrons move from cathode to anode they are multiplied producing a large number of secondary electrons. Thus if electron multiplication factor is greater than one, current will increase and if it is less than one current will decrease in the circuit. Fig 7 14 shows the variation of the POG signal as a function of current. After striking discharge the applied voltage is reduced to the minimum value and then increases so that the signal decreases considerably, but still have a positive value. Increase in
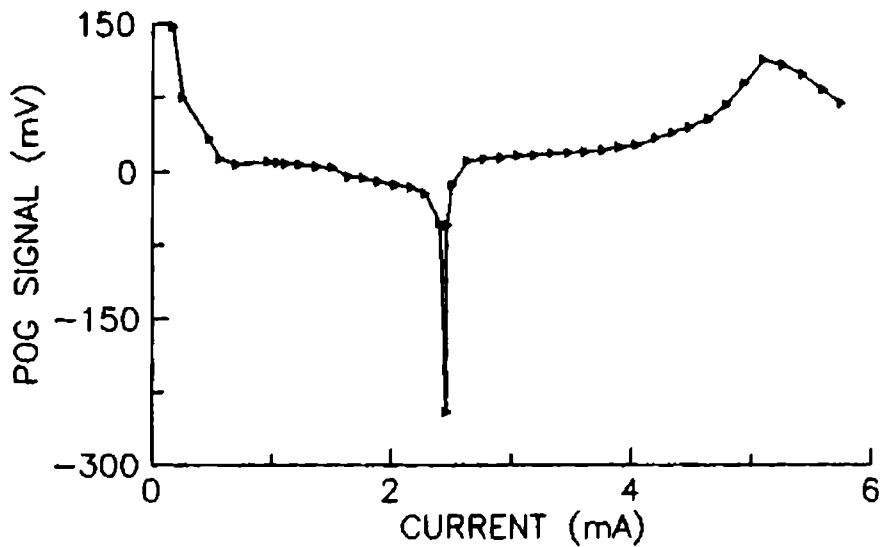
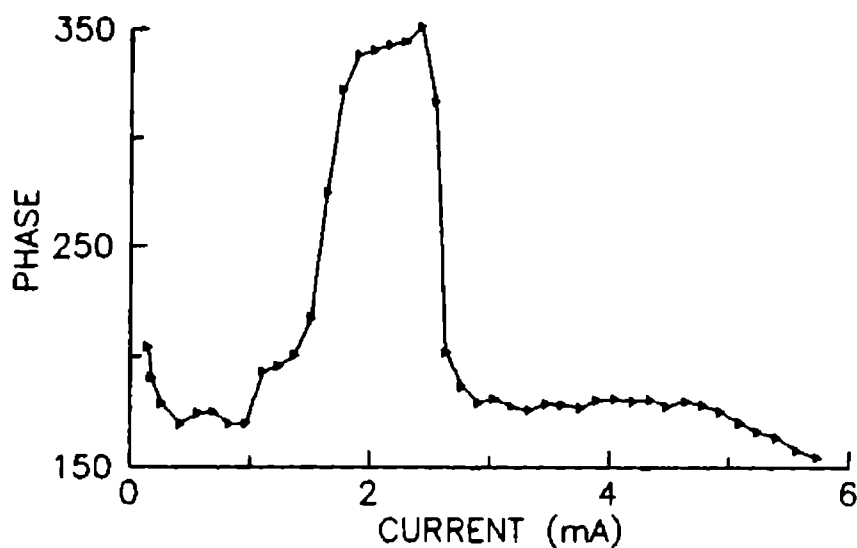Fig 7.14 Variation of the POG signal with discharge current.

Fig 7.15 Variation of phase of the POG signal
with discharge current.

current results in a sign reversal. The phase of the signal also
changes and at the maximum negative POG signal there is a phase
shift of 180° (fig 7.15). In this region photoelectrons
generated interact with the discharge such that instead of
producing more secondary electrons their number is reduced, ie.
the electron multiplication factor becomes less than one.
Further increase in voltage suddenly reverses the phase and the
sign of the signal also get changed to positive. This region at
which sudden sign and phase change of the POG signal takes place,
was found to move towards the lower current range after prolonged
running of the discharge or if the discharge is irradiated with
higher laser power. This is due to modifications in the discharge
characteristics by thermal effects. Further increase in current

indicates that the sign of the signal is always positive with a maximum at about 5mA.

Without laser excitation, self sustaining oscillations in the discharge have been observed when the CRO is terminated with 50Ω resistance. Details of such oscillations are given in chapter 8. This type of oscillations in voltage, current and emission intensity in the discharge have been reported earlier and were identified as quasi periodic or period doubling route to chaos [21] which has a strong dependence on the discharge characteristics [22]. Variation in the frequency (inverse of the adjacent time interval) of this self sustaining oscillations is shown in fig 7 16. The frequency of oscillations decreases with
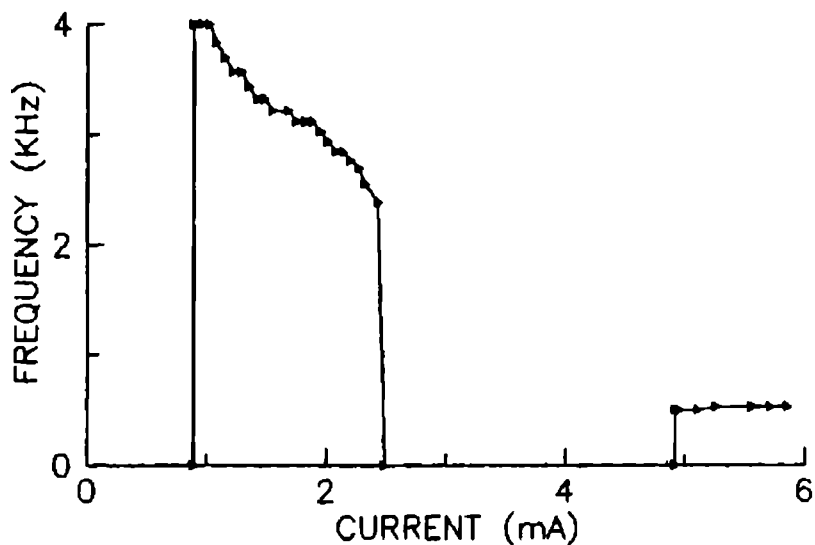

Fig 7.16 Variation of the frequency of oscillations with discharge current.

current and as the current approaches the instability region of the discharge where POG signal is negative maximum, the oscillations suddenly becomes zero. Again at about 5mA another oscillating state begins at about 550Hz as in the fig 7.16. This phenomenon in the dynamics of the plasma has been reported recently and has been identified as backward Hopf bifurcations in the bifurcation diagram in which oscillating state corresponds to a stable limit cycle and the non-oscillating state as stable fix point [23].

Fig 7.17 shows the time profile of the strength discharge noise at the instability region. This is obtained by recording the CRO pattern of the noise without irradiation near the instability. When the discharge current I is below I_c, the voltage across the resistance grows (ie. discharge noise) while when I is slightly above I_c the voltage across the resistance decreases as shown in the fig 7.17. It was not possible to fix current at $I = I_c$ where this instability signal is maximum. There are following points to be noted. 1) the amplitude of the negative signal (for $I > I_c$) is greater than that of the positive signal (for $I < I_c$). 2). Decrease of ballast resistance broadens the functional form and also decreases the amplitude of the instability signal.

Finally we have investigated this instability by monitoring the POG signal near the I_c. When the applied voltage is close to
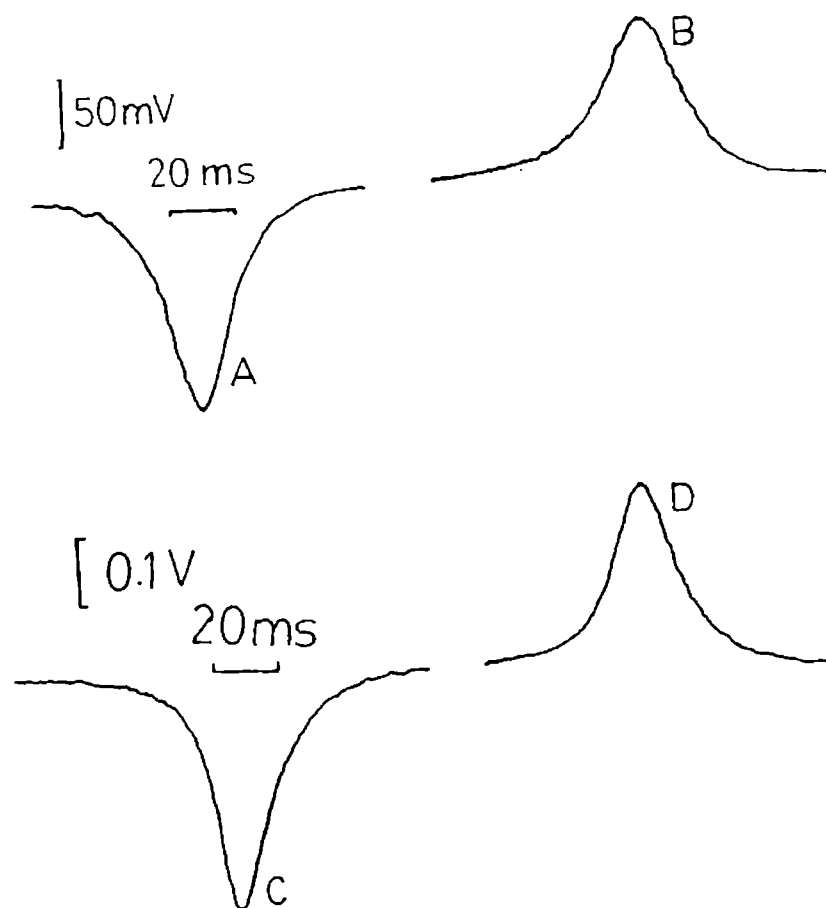
Fig 7.17 Time evolution of the discharge instability.

A) R = 66K, discharge current 2.29mA (discharge voltage is slightly above the instability).

B) R=66K, discharge current 2.28mA (discharge voltage is slightly below the instability).

C) R = 105K, discharge current 2.3mA (discharge voltage is slightly above the instability).

D) R = 105K, discharge current 2.3mA (discharge voltage is slightly below the instability).

the unstable region of the discharge, the POG signal grows and decays as shown in the fig 7.18 within a time scale of about ten minutes. This occurs till a stable condition is reached and within this period a number of oscillations are generated. Another noticeable observations was that the growth rate of POG signal was controllable by adjusting laser power which indicates the possibility of controlling this instability by adjusting an external parameters like laser power. The instability shows a strong dependence of the initial conditions such as the voltage and the laser power. The factors that cause the discharge instability are related to the processes that control the density of electrons (their production, removal and spatial distribution etc.). Depending upon the closeness of the set current to I_c the oscillations have one to three peaks. The large time scale of the signal suggests that the in stability is mainly created by thermal processes.

Following observations were made at the instability region.
1) The functional form of the instability signal is positive when $I < I_c$ and negative for $I > I_c$, where I is the discharge current and I_c is the current where the instability occurs.
2) The state changes from a stable oscillating state to a stable non-oscillating state.
3) The POG signal is negative ie. the interaction of photo electrons with the discharge reduces the current in the circuit so that a phase shift of 180° occurs for POG signal around the

instability region.

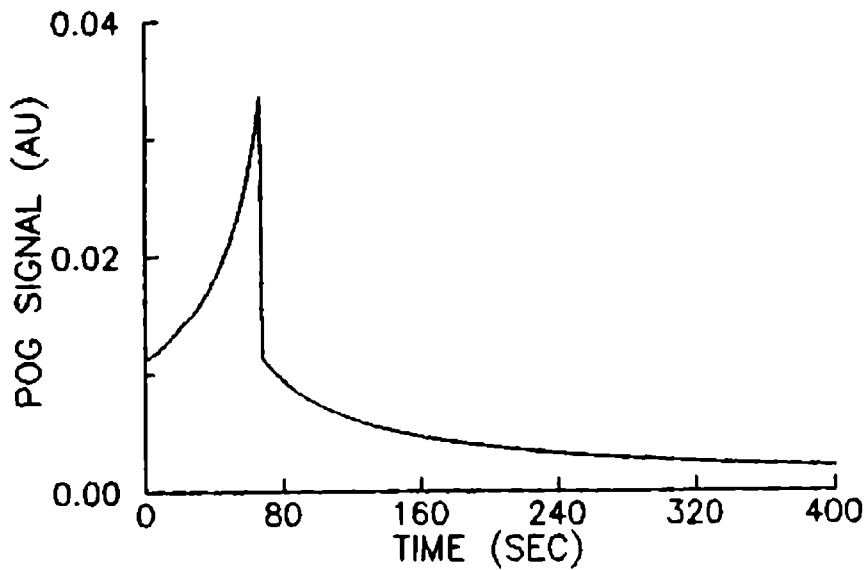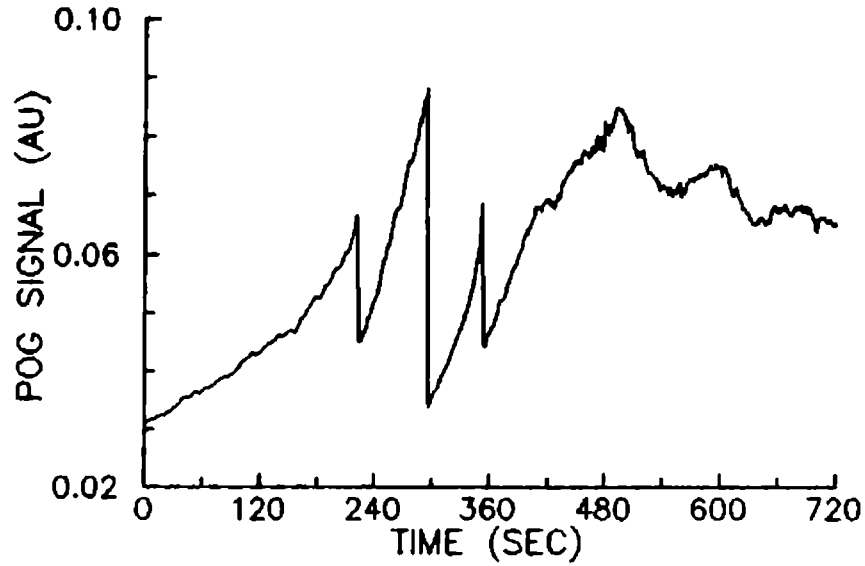4) Near the peak of the negative signal the POG signal is very unstable.

Fig 7.18 Variation of POG signal with time near the instability (laser power one watt).

7.8 OBSERVATION OF PULSATING POG SIGNAL

Moving striations, ionization waves, oscillations etc. are very interesting features of dc electrical discharges which are observed over a wide range of discharge parameters. These phenomena are not only a function of discharge current but also population of excited states and are manifestations of periodic changes in electron density caused by the production and removal of electrons. Instability leading to striations is generated due to repeated ionization processes [18].

Change in the number of electrons due to collision of excited state atoms with the electrons is believed to be one of the important mechanism of the OG effect. The contribution from multiphoton ionization will trigger the excitation wave and the change in the degree of ionization, either transient or oscillatory phenomena results into a change in impedance of the discharge plasma as a whole that causes the transient OG signal. Observation of laser induced striation in a hydrogen discharge plasma [24] as a result of direct photoionization of hydrogen atoms caused by the transient excitation of striations, suggested that striations can be excited by optogalvanic method. Tochigi et al [25] have reported damped OG oscillations at about 9 KHz in a neon hollow cathode on illumination by a pulsed dye laser at the resonant frequency of neon $2p_8 \rightarrow 1s_5$. The current and position dependence of illumination of the damped oscillation have lead these authors to conclude that the ionization caused by
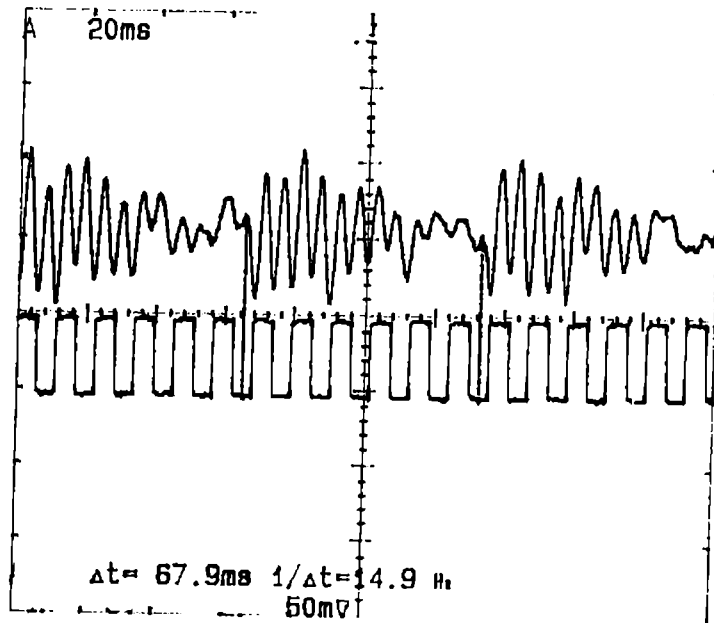
Fig 7.19 Pulsation of the POG signal
(discharge current 0.15mA, R=66KΩ,
laser power 160mW at 488nm).

the laser pulse inside that positive column region of the discharge lead to oscillations.

The experimental set up employed to observe the pulsation of the POG signal is same as in fig 7.5. The discharge current is decreased up to the minimum value required to sustain the discharge. The pulsation is observed only at this value of current which is of course due to certain instabilities created at this point. For all other discharge conditions, POG signal follows the chopping frequency, however at this instability region this pulsation decays as shown in fig 7.19. Since the POG signal indicates the number of electrons flowing in the circuit, the damping of the signal at this critical currents show that the number of electrons in the discharge also oscillate in the same manner and hence can be observed as pulsation in the plasma impedance. The pulsation phenomenon was found to be extremely sensitive to discharge current.

Optogalvanic effect generated by injecting photoelectrons into the discharge via photoelectric emission using pulsed and cw laser have been described. Studies on two photon absorption, voltage and laser power dependence and discharge instabilities were presented.

REFERENCES

1 B Feuerbacher, B Fitton and R F Willis, Photoemission and the
        electronic properties of surfaces, (John Wiley & Sons,
        New York, 1978).

2   J Irvi and L A Levin, Appl.Phys.Lett 62 (1993) 1338

3   B B Laud, Lasers and non-linear optics (Wiley Eastern Ltd,
        New Delhi, 1991)

4   K Shimoda, High resolution laser spectroscopy (Springer
        Verlag, Berlin, 1976)

5   S W Downey, A Mitchell and R A Gottscho, J.Appl.Phys. 63
        (1988) 5280

6   J E M Goldsmith and J E Lawler, Contemp.Phys. 22 (1981)235

7   G Erez, S Lavi and E Miron, IEEE J. Quantum Electron. 15
        (1979) 1328

8   G S Selwyn, B D Ai and J Singh, Appl.Phys.Lett. 52 (1988)
        1953

9   M B Schulman and D R Wooodward, Appl.Phys.Lett. 55 (1989)
        1618

10 R Yen, J Lin and N Bloembergen, Opt.Comm. 35 (1980) 277

11 J H Bechel, J.Appl.Phys. 46 (1975) 1585

12 R C Weast (ed) Hand book of Chemistry and Physics, 55 edn.
        (Chemical Rubber Co. Florida, 1975) p E-82

13 A G Gaydon and R W B Pearse, The identification of molecular
        spectra (Chapmann & Hall Ltd, London 1965)

14 D K Hsu, D L Monts and R N Zare, Spectral atlas of nitrogen
        dioxide 5530 to 6480 Å (Academic press, New York 1978)

15 M C Su, S R Ortiz and D L Monts, Opt.Comm. 61 (1987) 257

16 P R Sasi Kumar, Photoemission optogalvanic effect studied in
        Ar, N_2 and NO_2 discharges (M Phil Desertation Cochin
        University of Science & Technology, 1990)

17 R J Powel, J.Appl.Phys. 41 (1970) 2724

18 Yuri P Raizer, Gas discharge physics (Springer Verlag,
        Berlin 1991)

19 D E Gray (ed) American Institute of Physics Hand Book (Mc
        Graw Hill Book co, New York, 1972) p 9-173

20 R Naaman, A Petrank and D M Lubman, J. Chem. Phys. 79 (1983) 4608

21 T Donahue and G H dieke, Phys. Rev. 81 (1951) 248

22 T Braun, J A lisboa, R E Franke and J A C Gallas, Phys. Rev. Lett. 59 (1987) 613

23 R Singh, P S R Prasad, J K Bhattacharjee and R K Theraja, Phys. Lett A 178 (1993) 284

24 C P Ausschnitt and G C Bjoklund, Opt. Lett. 4 (1979) 4

25 K Tochigi S Meada and C Hirose, Phys. Rev. Lett. 57 (1986) 711

CHAOTIC BEHAVIOUR IN HOLLOW CATHODE DISCHARGE

8.1 INTRODUCTION

The phenomena of order and chaos occurring in non-linear dissipative systems have been the subject of intense research in recent years [1]. Universal characteristics of chaos have been observed both in numerical simulations and in experimental situations in various fields like optics [2,3], hydrodynamic flow systems [4], optical bistability [5], electrical circuits [6] etc. These studies have demonstrated transitions from order to chaos through various routes to chaos. Plasma is a typical non-linear dynamical system with a large number of degrees of freedom and it is an interesting medium to test these universal characteristics of chaos. Although, it was known theoretically that the plasma could exhibit deterministic chaos, it was only recently that the experimental observation of such behavior in gaseous plasma has been reported [7]. Much of the interest in gaseous discharges and plasma derive from their potential applications in the development of laser devices, controlled fusion etc., where the problems of instabilities and turbulence are very important. The study of chaotic behavior in gas discharges also enables one to understand the reproducibility of the plasma conditions in laboratory plasma experiments and their sensitive dependence on initial conditions.

Moving striations in gas discharges and electrical oscillations [8] have been detected in discharge plasmas under various experimental conditions. Even though this oscillatory phenomena in dc discharges have a long history, no quantitative nor even a unique qualitative explanation has been given [9]. Though an exact description of the mechanism responsible for the appearance of oscillatory behavior is still lacking, it is expected that the chaotic behaviour is generated from macroscopic properties of the discharge. These oscillatory behaviour of the discharge is a kind of self generated oscillation because the plasma system is not driven by any external periodic forces. The fundamental frequency of self oscillations varies with the change in the control parameters, like discharge current and there is no defined frequency of oscillation in these undriven chaotic systems.

It is reported that the voltage oscillations are closely related to moving striations in which the voltage and intensity of moving striations are always erratic and regular in the same way [9]. This shows that these two types of oscillations are different manifestations of the same phenomenon which is entirely due to atomic processes taking place in the discharge. The oscillations can be observed by monitoring the voltage, current or light emitted from the plasma. The characteristics of oscillations depend on the nature of the gas, total pressure, cell geometry, nature of electrodes, the external circuit

parameters etc. The discharge voltage and the intensity of plasma emission behaviour in an electrical discharge show striations, periodic or chaotic behaviour depending on the discharge current. Reports on such non-linear effects leading to chaotic dynamics in laser systems [10,11], moving striations in positive column discharge [12], self sustained oscillations in the hollow cathode discharges using optogalvanic effect [13] etc. are available in literature. Many experimental results on various universal routes to chaos such as period doubling [14-16], quasi periodic routes [17,18], intermittency [19] etc in steady state plasma have also been reported.

8.2 OSCILLATIONS IN A DC DISCHARGE

A qualitative description of oscillatory phenomenon in dc discharge has been presented by Cheung et al [13]. When an anode is biased positively with respect to the cathode, energetic electrons are ejected from the cathode. The electrons periodically ionize the back ground neutral gas and create a plasma between the electrodes. The two processes, viz., the generation of primary electrons from the cathode and the production of plasma are strongly coupled. The primary electrons ionize the gas and sustain the plasma while the plasma reduces negative space charge and facilitates electron emission. By varying the plasma discharge parameters, one can control this coupling or the feedback process and the resulting plasma

dynamics can be made unstable. This occurs when the plasma potential is negative with respect to the anode where the potential is unstable and current oscillations occur

The rate of plasma formation (determined by the rate of neutral ionization by primary electrons and the plasma decay time) can be written as,

$$\frac{dn_o}{dt} = n_p N_n \langle \sigma v_p \rangle - \frac{n_o}{\tau} \qquad (8.1)$$

where n_o and N_n are the density of the plasma electrons and neutral atoms respectively, n_p and v_p are the density and the velocity of the primary electron, σ is the ionization cross section and τ is the plasma decay time. Once a discharge is initiated the primary electron flux, $J_p = n_p v_p$ increases rapidly and the entire voltage is confined in a narrow potential sheath that exists between the plasma and the electrodes. The width of the sheath structure is typically of the order of tens of Deby length λ_D. In the steady state, primary electron flux $J_p \propto \lambda_D^{-2}$ and the efficiency of primary electron emission depends on how fast plasma ions can drift to form a stable potential sheath. An approximate rate equation for the primary-electron emission is

$$\frac{dn_o}{dt} = an_p (u_d/L') \qquad (8.2)$$

where a is a constant, u_d is the ion drift speed and L' is the

222

effective plasma radius. Above equations along with the angular discharge repetition frequency were well studied and have been shown to display chaotic behavior [13]. To maintain a stable sheath, the plasma ions have to enter the sheath from the plasma side with a minimum of drift speed of $u_d \geq c_s$; the ion acoustic speed   The ratio of the ion flux to primary electron flux is $J_i/J_p = (m_e/m_i)^{1/2}$; where m_e/m_i is the electron to ion mass ratio. The maximum ion flux generated through ionization is approximately given by $(J_i/J_p)_{ion} = N_n \sigma L' = L'/l_m$; where l_m is the mean free path. This ion flux must be large enough to neutralize the negative space charge due to primary electron, and sustain the sheath. As a result if $L'/l_m \geq (m_e/m_i)^{1/2}$, both the discharge current and the sheath are destabilized. This destabilizing process develops through the accumulation of negative space charge and the depression of the plasma potential to negative values forming a virtual cathode in the plasma. As a result, the effective energy of the primary electron is no longer a constant but depends on the spatial and temporal evolution of the plasma potential. This in turn affect the mean free path l_m and the particle flux J_i/J_p. In this unstable state, inherent shot to shot noise fluctuations of $\delta n/n \leq 0.1\%$ which make only a negligible changes in the initial discharge conditions, cause a considerable changes in the plasma and lead to chaotic behaviour.

8.3 BIFURCATION

In order to describe the complex behaviour of plasma

instability, we take a standard model the non-linear forced oscillator which is known to exhibit chaotic behaviour[4]. The equation for the forced non-linear oscillator (which is also known as Van der Pol equation) is,

$$\frac{d^2\Theta}{dt^2} - (\varepsilon - \Theta^2) \frac{d\Theta}{dt} + \Theta = 0 \qquad\qquad (8.3)$$

where Θ is the amplitude of oscillation and ε is a control parameter. Whenever the solution of a system of equations changes qualitatively at a particular value of the control parameter, a bifurcation is said to be taken place. A point in parameter space where such an event occurs is defined as the bifurcation point. From a bifurcation point emerges solution branches, which are either stable or unstable. The representation of any characteristic property of the solutions as a function of the bifurcation parameter constitutes a bifurcation diagram (fig 8.1).

Hopf bifurcation

For all values, positive or negative of the bifurcation parameter ε the origin $\Theta = \dot{\Theta} = 0$ is always a singular point. The origin is stable - called a fixed point (an attractor) - for $\varepsilon < 0$ but becomes unstable for $\varepsilon > 0$ and is replaced by another attractor, called the limit cycle. A change in the nature of the stable solution thus occurs, for the critical parameter value ε_c
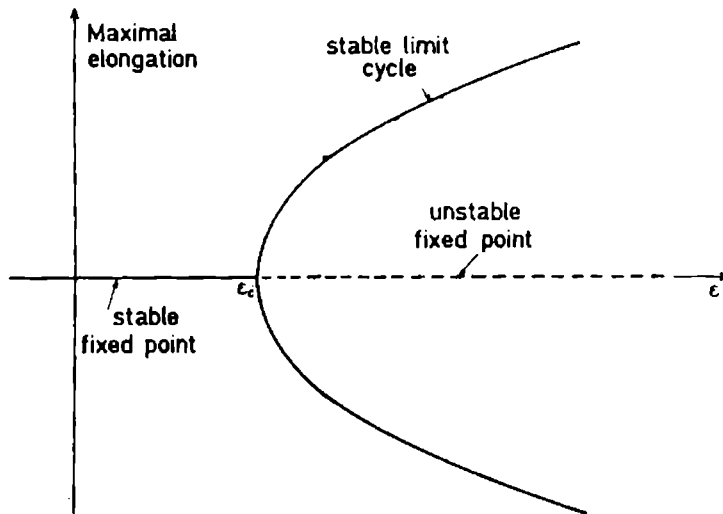
In Hopf bifurcation, a fixed point gives rise to a limit cycle as the critical parameter is crossed. The limit cycle is created with a zero amplitude at the bifurcation point, and the system is in a state of marginal stability. The amplitude of the limit cycle increases as the control parameter is increased beyond the bifurcation point. The bifurcation that gives rise at $\varepsilon = \varepsilon_c = 0$ is called as super critical or normal.

Subcritical Hopf bifurcation

As traversing along the ε axis from right to left (ie. decreasing ε), an unstable fixed point gives rise to a stable fixed point and an unstable limit cycle. This is the inverse of the normal bifurcation and is called inverse bifurcation or subcritical Hopf bifurcation. In the interval $(\varepsilon_c', \varepsilon_c)$ two stable solutions coexist; one is stationary (an attracting fixed point) and the other is oscillatory (a limit cycle). The solutions are not simultaneously observable in the same system and it is the initial condition which determines the actual state. In the case of subcritical Hopf bifurcation the stable limit cycle start with a finite amplitude.

Another characteristics of subcrtical Hopf bifurcation is that if we vary the parameter ε successively in one direction and then reversed, a hysteresis phenomenon is observed. In other words when we increase the bifurcation parameter the transition from the fixed point to the limit cycle takes place at $\varepsilon = \varepsilon_c$
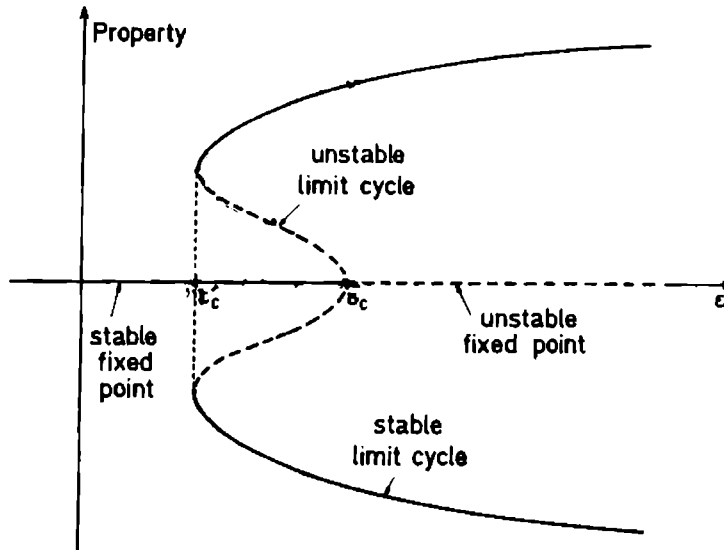
Hopf bifurcation

Maximal elongation

stable limit cycle

unstable fixed point

ε_c

stable fixed point

ε

Subcritical Hopf bifurcation

Property

unstable limit cycle

stable fixed point

ε_c'

ε_c

unstable fixed point

stable limit cycle

ε

Fig 8.1 Bifurcation diagram

while the inverse transition, obtained by diminishing ε occurs at ε_c^i instead of at $\varepsilon = \varepsilon_c$ ($\varepsilon_c^i < \varepsilon_c$). Thus, the absence of marginal stability, a non zero oscillation amplitude at transition, and hysteresis are properties of a subcrtical bifurcation that are qualitatively different from those of normal Hopf bifurcation. Sub critical Hopf bifurcation is also known as backward Hopf bifurcation. In this chapter, we describe the details of Hopf bifurcation observed in hollow cathode discharge.

8.4 OBSERVATION OF HOPF BIFURCATION IN HOLLOW CATHODE DISCHARGE

Experimental

Schematic diagram of the experimental set up is shown in fig 8.2. A commercial hollow cathode lamp (Cathodean UK) which contains Nd cathode and neon buffer gas is operated at low current. The discharge was excited by applying a stable ripple free dc voltage using a highly regulated power supply (Thorn EMI, PM28B). The discharge current is limited using a resistance which is in series with the power supply. The output signal, across the resistance was monitored using a 200 MHz digital storage oscilloscope (Iwatzu, DS-8821) with 50 Ω termination through a blocking capacitor. Thus when we talk of signal it is the ac signal and in the non-oscillating state the output is zero.

To strike the discharge in the hollow cathode, a higher current is momentarily applied. The current is then decreased to
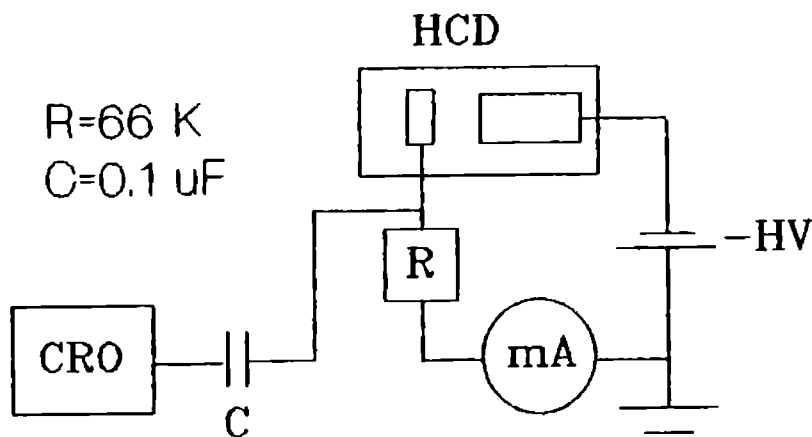
Fig 8.2 Experimental setup

a lower value at which the discharge is sustained and stable. The dc current, which is the control parameter, in the plasma dynamics is slowly increased by varying the applied voltage. Variation of the current through the lamp was measured from the voltage drop across the ballast resistance and displayed on the screen of a storage oscilloscope after conveniently de-coupling the dc component by a capacitor. The non-linear element in the circuit is the lamp operating in the glow region excited by a steady ripple free continuously adjustable dc voltage. By monitoring the temporal evolution of the signal different distinct states can be observed and recognized under various experimental conditions. The time it takes to reach a stable

state strongly depends on the set control parameter (input current).

When the current is gradually increased in presence of the discharge it was found that pure sinusoidal oscillations starts with a finite amplitude at the threshold current $i = i_1$. As the current is further increased, at $i = i_2$ oscillations stops abruptly corresponding to dc state which is continued till $i = i_3$. Above i_3 oscillations with complex wave form (having more than one frequency) starts again with finite amplitude till $i = i_4$ and after that the oscillations stop and it goes to dc state. We were not able to go beyond $i_4 \sim 5mA$ due to the limitations of the power supply. Various state in the dynamics of the plasma are designated as follows.

state I $i \leq i_1$ non-oscillating state

state II $i_1 \leq i \leq i_2$ oscillating state - stable 5.26 - 2.27 KHz

state III $i_2 \leq i \leq i_3$ non-oscillating state

state IV $i_3 \leq i \leq i_4$ oscillating state - metastable 526 - 434 Hz

state V $i > i_4$ non-oscillating state

where $i_1 = 0.83$ mA, $i_2 = 2.46$ mA, $i_3 = 4.2$ mA, $i_4 = 4.96mA$

Fig 8.3 above these regions in the bifurcation diagram in which amplitude of oscillations as a function of discharge current in the dynamics of the plasma is given. CRO traces of the discharge oscillations at various states are shown in fig 8.4.
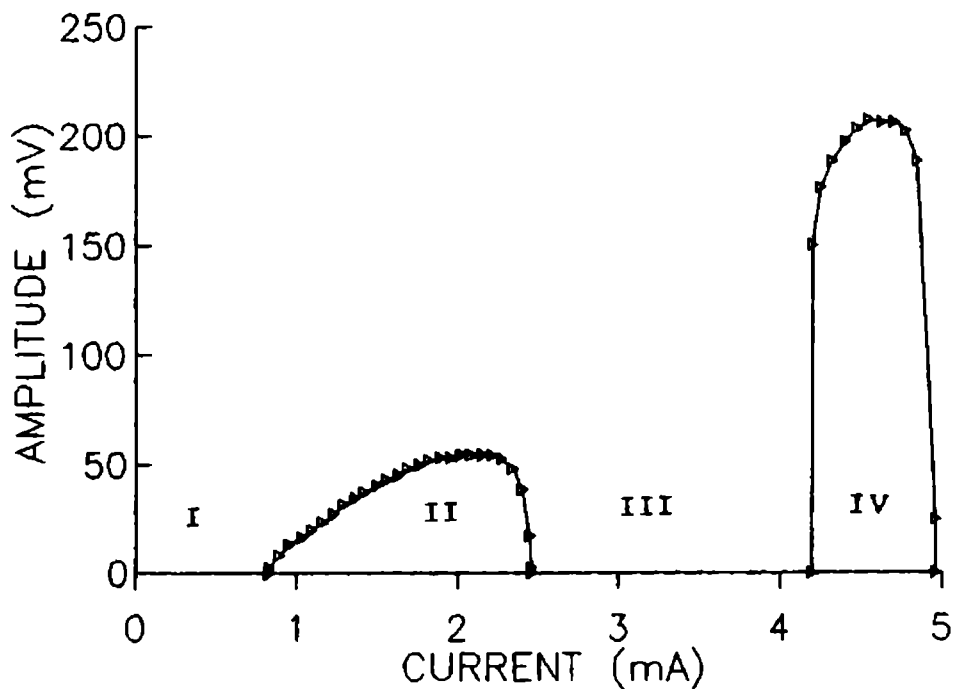
Fig 8.3 Bifurcation diagram of the plasma dynamics with discharge current as the control parameter.
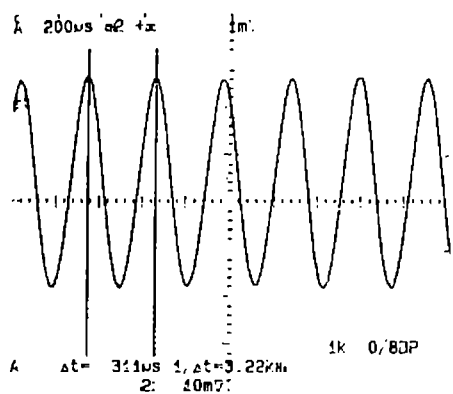Variation of signal amplitude with discharge current.

Fig 8.4A
Time evolution of
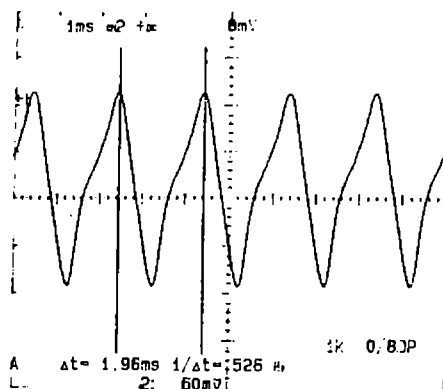the oscillation
for state II

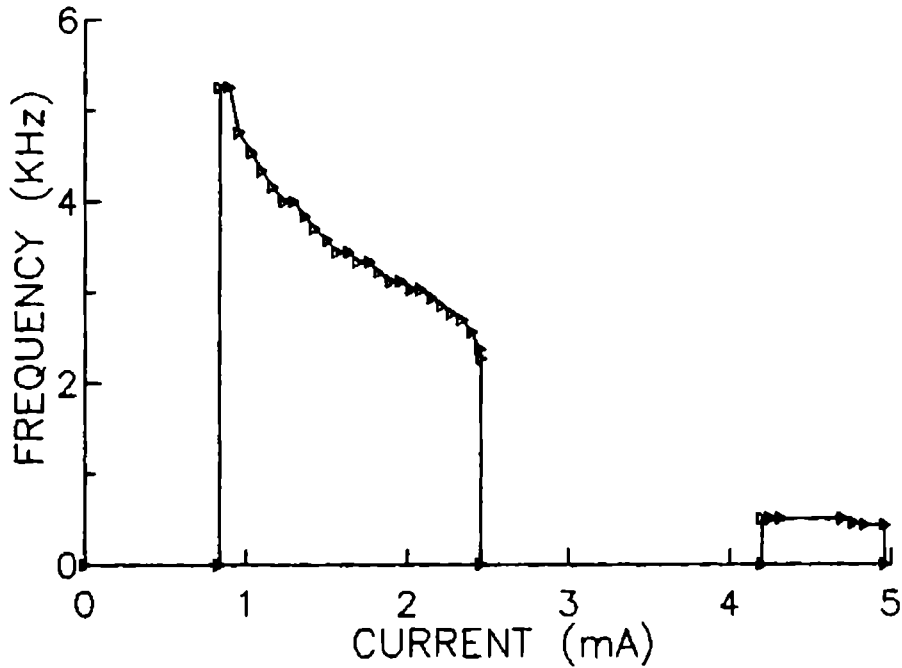
Fig 8.4B
Time evolution of
the oscillation
for state IV

Fig 8.5 Variation of frequency with discharge current

Even though observation of an intermediate oscillating state in the bifurcation has been reported recently [20] it is quite interesting to observe a non-oscillating intermediate state in the plasma dynamics as the discharge current is varied. Oscillations in the state II start at 0.83 mA with a frequency of 5.26 KHz and the frequency of oscillation in this state decreases with current to 2.27 KHz at 2.46 mA. For state IV also the frequency decreases with current (fig 8.5) from 526 Hz (at 4.2mA) to 434 Hz at (at i_4 = 4.96 mA).

The oscillating state II is found to be very stable ie. the oscillation amplitude remains constant with time if we fix the current between i_1 and i_2. When the discharge current is in the vicinity of $i = i_4$, the state IV decays to nonoscillating state V.
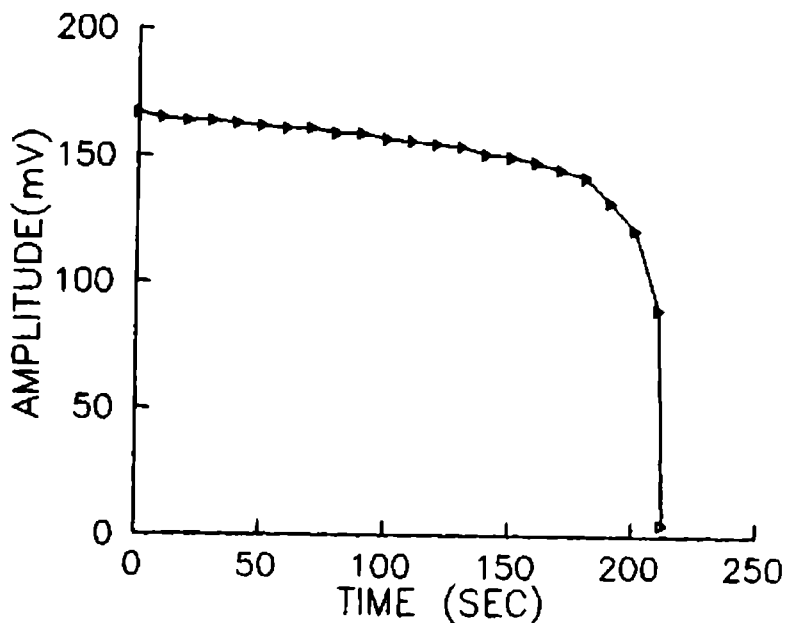
Fig 8.6 Relaxation from the oscillating
state IV to the non-oscillating state V

The relaxation of the state from IV to V is fast when i is close
to i_4 while it is slow when i is near to i_3. Fig 8.6 shows the
variations of the amplitude of oscillation as a function of time
in the left edge of the second oscillating regime. This
indicates that the state IV is a metastable state. Values of
critical currents i_1, i_2, i_3 and i_4 depends on aging and time
duration of the discharge operated.

When we go in the reverse direction, by decreasing the
discharge current, the critical currents are found to be shifted
to lower values demonstrating the existence of hysteresis (fig
8.7). This hysteresis is an indication of subcritical Hopf
bifurcation in which dc state is a fixed point and oscillating
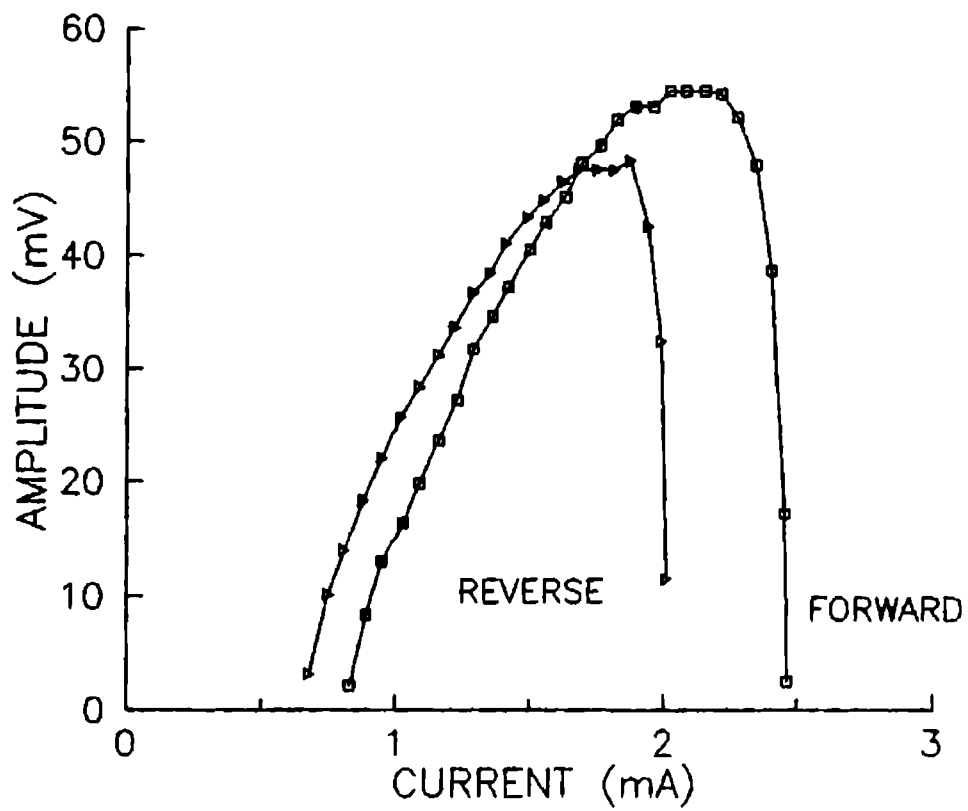state is a limit cycle. In the reverse direction the frequency of

Fig 8.7 Hysteresis in the amplitude

oscillation is less than that in the forward direction of i (fig 8.8). From the presence of two oscillating state (II and IV) and three non oscillating states (I, III and V) we can think of a series of subcritical Hopf bifurcations in the dynamics of the discharge plasma with windows of non-oscillating state in between them. The observation of "windows" may be due to the presence of noise in the discharge system. A quantitative analysis is not
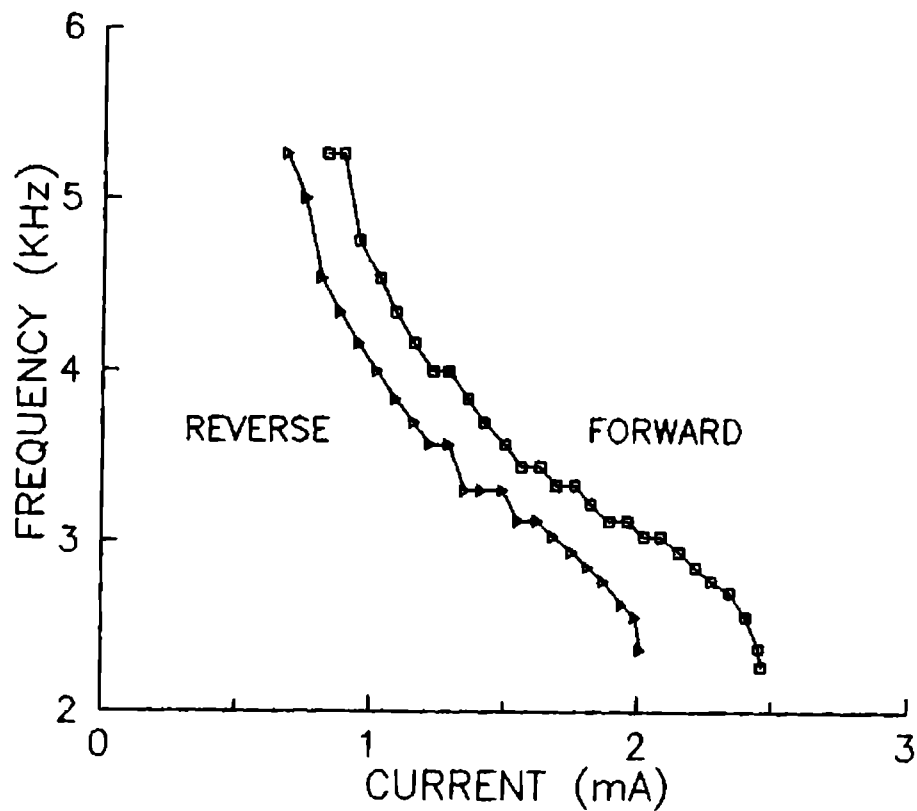

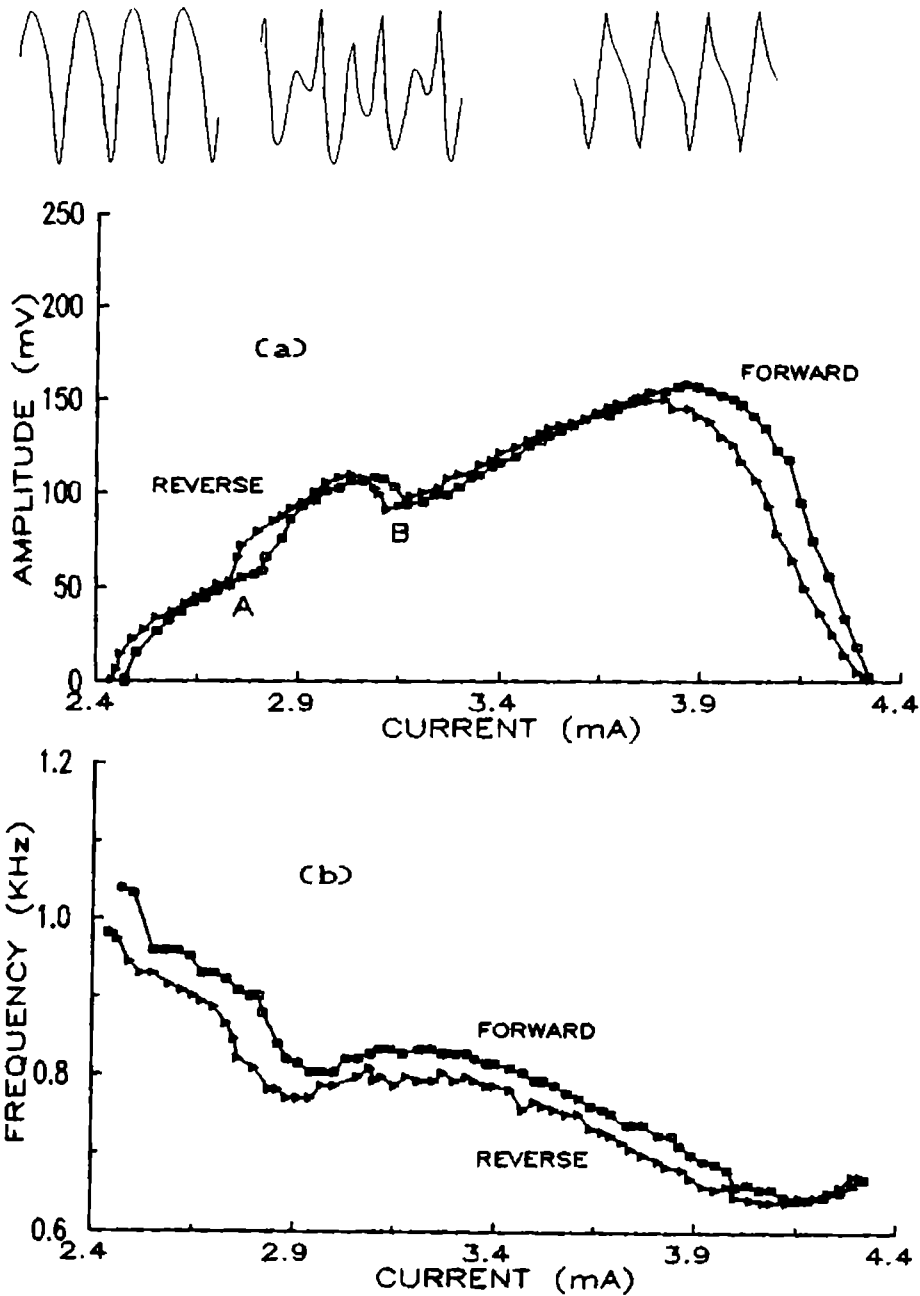Fig 8.8   Hysteresis in the frequency

Fig 8. 9 Bifurcation diagram of the plasma dynamics in Ne/Mo hcd with discharge current as the control parameter. R=86KΩ a) Variation of signal amplitude with discharge current, b) variation of frequency with current and shape of oscillations (not scaled).

possible because most of the understanding about the processes in hollow cathode is qualitative in nature. However, a general mechanism that leads to chaotic behaviour in discharge and modeling of the plasma dynamics showing the windows in the bifurcation diagram have been discussed in a few papers [4,20].

Fig 8.9 shows the bifurcation diagram and the frequency of oscillations obtained in a Ne/Mo hollow cathode discharge. In this case also hysteresis property is observed. The presence of quasi periodic oscillations in the bifurcation phenomena and its hysteresis (region A to B in fig 8.9a) are the noticeable observation as compared to that in Nd hollow cathode discharge.

8.5 PERIOD DOUBLING ROUTE TO CHAOS

We have also observed period doubling route in the plasma dynamics. When the discharge current is varied keeping all the parameter constant, the system bifurcates to a period doubling state and the temporal evolution is very different from the periodic oscillation. Above 0.5 mA just a stationary dc value is observed. Then a self generated oscillation appears which is superimposed to the dc level. By lowering the current in the circuit it is possible to see a very clear period doubling sequence as displayed in the fig 8.10. It can be seen that the temporal evolution of the signal displays chaotic oscillation and the power spectrum shows a substantial increase of band broadening. The power spectra of the signal can be obtained by
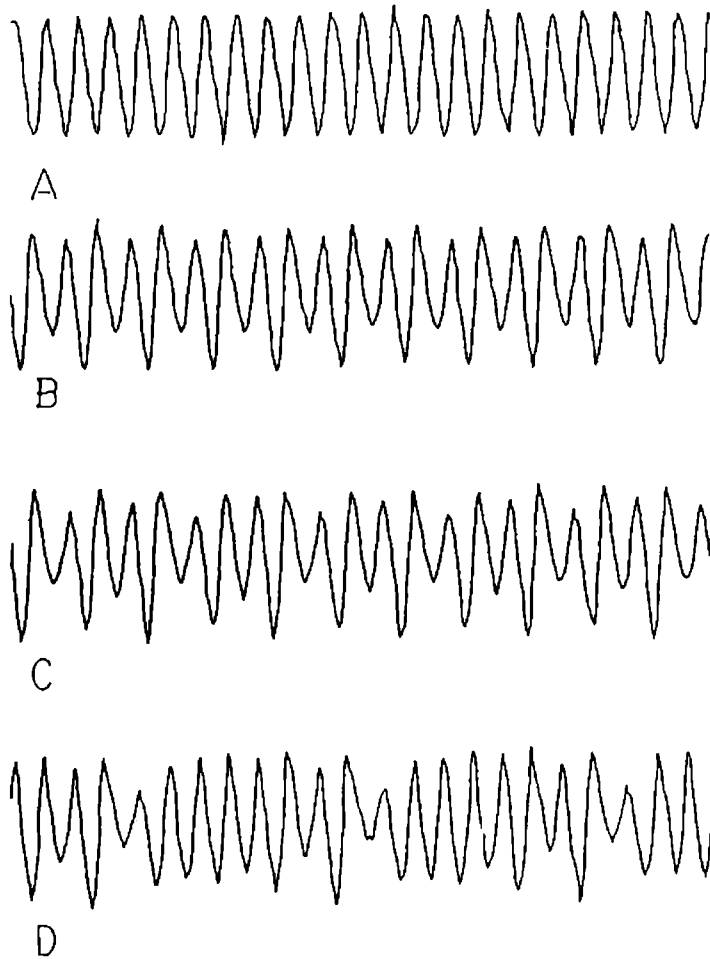
Fig 8.10 Period doubling route to chaos.

Self generated oscillations at different discharge currents
(R=33KΩ A-O.72mA, B-O.55mA, C-O.51mA and D-O.50mA)

fast fourier transform algorithm. The power spectrum and the phase space plot analysis obtained from the manual digitization of the CRO traces of the oscillatory pattern have also been used to confirm the existence of the period doubling route to chaos.

By measuring the ratio of the difference of the observed current I_i (δ), $i = 1,2,3$ signifies the various bifurcation states where the successive bifurcation occurs. Universal scaling factor (α) which gives the scale change of the differences between the neighboring values of the dynamical variable before and after a bifurcation can be obtained as follows [6,11].

$$\delta = \frac{I_3 - I_2}{I_4 - I_3} \qquad\qquad (8.4)$$

$$\alpha = \frac{\Delta V_1 - \Delta V_2}{\Delta V_3 - \Delta V_4} \qquad\qquad (8.5)$$

With in the limitations of the experimental accuracy (to tune the discharge current exactly at the bifurcation point) the measured value for δ is 4 and for α it is 2.5 which compares with the numerical results (theoretical values for $\delta = 4.6696$ and $\alpha = 2.503$ [11]. The favorable comparison with the theoretical result demonstrate that this region, the Fiegenbaum scenario of the route to chaos is relevant.

In summery, non-linear properties in the dynamics of Ne/Nd and Ne-Mo hollow cathode discharges with discharge current as the control parameter is studied. The existence of the non-oscillating state windows in the bifurcation diagram, the amplitude and the frequency of oscillations, hysteresis, period doubling route to chaos,etc. are investigated.

REFERENCES

1 J P Eckmann, Rev.Mod.Phys. 53 (1981) 655.

2 C O Weiss, W Klische, P S Ering and M Cooper, Opt.Commn. 52
        (1985) 405.

3 T Midavaine, D Dangoisse and P Glorieux, Phys.Rev.Lett. 55
        (1985) 1989

4 P Berge, Y Pomeau and C Vidal, Order within chaos (Wiley,
        New York, 1984).

5 H M Gibbs, F A Hopf, D L Kaplan and R L Schoemaker,
        Phys.Rev.Lett. 46 (1981) 46

6 P S Linsay, Phys.Rev.Lett. 47 (1981) 1349

7 T Braun, J A Lisboa, R E Francke and J A C Gallas,
        Phys.Rev.Lett. 59 (1987) 613.

8 Yuri P raizer, Gas discharge Physics (Springer verlag,
        Berline 1991)

9 T Donahue and G H Dieke, Phys.Rev. 81 (1951) 248.

10 C O Weiss, N B Abraham and U Hubner, Phys.Rev.Lett. 61
        (1988) 1587

11 P W Milouni, M L Shih, and J R Ackerhalt, Chaos in laser
        matter interactions (World Scientific, Singapore,1987).

12 A Garscadden and P Bletzinger and E M Friar, J.Appl.Phys. 35
        (1964) 3432

13 K Tochigi, S Maeda and C Hirose, Phys.Rev.Lett. 57 (1986) 711

14 P Y Cheung and A Y Wong, Phys.Rev.Lett. 59 (1987) 551

15 J Qin, L Wang, D P Yuan, P Gao and B Z Zhang Phys.Rev.Lett. 63 (1989) 163.

16 V O Papanyan and Y I Grigoryan, Phys.Lett.A 164 (1992) 43.

17 S H Fan, S Z Yang, J H Dai, S B Zheng, D P Yuan and S T Tsai, Phys.Lett.A 164 (1992) 295

18 D Weixing, H Wei, W Xiaodong and C X Yu, Phys.Rev.Lett. 70 (1993) 170.

19 P Y Cheung, S Donovan and A Y Wong, Phys.Rev.Lett. 61 (1988) 1360.

20 R Singh, P S R Prasad, J K Bhattacharjee and R K Thareja, Phys.Lett.A 178 (1993) 284.

CHAPTER 9

GENERAL CONCLUSIONS

The properties and behavior of gas discharges have been the subject of numerous investigations due to their growing interest in both fundamental and technological applications. It is widely used in gas lasers, radiation sources for generating light and for many spectrochemical applications. The characteristics of a gas discharge depend on various parameters like the electrode material, properties of gas, cell configuration, discharge condition and so on. Various techniques like emission or absorption spectroscopy, Langmuir probe, optogalvanic effect, etc. have been employed to characterize the discharge. Of these, the optogalvanic effect is unique and has several advantageous over other techniques. Here one essentially measures the change in discharge impedance as a result of absorption of radiation. Since the measurements are in terms of voltage change, all the spectroscopic and analytical studies can be made without any optical detection technique, so that the sensitivity is considerably high.

The spectroscopic investigations in gas discharges by laser induced optogalvanic effect and non-linear properties in the dynamics of the discharge plasma such as instability and various possible routes to chaos have been described in the present thesis. The discussion and results obtained from the present

<center>241</center>

investigations were included in the previous chapters. This chapter gives the general conclusions derived from the present studies.

The work presented in the chapters can be broadly divided as follows.

(I)   Optogalvanic study in nitrogen and neon discharges

(II)   Photoemission optogalvanic studies in Ne-Nd hollow cathode under cw laser excitation and two photon POG effect under pulsed laser excitation.

(III)   Experimental study of non-linear properties in the dynamics of the hollow cathode discharge.

The optogalvanic studies were carried out in two ways; a) by resonant absorption of radiation usually known as optogalvanic effect and b) non-resonant absorption of radiation by the electrode material known as photoemission optogalvanic effect. In the first case, the wavelength of the radiation is required to be resonant to a transition related to any of the discharge species for generating the signal, where as in the later case, it is generated by injecting photoelectrons into the discharge via photoelectron emission from the cathode. Even though the experimental procedure for these studies are simple and convenient, the presence of discharge noise as a result of random variations in current and gas pressure is a serious problem that limit the sensitivity of detection. However, this can be

minimized considerably by choosing a suitable cell configuration and operating the discharge in a stable region of the discharge using a highly regulated power supply and by maintaining a constant gas pressure in the cell.

Home made cells with positive column and glow discharges as well as commercial hollow cathodes and indicator glow lamps were used in the present studies. Continuous gas flow cells with de-mountable electrodes are found to be suitable for the spectroscopic study of molecular gases.

The first positive system $(B^3\Pi_g - A^3\Sigma_u^+)$ of nitrogen molecule has been studied by using Doppler limited high resolution OGS. Due to a good sensitivity of the method, OG resonances for a large number of rotational lines belonging to $(10,6)$, $(11,7)$ and $(12,8)$ bands of this system have been observed. The studies show that the method can be extend to investigate other band system by varying the discharge conditions such as gas pressure or current and a far better line accuracy and resolution can be obtained by adopting Doppler free methods.

Simultaneous investigations of OG effect carried out for $1s_5 \rightarrow 2p_2$ and $1s_5 \rightarrow 2p_4$ transition in neon and the fluorescence properties under resonant absorption of laser gives some very interesting results. These are very useful techniques to investigate the population distribution and hence the modifications in the electrical and emission properties of the discharge. Monitoring of these effects can also be used to

elucidate the mechanism of the optogalvanic effect.

As an alternative to conventional spectroscopic methods, the spectral profile of transitions belonging to highly excited state can be easily investigated by OG spectroscopy. The line spectral profile measurement has been carried out using OG effect and the line broadening coefficient, collision cross section, temperature etc have been evaluated for certain transitions in neon discharge. The spatial dependence of the OG signal has been found to give very interesting information on population distribution of species in the discharge.

The interaction of radiation with discharge medium by non-resonant process can be investigated by photoemission optogalvanic effect. This is useful for the study of photoelectric properties of the cathode material in presence of discharge as well as the physical processes involved in the interaction of photoelectrons with the plasma. The non-linear properties of the gas discharges such as multi photon absorption, discharge instability etc. have been studied here in detail by monitoring POG effect.

The order and chaos in dissipative system has been the subject of intense research due to their numerous potential applications. The gas discharge is a typical non-linear dynamical system with a large number of degrees of freedom. The non-linear behavior in gas discharges enables one to understand the chaotic behavior in the dynamics of a plasma discharge and

their sensitive dependence on the initial conditions. Here the existence of these non-linear properties that lead to various routes to chaos such as period doubling, Hopf bifurcation etc. are investigated by monitoring the discharge current as the control parameter.

In summary the various properties of gas discharges investigated by laser induced OG effect, POG effect and the current oscillations have revealed some of the interesting spectroscopic features and yielded information useful on non-linear behaviour in the dynamics of the gas discharges.